RADIATED NOISE AND WALL PRESSURE MEASUREMENTS IN TURBULENT BOUNDARY LAYERS IN DILUTE POLYMER SOLUTIONS

Thesis by

Steven J. Barker

In Partial Fulfillment of the Requirements

For the Degree of

Doctor of Philosophy

California Institute of Technology

Pasadena, California

1971

(Submitted August 20, 1971)

ACKNOWLEDGMENTS

The author gratefully acknowledges the guidance and assistance of Professor Donald Coles, whose expert advice made possible the success of this experiment. He also wishes to thank Dr. J. W. Hoyt, Mr. Paul Roberts, and Mr. John Mayr of the U. S. Navy Research and Development Center. Their assistance and support in the design and construction of the experiment and in the analysis of the data are appreciated.

The author is also indebted to Mr. Lewis Balthasar and Mr. Ray Wagoner for their help in the construction of the apparatus, and to Mrs. Geraldine Krentler, who typed the manuscript.

ABSTRACT

Measurements of radiated noise and wall pressure fluctuations in a turbulent boundary layer in water are described. A comparison is made between measurements in pure water and in dilute solutions of high molecular weight polymers. To obtain these measurements, a new experimental geometry was developed.

The principle of the experiment is as follows: A flat steel plate 205 cm long by 80 cm wide is rolled into a single-turn spiral, with a radial gap of 4.5 cm between the two overlapping ends. The spiral is submerged in water and rotated about its axis, creating a boundary layer on the inner surface which leaves the interior of the spiral through the radial gap. The fluid leaving the interior through the gap is replaced through the two open ends of the spiral by means of stationary honeycomb filters which remove residual turbulence and vorticity.

Measurements of the mean velocity profile show that the turbulent boundary layer on the inside surface of the spiral resembles that on a flat plate in a uniform free stream. A Reynolds number based upon plate length of 5×10^6 is obtained.

Wall pressure fluctuations under the boundary layer are measured with piezoelectric transducers mounted flush in the wall of the spiral. Radiated noise is measured with a

stationary transducer located outside of the boundary layer, near the center of the spiral. It is shown that the polymer additives cause significant reductions in both the radiated noise and wall pressure spectra. The reductions are greatest at high frequencies, or at Strouhal numbers greater than one.

TABLE OF CONTENTS

LIST OF FIGURES

LIST OF FIGURES (cont.)

LIST OF FIGURES (cont.)

LIST OF FIGURES (cont.)

I. INTRODUCTION

The purpose of this experimental study is to find a rough answer to a difficult question: what effect do high-polymer additives have upon turbulent boundary layer radiated noise and wall pressure fluctuations? Although the fluctating wall pressure in polymer flows has been measured in previous experiments, there have been few, if any, measurements of the boundary layer radiated noise. In order to help fill this void, we have used a new experimental geometry designed specifically to facilitate radiated noise measurements.

The phenomenon of radiated noise from turbulent boundary layers in dilute polymer solutions combines two subjects in which little theoretical progress has been made. We shall present in this section a very brief summary of what has been done in these two fields, both in theory and in experiment, and give some references for the interested reader.

A. The Toms' Effect.

In 1948 B. A. Toms discovered that the addition of minute quantities of high molecular weight polymer to a solvent resulted in a significant increase in the flow rate through a pipe for a fixed pressure drop. Since that discovery there have been numerous experimental studies of the properties of these dilute polymer solutions, as well as many attempts to explain the phenomenon of viscous drag reduction.

Most of the drag reduction data presently available are for pipe flow, this being the simplest type of turbulent wall flow to create in the laboratory. Typical experiments are described in the proceedings of the 1968 Drag Reduction Symposium, held at Dallas (Ref. 1). The results of these experiments show that viscous drag reduction occurs only in turbulent flows, and that for a given polymer solution there exists a critical wall shear stress above which drag reduction begins. The critical shear stress is a weak function of concentration: it is slightly lower for the more concentrated solutions. At a wall shear stress less than the critical value, the solutions behave much the same as the pure solvent.

Experiments such as these have also shown that the polymer solutions are subject to shear degradation; that is the drag reducing characteristics of the solution will decay if the fluid is subjected to high shear rates for any period of time. The degradation phenomenon has been measured experimentally by Paterson (Ref. 2) in a pipe flow in which the properties of the polymer solutions were monitored as functions of time.

Although most of the experimental data are for drag-reduced wall flows, there have been a few measurements in free turbulent flows. Jackley (Ref. 3), and White (Ref. 4) measured velocity profiles in free turbulent jets of polymer solutions. The results of these two experiments are contra-

dictory. Jackley found that the additives have no measurable effect upon the jet, while White reported an increase in both spreading angle and center-line velocity. Fabula (Ref. 5) made a study of turbulence generated by flow through a grid in polymer solutions. He found no effect of the polymers upon the turbulence spectrum other than that attributable to the influence of the additives upon the measuring apparatus.

On the theoretical side of the Toms' effect the picture is rather bleak. There is at present no theory which can quantitatively explain the occurrence of viscous drag reduction. Many mechanisms have been proposed, most of which involve a non-Newtonian effect near the wall. Evidence cited above that free turbulent flows are not affected by the polymers seems to support such wall effect theories, which propose that the influence of the polymer is felt chiefly in the viscous sublayer of the flow. Other theories, however, postulate a suppression of turbulence by particulate effects of the molecules or agglomerations thereof. Reviews of most of the mechanisms for drag reduction that have been proposed have been written by Deavours (Ref. 6) and Walsh (Ref. 7). A statement of the theoretical problems associated with polymer flows has been written by Lumley (Ref. 8).

Although the viscous drag reduction phenomenon has been fairly well characterized in experiments, further

knowledge of the other hydrodynamic properties of these solutions is needed before the Toms' effect can be fully understood.

B. Radiated Noise from Turbulent Flows.

Even though the sound radiated from turbulent shear flows has been a subject of interest for many years, the theory of radiated sound is but little more advanced than the theory of the Toms' effect. Lighthill's 1952 paper (Ref. 9) is usually considered the foundation of this subject. In it he transforms the usual momentum equation for a fluid into a wave equation for the fluid density, with the Reynolds stresses appearing on the right hand side as a forcing function. In this way, he drives his "acoustic analogy" between a turbulent shear flow radiating sound and a uniform acoustic medium at rest. While this is a very elegant formulation of the problem, it only expresses the unknown radiation field in terms of another unknown field -- the Reynolds stresses in the shear layer.

Lighthill's analogy has been applied to turbulent boundary layers by Curle (Ref. 10), and to turbulent jets by Lighthill himself (Ref. 11). Phillips (Ref. 12) derived a qualitative explanation of boundary layer radiated noise expressed in terms of dipole sources rather than the quadrupoles of Lighthill. A different acoustic model was proposed by Liepmann (Ref. 13), who represented the noise

sources in the boundary layer by fluctuations in the displacement thickness. This approach is more practical in that the displacement thickness is probably easier to measure than Lighthill's quadrupole density function.

None of these theories is able to predict experimental results with any accuracy or consistency. An excellent survey of the theoretical work in radiated noise has been written by Laufer, et al. (Ref. 14).

Experimental data on radiated noise from turbulent boundary layers are scarce. Due to the extremely low intensity of this noise, it is difficult to create an experimental geometry in which it can be accurately measured. Results have been obtained for the radiated sound from the outside of a rotating cylinder in water, but the flow around a rotating cylinder does not resemble a turbulent boundary layer on a flat plate, due to its inertial instability. Radiated noise has also been measured with buoyancy-propelled cylindrical bodies in water (Ref. 15), but in this case it is difficult to distinguish noise from the turbulent boundary layer itself from noise generated by the stabilizing fins on the tail of the body.

Although data on radiated noise from boundary layers are lacking, there have been many experimental measurements of the fluctuating wall pressure. These include measurements using wind tunnels, pipe flow, water channels, rotating cylinders, and rising bodies in water (Refs. 16, 17, 18, 19,

20, 21, 22, 23). Some of these results will be compared with the data of the present experiment later in this paper.

Further experiments are needed to determine the effects of polymer additives upon radiated noise from turbulent boundary layers. In addition, wall pressure measurements in polymer solutions for a boundary layer which closely resembles that of a flat plate in a uniform free stream are needed. It is to these purposes that the present experiment was designed.

II. DESCRIPTION OF EXPERIMENT

A. Apparatus.

In the design of an experiment for measuring radiated noise from a boundary layer in dilute polymer solutions, several requirements must be met. In order to be as fundamental as possible, the experimental flow should closely simulate the flow over a flat plate in a uniform free stream. Unfortunately this criterion excludes all of the easier experimental geometries, such as pipe flows and rotating cylinders.

To make radiated noise measurements possible at flow velocities realizable in the laboratory, extraneous noise sources in the experiment must be kept to a minimum. This requirement is very difficult to meet in experiments which require complicated machinery, such as tow basin facilities.

Another requirement is that the radiated noise receiver must be nearly stationary with respect to the fluid surrounding it. If this is not the case, the turbulent flow over the surface of the receiver will create a fluctuating pressure field of its own. The signal from the receiver due to this "self noise" field will then mask out the radiated noise from the relatively distant experimental boundary layer.

A final consideration is the fact that the polymer solutions are shear degradable, as mentioned above. If steady state experimental conditions are to be obtained long

enough to make consistent measurements, the apparatus can contain no pumps or other sources of high shear rates which would seriously affect the drag-reducing properties of the solution.

The present experiment was designed to satisfy these conditions as closely as possible. The principle is as follows. A .23 cm thick stainless steel plate, 80 x 214 cm, is rolled along its length into a single-turn spiral, with the two ends overlapping by 9 cm and separated radially by a gap of 4.5 cm. The resulting shape is then a nearly cylindrical shell, open at both ends, whose inside radius is given by $R = (30.5 \nearrow 4.5 \frac{\theta}{2\pi})$ cm (see Fig. 1). This spiral plate, henceforth called a "scroll", is held to its proper shape by three external rings which have had their inside edges cut to the equation given above by a numerically controlled milling machine. The edge of the plate closest to the center of the scroll is now called the leading edge (where $\theta = 0$ in the formula above), and the edge further out is the trailing edge ($\theta = 2\pi$). The inner surface of the scroll is polished to approximately a 20 micro-inch finish.

This scroll is then rotated about its axis in a stationary fluid in the direction of the leading edge, creating a boundary layer along the inner surface. Most of this boundary layer will leave the interior of the scroll through the radial gap (Fig. 1). If the boundary layer is thin

relative to the radius of curvature of the scroll, it can be expected to resemble the boundary layer on a flat plate.

To make the flow steady-state, the outflow of vorticity-containing fluid through the radial gap must be replaced by non-rotating fluid supplied through the two open ends of the scroll. Thus the flow in the interior of the scroll will have both an axial and a radial component, and should closely resemble the axisymmetric stagnation point flow: $u_r = Ar$, $u_z = -2Az$. To match this external flow, the wall should really be a logarithmic spiral, $r \sim e^{\theta}$, but its actual shape is a close enough approximation.

Since it was desired to make the experiment a closed, recirculating system, a means had to be devised to remove the residual turbulence and vorticity from the fluid which exits the scroll through the radial gap, and then return it through the two ends. This was accomplished in the following way (see Figs. 2 and 2a). The scroll is mounted inside of a cylindrical tank 91 cm in diameter and 152 cm long (3' x 5'). It is supported exactly in the center of this tank by means of two perforated rings attached to the outside of the scroll at either end (see Fig. 2b). These rings fit closely inside the tank wall and are held there by set screws. The tank itself, the rings and the scroll all rotate. The perforations in the rings allow the fluid flow from the radial gap of the scroll to reach the two ends by moving vertically in the space between the scroll and the

tank. Each of these rings consists of two rings, one on top of the other, which can be slightly rotated with respect to one another to vary the size of the perforations and thus control the external flow. The open area of the rings can be varied in this way from 55% of the total area to about 10%.

The two ends of the scroll are covered by two non-rotating cylindrical honeycomb filter assemblies, which remove the mean rotational velocity component and reduce the residual turbulence of the fluid passing through them. These filters are held stationary by two fixed steel shafts which come through the top and bottom of the tank along the axis of rotation and attach to the honeycombs. The lower shaft enters the tank through a neoprene seal which prevents leakage. Around the outside of each of the honeycombs is a series of eight stator vanes mounted at an angle of incidence such that they deflect the rotating flow in the region between the scroll and the tank wall, thus pumping the fluid through the honeycombs and back into the interior of the scroll (Fig. 2a). Nowhere in this process is the fluid subjected to shear stresses which are substantially greater than those in the boundary layer itself.

Each of the honeycomb assemblies consists of about 20,000 polypropylene soda straws, .32 cm in diameter and 15.3 cm long (1/8 x 6"). The straws are bonded together side by side with contact cement to form a cylinder 15.2 cm thick

and 58.5 cm in diameter. The outside of this cylinder is surrounded by a .64 cm thick aluminum shell, and it is to this shell that the stator vanes are attached. There are eight vanes around each cylinder, spaced such that the leading and trailing edges of consecutive vanes overlap slightly. The vanes are shaped so that their outside edges are a constant 1.2 cm from the inner wall of the tank. The angle of incidence of the vanes is about 15^{o}, as calculated from the flow rate through them required to equal the flow through the radial gap. It is important to remember that the vanes, the honeycombs, and the central shafts are stationary while the rest of the apparatus rotates. Thus most of the fluid in the scroll interior (except for the boundary layer) does not rotate, while most of the fluid in the region exterior to the scroll does.

The ratio of the mean fluid velocity through the honeycombs to the rotational velocity of the scroll wall is roughly equal to the ratio of the area of the radial gap to the area of the two honeycombs. The latter area is 5350 cm^2 while the area of the radial gap of the scroll is 340 cm^2. Thus the velocity ratio is of the order 1:20, and so the axial velocity component in the interior of the scroll can be neglected for most purposes. For a typical wall velocity of 200 cm/sec the mean flow velocity through the honeycomb is about 10 cm/sec. The resulting pipe flow Reynolds number in the soda straws is 300. Since the straws are fifty

diameters in length, the flow issuing from them should be free of small-scale turbulence.

The two steel shafts which hold the honeycombs are 6.35 cm (2½") in diameter, and extend through the centers of the honeycombs, ending 2.5 cm beyond the ends of the straws. These two ends of the shafts are joined by a plexiglass tube of the same diameter, 74 cm in length. This non-rotating tube running along the central axis of the scroll is used to mount the stationary hydrophone used for the radiated noise measurements.

Mechanical noise was the chief consideration in the design of the external apparatus for rotating the tank. For this reason ball bearings were immediately excluded. However, the tank weighs about 3,000 lbs when full of water, and so requires a thrust bearing of reasonably low friction coefficient as well as low noise to support it. For these reasons a hydrodynamic bearing was chosen, in which oil is pumped at high pressure between a disc of teflon and one of steel. This bearing is essentially noiseless and quite low in friction. There are two other bearings for carrying radial loads -- one at the top and one at the bottom of the tank. These are friction bearings made of a self-lubricating, graphite-impregnated teflon (Garlock DU material), with polished steel journals.

To minimize transmission of noise from the drive motor to the tank, a rubber drive belt is used rather than a chain

or gear train. The belt is of the "poly V" type, having a sawtooth pattern (parallel to the belt length) on its inside face. This pattern matches a similar pattern on the sheaves, thus providing a large area of contact. The belt drives a 30.5 cm (12") diameter sheave attached to the bottom of the tank, and is driven by a 10.2 cm (4") diameter sheave. Both sheaves are in the horizontal plane. The smaller sheave is on the output of a right angle drive transmission, which has a vertical output shaft and a horizontal input shaft. This is in turn driven by a Graham "Varidrive" 1.5 hp motor-transmission. The Varidrive provides a continuously variable output shaft rpm while its AC motor runs at constant speed. It is surrounded by a plywood box lined with glass wool, which absorbs noise radiated from the motor and transmission. The Varidrive unit is also isolated from the right angle transmission by two flexible couplings, designed to absorb vibration. Both the Varidrive and the right angle transmission are isolated from the floor of the laboratory by shock mounts.

The thrust bearing which supports the tank is mounted in the center of a horizontal H-shaped frame of steel I-beams. The four corners of this frame are mounted on rubber pads on the floor. The frame has vertical extensions which support the upper stationary shaft of the experiment. This system of suspension provides good isolation of the apparatus from the floor at frequencies above 20 Hz.

(Accelerometer measurements on the floor show an ambient vibration peak at 25 Hz in the vertical mode, and a smaller peak at 9 Hz in the horizontal mode.)

The maximum attainable speed of the experimental tank is 70 rpm, which corresponds to a scroll wall velocity of 238 cm/sec. The usable length of the wall is 205 cm, so that the maximum Reynolds number based on plate length is 5×10^6.

B. Preparation of Polymer Solutions.

For most of the tests of dilute polymer solutions, the most widely used drag-reducing polymer was chosen: Union Carbide polyox, WSR-301. The compound is poly(ethylene oxide), a single-chain polymer with an average molecular weight of about 4×10^6. Typical friction reduction data for WSR-301 in a pipe flow of Re = 14,000 are shown in figure 3 (Ref. 24). From these results it is evident that concentrations between 20 and 100 parts per million by weight yield the best friction reduction. Therefore most of the tests were performed with solution concentrations of 20, 50 and 100 ppm.

It is known that drag reduction is very sensitive to polymer molecular weight, which is a very difficult quantity to measure. Attempts to measure the distribution curve of molecular weights in WSR-301 have yielded only approximate results. Attempts to fractionate this polymer into a single molecular weight species have failed (Ref. 2). Although

WSR-301 has a narrower distribution curve than most commercially produced polymers, it contains several hundred thousand molecular weight species. Thus a measurement of the average molecular weight, which can be defined in half a dozen different ways, is not sufficient to characterize the polymer solution. For these reasons no molecular weight measurements were attempted in this experiment. To insure consistency, all of the polyox used came from the same barrel.

The polymer solutions were prepared as follows. First a 150 liter master solution was prepared, containing the amount of polymer necessary to yield the desired concentration in the final solution in the experiment. By sheer coincidence, the apparatus holds 1.00×10^6 cc of water. Thus the number of grams of polymer dissolved in the master solution is equal to the parts per million by weight concentration of the final solution in the tank. The concentration of the master solution is then of the order of 1%.

The polymer is dissolved by sprinkling the powder thinly and evenly over the surface of the master solution while stirring with a very slow (60 rpm) motor. The master solution is allowed to stand overnight to insure homogeneity. The experimental tank is then filled about half full with water, and the master solution is added. The tank is filled the rest of the way with water, and the experiment is run at a low speed of 25 rpm for ten minutes to insure that the

master solution is thoroughly dissolved in the water before any tests are performed. This procedure was used throughout the tests, and gave quite repeatable results.

III. VELOCITY FIELD MEASUREMENTS

A. Flow Visualization.

The first order of business after the construction of the experiment had been completed was to see if the flow was qualitatively as expected; that is, the fluid outside of the boundary layer in the interior of the scroll should exhibit little or no solid body rotation and a relatively low degree of turbulence. This was accomplished by a simple flow visualization study, involving no quantitative measurements.

The tank was filled half full with water, to the center of length of the scroll, and the upper honeycomb assembly was left out. The free surface inside the scroll was covered by a flat plexiglass disc, held by the upper stationary steel shaft. This procedure is then equivalent to cutting the experiment in half and studying the lower half. The water in the scroll can be viewed through the plexiglass top of the tank, and the additional plexiglass disc on the free surface suppresses the surface waves. The tank was run in this way at several speeds, and dye streaks were injected into the water at several positions in the flow of the scroll interior. Small styrofoam tracer particles were also used to observe the flow.

This study showed that the fluid mean angular velocity in the scroll interior is less than 1/20 of the wall angular velocity everywhere except within the boundary layer itself.

Small crystals of potassium permanganate placed on top of the lower honeycomb showed that the flow emerging through the honeycomb is nearly laminar, as expected.

B. Static Pressure at the Leading Edge.

Another preliminary measurement was the determination of the static pressure jump across the surface of the scroll at a point 1 cm behind the leading edge. This measurement gives an indirect indication of whether or not the stator vanes are pumping the fluid into the scroll at the proper rate. In the ideal case, the front stagnation point would be located precisely on the leading edge. Then the static pressure measured on both sides of the leading edge a short distance back would be the same. However, if the stator vanes are not pumping the fluid at a sufficient rate, the front stagnation point will be displaced toward the outside of the leading edge. This will result in a higher static pressure on the outside than on the inside. Conversely, if the vanes are pumping the fluid at too great a rate, the stagnation point will be displaced toward the inside of the leading edge, and the static pressure will be greater on the inside.

If these measurements show the pumping rate to be incorrect, the situation can be rectified in one of two ways. First, the angle of incidence of the deflector vanes can be varied. In addition, the perforated rings which hold

the scroll to the inside of the tank can be varied in their open area from 10% to 55% by the method described above. A reduction in the open area of the rings has the effect of increasing the pressure drop through them and thus reducing the fluid pumping rate.

The leading edge static pressure measurements are made in the following way. Two brass tubes, .152 cm (.060") in diameter, are soldered together side by side and then bent into a U-shape at one end (Fig. 14). This U is made to fit over the leading edge of the scroll such that the two tubes lie flat against the wall on both sides. A small static pressure hole is drilled in the side of each tube in such a way that there is one hole on each side of the leading edge. The ends of the tubes are closed on the inside of the leading edge. The ends on the outside are connected through plastic tubing to a pair of manometer tubes on the top of the tank. These two manometers are mounted vertically on the ouside of the tank, and they rotate with the experiment. A simple flash photography system is used to read the fluid levels in the tubes. A Polaroid camera and high intensity flash lamp are located opposite the tank in the laboratory. When the manometer tubes are directly in front of the camera lens, a cam on the outside of the tank closes a microswitch, which then opens the shutter. The cam closes a second microswitch 20 milliseconds later, which fires the flash lamp. The manometer levels on the resulting photographs are read to

the nearest millimeter of water.

From this measurement we can obtain an estimate of the difference in mean velocity at the two static pressure points by assuming that the stagnation pressure, $p + \frac{1}{2}\rho u^2$, is the same at both points. This is a reasonable assumption since both points are located on the dividing streamline. Thus the measured pressure difference, $\Delta p = p(\text{outside}) - p(\text{inside})$, is equal to the change in the dynamic head, $\frac{1}{2}\rho\Delta(u^2)$. This can be approximated by

$$\Delta p = \tfrac{1}{2}\rho(u_1^2 - u_2^2) = \tfrac{1}{2}\rho(u_1 - u_2)(u_1 + u_2)$$

$$\approx \rho U(u_1 - u_2) ,$$

where u_1 and u_2 are the inside and outside velocities, respectively, and U is the wall velocity, which is nearly equal to $\frac{1}{2}(u_1 + u_2)$. Thus we can write the fractional change in velocity across the leading edge as

$$(u_1 - u_2)/U = \Delta p/\rho U^2 .$$

This quantity is the best indication of the degree of displacement of the stagnation point from the leading edge, and is plotted versus vertical distance from the center of length of the leading edge in figure 5. Note that a positive value of Δp implies that the stagnation point is shifted toward the outside, while a negative value means it is shifted to the inside.

With this in mind, the results shown in figure 5 can be easily interpreted. Fluid is entering the scroll interior through the honeycombs at the ends, and once it leaves the scroll through the radial gap it must move back towards the ends and through the perforated rings. This axial circulation causes the pressure drop through the radial gap to be greater near the ends of the scroll than at the middle (see Fig. 2). Thus the fluid is pumped through the radial gap more efficiently near the ends of the scroll. This results in the shift of the stagnation point to the outside of the leading edge at the middle, and the shift in the opposite direction near the ends.

These measurements were made at four different positions along the leading edge: the three shown in figure 5, and also at $z = -37$ cm. This provides a comparison of the leading edge pressure jump at points near both ends of the scroll, and thus checks the symmetry of the flow at the two ends. The results for these two positions are the same to within experimental error.

The conclusion to be drawn from these measurements is that the flow near the leading edge is about as expected. The velocity difference between the two points 1 cm back from the leading edge is less than 7% for the highest wall speed. The pumping of fluid through the radial gap is more efficient near the ends than at the middel, which is predictable from the experimental geometry. We might expect from this that the boundary layer thickness will grow more rapidly

with distance from the leading edge near the middle of the scroll than it does near the ends. It will be shown below that this is indeed the case. In view of these results no further changes were made in the angle of incidence of the stator vanes or the open area of the perforated rings.

C. Mean Velocity Profile.

Having established that some sort of boundary layer does indeed develop on the inside surface of the scroll, the next step was to measure the mean velocity profile of this boundary layer as a function of free stream velocity and position on the wall. The results can then be compared with velocity profiles for flat plate turbulent boundary layers from other experiments.

The velocity profiles were measured with an array of eleven pitot tubes, made of stainless hypodermic tubing .076 cm (.030") in diameter. The tubes are spaced .3 cm apart near the wall, with spacing gradually increasing to 1 cm further out. The pitot tube array is mounted on the wall of the scroll in such a way that the innermost tube lies against the wall and can be used as a Preston tube. The outermost tube is 6.35 cm from the wall, and is in the free stream flow under all conditions.

The pitot tubes are connected through the wall to plastic tubing which leads to the outside of the tank. The plastic tubing is connected to a row of manometer tubes mounted on the outside of the tank at the top. These

manometer tubes are restricted to a height of 44 cm above the top of the tank, due to the supporting framework of the experiment. Since this is not enough height to measure the total head at the highest wall speeds, the manometer tubes are slanted inward toward the axis of rotation, taking advantage of the centrifugal pressure gradient caused by the rotation of the tubes. To measure the fluid levels in the manometer tubes, the flash photography technique described in the leading edge measurements is used.

Both centrifugal and hydrostatic pressure gradients must be considered in the conversion of the levels in the manometer tubes to pitot pressures at the probe locations. Since all of the fluid in the manometers, pitot tubes, and connecting tubing is undergoing solid body rotation, the radial pressure gradient is given by $\rho\omega^2 r$, where ω is the tank angular velocity. This is integrated from the pitot tube to the liquid surface in the manometer tube to give

$$\Delta p_r = \tfrac{1}{2}\rho\omega^2 (r_m^2 - r_p^2) ,$$

where r_m is the radial coordinate of the liquid surface in the manometer, and r_p is that of the pitot tube. This pressure change due to centrifugal force is subtracted from the hydrostatic pressure to give the pitot pressure:

$$p_t = \rho g z - \tfrac{1}{2}\rho\omega^2 (r_m^2 - r_p^2) ,$$

where z is the vertical coordinate of the manometer fluid

level. Defining h as the level in the manometer as measured along the length of the tube (this is the quantity measured in the photographs), then

$$z = 79.5 \neq h \sin \theta$$

$$r_m = 54.0 - h \cos \theta \ ,$$

where θ is the angle of elevation of the manometer tubes, 47.5°. Using these formulae with the known values of r_p, we have the pitot pressure in terms of h and ω.

Located near the pitot tube array is a small hole in the wall for measuring the static pressure. The static pressure at the wall is read from a manometer tube in the same way as the pitot pressure. In plane, two-dimensional boundary layer theory the static pressure is found to be constant across the boundary layer, so that the measurement of p at the wall combined with the pitot measurements of $p \neq \frac{1}{2}\rho u^2$ is sufficient to determine the mean velocity profile. However, in the case of flow over a curved wall the fluid velocity in the boundary layer creates a radial pressure gradient which balances the centripetal fluid acceleration. Since this pressure gradient, given by $\rho u^2/r$, depends upon the velocity we wish to measure, it cannot be calculated a priori. Hence a method of successive approximations must be used. First the velocity profile is calculated from the pitot pressure assuming constant static pressure throughout the boundary layer. The velocity profile found in this way

is then converted to velocity in non-rotating laboratory coordinates by subtracting the rotation of the probes, ωr. The velocity profile in the Newtonian frame is used to calculate numerically the integral

$$\int_{r(\text{wall})}^{r(\text{probe})} (\rho u^2/r)dr \ ,$$

which is the static pressure change from the wall to the pitot probe due to the centrifugal pressure gradient. This pressure change is applied as a correction to the static pressure measured at the wall and the velocity profile is re-calculated from the pitot pressure and corrected static pressure. The new velocity profile is used to calculate the static pressure correction again, and so on. This process is carried out by a digital computer, with the iteration just described being done five times. The results are observed to converge rapidly.

To estimate the mean wall shear stress from the Preston tube pressure, we use the following result of Patel (Ref.25). Define:

$$x^* = \log(\Delta p d^2/4\rho\nu^2) \ , \qquad y^* = \frac{d}{2\nu}\sqrt{\frac{T_o}{\rho}} \ ,$$

where Δp is the Preston tube pressure minus the static pressure, d is the diameter of the Preston tube, and T_o is the wall shear stress. Then for the y^* range $5.6 < y^* < 56$ we have

$$\log(y^{*2}) = 0.8287 - 0.1381x^* + 0.1437x^{*2} - 0.0060x^{*3} \ .$$

It was found that the measured values of y* for the Preston tube always fell within the range given above, so this formula was used throughout.

Typical velocity profile data for a distance behind the leading edge of x = 30 are shown in figure 6. Since the free stream flow relative to the probes is a solid body rotation rather than a uniform flow, it is convenient to define an angular fluid velocity by v = uR/r, where R is the radial coordinate of the wall and r is that of the probe. If y is the distance inward from the scroll wall, then r = R - y. Profiles of angular velocity defined in this way will approach a constant value with increasing distance from the wall. Typical profiles of this form are shown in figure 7, for x = 196 cm. The most important feature of these velocity profiles is that they show that the mean vorticity is contained in a thin layer near the wall, and the flow relative to the wall rapidly approaches solid body rotation outside of this layer.

Wall shear stress as measured by the Preston tube is shown in figure 8, plotted as a function of both wall velocity and distance from the leading edge. The wall stress of a flat plate turbulent boundary layer is expected to vary as $U_w^{9/5}$. The Preston tube results are rather approximate, and they show this speed dependence to within experimental error.

It was stated above that the pumping of fluid through

the radial gap of the scroll is more efficient near the ends than at the middle. To see what effect this has, two velocity profiles were measured for the same distance from the leading edge -- one at the center of length, and the other near one of the ends. Some of the results of this are shown in figure 9. This figure shows that the previous hypothesis is correct; the boundary layer is indeed thinner near the ends of the scroll, and the wall stress there is greater.

To permit a comparison of the mean velocity profiles of this experiment with those of other turbulent boundary layer experiments, the data are transformed to "law of the wall" coordinates. Define $y^+ = yu_\tau/\nu$, where $u_\tau = \sqrt{T_o/\rho}$ is the so-called friction velocity. Also define $u^+ = u/u_\tau$. The law of the wall states that there exists a range of y^+, usually between 50 and 1,000, for which

$$u^+ = (1/k)\ln(y^+) + C \ .$$

It has been demonstrated by Coles (Ref. 26) that nearly all existing mean velocity profile data for turbulent boundary layers can be fitted to this law, and that the constants k and C can be set equal to .4 and 5.1 respectively.

Figure 10 shows data from the present experiment plotted in law of the wall coordinates. It also shows wind tunnel data by Weighardt (Ref. 27) for constant free stream velocity. Two of these curves have been shifted upward along the y-axis to permit a comparison. The straight lines

shown correspond to k = .4 and C = 5.1. Note the close resemblance between the x = 161.5 cm data from the present experiment and the Weighardt data. This is one indication that the boundary layer of this experiment is similar in nature to the turbulent boundary layer on a flat plate in a uniform free stream. The two profiles for x = 30.5 and 161.5 include data for four different wall speeds: U_w = 103, 150, 190, and 221 cm/sec. The data for the four speeds fall nearly on the same curve for each location.

Measurements of mean and fluctuating velocities in dilute polymer solutions are made extremely difficult by the anomalous behavior of both pitot tubes and hot-film anemometers in these fluids (Ref. 28). However, approximate results can be obtained with pitot tubes at the lowest polymer concentrations. Therefore velocity measurements were attempted in this experiment for polymer concentrations of 20 and 50 ppm. Some of the results are shown plotted in law of the wall coordinates in figure 11. There appears to be a slight upward shift in the profiles when compared with those of pure water, caused by the decrease in the measured value of u_τ. This is equivalent to an increase in the law of the wall constant C, and can be interpreted as a thickening of the viscous sublayer. Note that the scatter of the data is much greater for the polymer solutions than for pure water. The degree of scatter is a strong function of concentration, but has no apparent dependence upon wall speed.

Wall shear stress measured by the Preston tube for concentrations of 20 and 50 ppm and for pure water is shown in figure 12, for x = 161.5 cm. While the polymer causes a significant decrease in the apparent wall shear stress at this location, there is virtually no change in wall shear at x = 30.5 cm.

A boundary layer momentum integral of the von Karman type was computed in order to give a qualitative check on the wall shear stress measurement. Static pressure measurements at several locations along the wall show that $\frac{\partial p}{\partial x} \approx 0$, a result which is expected from the circular geometry of the experiment. Using this simplification in the θ-momentum equation in cylindrical coordinates, and forming the conventional momentum integral across the boundary layer we obtain the approximate formula:

$$T_o/\rho = V^2 \frac{d}{dx} \int v/V(1 - v/V)dy \ ,$$

where v is the angular fluid velocity as defined above, and V is the wall angular velocity. Terms of the order δ/R have been neglected, where δ is the boundary layer thickness and R is the wall radius. The factor δ/R is less than 1/30 in the present experiment. Note that the integral above has the same form as the momentum thickness in a plane, two-dimensional boundary layer, except that in this case v is the angular velocity rather than the translational velocity.

To calculate the wall shear stress using this equation, velocity profiles for at least two values of x must be known.

Then the momentum integral can be calculated at the two locations and the x derivative can be evaluated approximately by taking the difference of the two momentum integrals and dividing it by Δx. The wall shear stress computed in this way is expected to lie between the two measured Preston tube values at the two locations.

The calculation was carried out by digital computer, using the trapezoid method to evaluate the momentum integrals from the measured velocity profiles. Results for water and for 20 ppm polyox are shown in the table below. The momentum integral and Preston tube results are in reasonable agreement for pure water and for the higher speeds of the 20 ppm polyox solution.

Table I.

	U_w	T_o: Preston tube x=30.5 cm	Preston tube x=161.5 cm	Momentum Integral
water:	103 cm/sec	20 dynes/cm^2	18	20
	150	43	36	41
	190	59	51	60
	220	71	62	73
20 ppm:	103	30	17	14
	150	42	35	44
	190	59	47	52
	220	69	57	60

The boundary layer displacement thickness was also calculated from the measured velocity profiles in the same way as the momentum thickness. The results show that the displacement thickness δ^* is nearly independent of wall speed, having a value of .25 cm at x = 30.5 cm and .58 cm

at x = 161.5 cm. This is not surprising in view of the expected result that $\delta^* \sim U^{-1/5}$ for turbulent boundary layers. Comparing these values with those of the momentum thickness at the same locations, we obtain the boundary layer shape factor, H = (displacement thickness)/(momentum thickness). H has a value of 1.47 at x = 30.5 cm, and a value of 1.35 at x = 161.5 cm. These results are slightly higher than those obtained by Willmarth (Ref. 17), but they are in good agreement with Bull (Ref.19), who measured H = 1.36.

When plotted as a function of x, the displacement thickness exhibits a power law dependence of $\delta^* \sim x^{.52}$. Although this does not agree with the usual $x^{4/5}$ growth law for turbulent boundary layers, the reason may be simply that the "effective" leading edge is displaced considerably ahead of the actual leading edge. This is due to the fact that not quite all of the boundary layer goes out through the radial gap; some of it is left over and becomes a part of the boundary layer of the next revolution of the wall. It is also possible that the inertially stabilizing influence of the wall curvature causes the boundary layer to grow more slowly than on a flat plate.

D. Free Stream Turbulence.

Measurements of the turbulence level of the free stream flow in the scroll interior was made with two Thermo-Systems cylindrical hot-film anemometers. One of these was located

30.5 cm behind the leading edge and 10.2 cm inward from the wall. This sensor rotated with the scroll wall, and the electrical connections were brought out through a set of slip rings. The sensor was 21 cm from the axis of rotation, so that the mean velocity at the point of measurement is given by $U = 21\ \omega$.

The second hot-film sensor was mounted on the stationary central shaft at a point 5 cm above the lower homeycomb and 10 cm outward from the axis. This probe was not rotating, so that the mean velocity at the probe is determined by the relatively slow axial flow through the lower honeycomb. Both probes were calibrated by using the known values of the mean velocity. An overheat ratio of $(R - R_c)/R_c = .10$, where R is probe resistance and R_c is cold probe resistance, was used in all measurements. Table II shows the measured values of $\sqrt{\overline{u'^2}}$, and of the turbulence level $\sqrt{\overline{u'^2}}/U_w$, as functions of the wall velocity U_w.

In view of the uncertainty in the mean velocity at the non-rotating end probe, the agreement of the results is reasonable. Thus the upper bound of the turbulence level in the free stream flow of the scroll interior is about 1%.

Table II.

Free Stream Turbulence

U_w	$\overline{u'^2}$	$\overline{u'^2}/U_x$
Probe #1:	rotating with wall	
63	0.3	.0048
112	0.8	.0072
141	1.3	.0096
171	1.9	.0112
201	2.2	.0112
231	2.4	.0104
Probe #2:	non-rotating	
112	0.4	.0035
171	1.0	.0059
201	1.2	.0060
231	1.5	.0063

IV. WALL PRESSURE FLUCTUATIONS

The fluctuating component of the pressure on the scroll wall was measured at two locations with piezoelectric transducers. The sensitive surface of these transducers is circular and .32 cm (1/8") in diameter. They are mounted flush with the wall, and their surfaces have been smoothed by paint and fine sandpaper. Water-tight coaxial cables are connected to the transducers on the outside of the scroll. These cables lead to low noise pre-amplifiers mounted on the top of the tank. The pre-amps (Ithaco model #143M39) have an input impedance greater than 1,000 megohms, and an output impedance of 50 ohms. They have 40 db gain and a broad band noise level of less than .5 microvolt referred to the input.

The amplified wall pressure signal then passes through a set of slip rings which are mounted on the stationary vertical shaft at the top of the tank. The brushes of these slip rings are mounted on the rotating tank lid. The slip rings themselves are gold-plated; the brushes are silver-graphite. There are four brushes for each ring, and every second ring is connected to ground. The low noise pre-amps on the top of the tank receive their power through one of the rings.

The wall pressure signal is amplified an additional 40 db after passing through the slip rings, making a total gain of 80 db. The advantage of placing the slip rings between two successive stages of amplification is that the

signal current through the rings is kept small while the load on the transducer is kept to a maximum. The 50 ohms impedance signal from the output of the first pre-amp is loaded only by the 1,000 megohms input impedance of the second pre-amp. Therefore the signal voltage into the second pre-amp is quite insensitive to small fluctuations in the series resistance between the two. The noise generated by slip rings is primarily in the form of a small fluctuating series resistance, typically about 5 milliohms rms. This type of slip ring noise will have no measurable effect upon the signal.

The amplified signal is recorded on an Ampex model SP-300 magnetic tape recorder, whose frequency response is from 40 to 25,000 Hz. The magnetic tapes are played back through a General Radio Audio Spectrometer, which filters the wall pressure signal into frequency bands 1/3 octave in width. The output of the spectrometer is then rectified and the rms band levels are recorded on a strip-chart recorder. The level for each 1/3 octave band is averaged over a five second period. These band levels are converted to power spectral density in db referred to 1 dyne/cm^2 by applying the proper correction factors for bandwidth, amplifier gain, and transducer sensitivity.

The background noise level of the slip rings and pre-amps was determined by running the tank at various speeds with the output of the wall pressure transducers short

circuited. These data were recorded and analyzed in the same way as the wall pressure signal. The results of this test show that the electrical background noise level is about 35 db below the measured wall pressure spectral density at all frequencies below 1 kHz, and at least 10 db below it at the highest frequencies analyzed.

The two transducers were located at distances from the leading edge of x = 51.5 cm and 154.5 cm. Both were on the vertical center of length of the scroll. Measurements were made at two wall speeds: U_w = 171 cm/sec and 238 cm/sec. The lower of these was the lowest speed at which a reasonable signal to noise ratio could be obtained. The Reynolds number based upon distance from the leading edge at the point of measurement varies from 8.8×10^5 to 3.7×10^6.

The wall pressure spectrum for pure water is shown in figure 13 for both speeds at x = 51.5 cm. The same data for x = 154.5 cm are shown in figure 14. The apparent leveling out of the spectrum above 3 kHz for the low speed data is undoubtedly caused by poor signal to noise ratio at high frequencies. However, these data are retained for comparison with spectra for the polymer solutions. The average slope of the power spectrum for U_w = 238 cm/sec, x = 51.5 cm is about 6.3 db/octave, which means that the spectrum level behaves approximately as $1/f^2$. This slope is nearly constant across the entire measured spectrum.

In figure 13, the average difference between the

spectra for the two speeds in the frequency band from 80 to 250 Hz is 5 db. This implies that the wall pressure spectrum varies as $U_w^{3.5}$ in this frequency range. In the band from 1 to 3.5 kHz, the average difference between the two spectra is 7.9 db. The spectrum level dependence in this frequency range is $U_w^{5.5}$. The spectra of figure 14, for x = 154.5 cm, shows nearly the same speed dependence, with spectrum level being proportional to $U_w^{3.5}$ and $U_w^{4.9}$ in the same two frequency bands. Thus the high frequency end of the spectrum exhibits a stronger dependence upon speed than does the low frequency end.

The wall pressure power spectra can be normalized by multiplying the spectral density by $U_w/(q^2\delta^*)$, where $q = \rho U_w^2$ and δ^* is the displacement thickness. The frequencies are transformed to the usual Strouhal numbers by multiplying them by δ^*/U_w. The wall pressure spectra of figures 13 and 14 are shown in normalized form in figures 15 and 16. It is evident that the high frequency part of the spectrum normalizes in the expected manner -- data of both speeds fall nearly on the same curve. At the low frequencies, however, the normalized low speed data are about 2 db higher than the high speed data. The same tendency can be observed in data from previous experiments, as in the pipe flow results of Corcos (Ref. 20), and those of Clinch (Ref. 21).

Comparing the data of figure 15, x = 51.5 cm, with those of figure 16, x = 154.5 cm, we see that the normalized

power spectrum is uniformly higher at the greater distance from the leading edge. This is chiefly due to the shifting of frequencies to the right, caused by the increase in δ^* with increasing x. Thus while the normalized spectra are nearly independent of wall speed, they are not independent of distance from the leading edge.

It is a well known fact that high frequency components of the wall pressure fluctuations are attenuated by the finite size of the pressure transducer, due to the partial cancellation of signals from disturbances which are smaller than the transducer itself. However, the calculation of the degree of attenuation as a function of frequency is a difficult matter. The attenuation can be expressed as a function of the space-time correlation function of the wall pressure:

$$R_{pp} = \frac{\overline{p(\underline{x}', t')\, p(\underline{x}' + \underline{\xi}, t' + \tau)}}{\overline{p^2}} ,$$

or, equivalently, as a function of the wave number-frequency spectrum, which is the Fourier transform with respect to space and time of the correlation. In other words, we must assume the properties of the spectrum we wish to measure before we can measure it. This is done by constructing a mathematical model of the correlation function, as Corcos did in 1962 (Ref. 20).

More recently Chandiramani (Ref. 30) reported results of several correlation models which were based on different

assumptions from those of Corcos. While the size effect correction factor of Corcos behaves as $1/f^2$ at high frequencies, that of Chandiramani reaches a nearly constant value. Thus the results of this type of analysis are extremely sensitive to the assumptions made in the mathematical model. Figure 17 shows wall pressure data of the present experiment corrected for transducer size effect by both the Corcos and the Chandiramani results. The Chandiramani correction gives much more reasonable results in this case.

Figure 18 shows a comparison of the wall pressure spectrum for x = 154.5 cm, U_w = 238 cm/sec with the results of Willmarth (Ref. 17), Bull (Ref. 19), and Bradshaw (Ref. 22). The data of the present study are in agreement with the other data at the high and the low frequency ends of the spectrum, but lie somewhat below the other data at the intermediate frequencies. This is reflected in the fact noted above that the spectrum in this cas has an almost uniform slope throughout the measured frequency range, rather than the downward curvature exhibited by the spectra of most other experiments. This difference in the spectral shape could be an effect of the curvature of the scroll wall. This curvature has a stabilizing influence upon the flow, since the mean angular momentum increases with increasing distance from the center of curvature (Goertler stability criterion). The difference in the shape of the spectrum could also be a result of the free stream turbulence, which has been shown

to have a level as high as 1%.

The order-of-magnitude agreement between the present wall pressure spectra and those of other experiments is further evidence that the flow over the scroll wall resembles a turbulent boundary layer on a flat plate. The real importance of these measurements, however, lies in the comparison of wall pressure spectra in pure water with those in dilute polymer solutions. Figure 19 shows the normalized pressure spectrum for pure water and for 20 and 100 ppm polyox solutions, for x = 51.5 cm and U_w = 238 cm/sec. Note that while the spectra are practically the same for Strouhal numbers less than 0.7, above this value the two polymer spectra fall considerably below the pure water spectrum. The 100 ppm polyox solution yields reductions of from 6 to 12 db in the Strouhal number range from 1.0 to 7.0, and the average reduction in this range is 9 db. The 20 ppm solution exhibits somewhat smaller reductions, having an average reduction of 6.5 db in the same frequency range.

Figure 20 shows wall pressure spectra for the same position and wall speed for solutions of 200 ppm polyox and 300 ppm guar gum. In this case there is apparently a slight reduction at low frequencies, from 1 to 3 db, in addition to the larger reductions at the high frequencies. The 200 ppm polyox solution yields an average reduction of 7.6 db in the 1 to 7 Strouhal number range, and 2.5 db in the .06 to .8 Strouhal number range. The guar gum solution gives slightly

lower reductions at all frequencies. Thus the higher concentrations show measurable reductions at low frequencies, but they are not as effective at high frequencies as the 100 ppm polyox solution.

Figures 21 and 22 show wall pressure spectra for water and the four polymer solutions discussed above for the same wall speed (U_w = 238 cm/sec) at x = 154.5 cm. In these figures the large reductions in spectrum level begin at higher values of the Strouhal number than for x = 51.5 cm. However, the actual frequencies at which the reductions begin are the same. In the Strouhal number range from 2.0 to 10.0, the average reduction for the 20 ppm solution is 8 db, while for 100 ppm it is 10 db, and for 200 ppm it is 9 db. Again there is no reduction at low frequencies for 20 and 100 ppm, while for 200 ppm there may be a slight reduction, although it is obscured by the unexplained peak at Strouhal number .17, For both wall positions the effect of increasing concentration is to lower slightly the lowest frequency at which the large reductions occur.

We turn now to the data for the lower wall speed, U_w = 171 cm/sec. Figures 23 and 24 show wall pressure spectra at this speed at x = 51.5 cm for water and the four polymer solutions. The reductions in spectrum level at the high frequencies are now considerably less than they were for the higher speed. In the range of Strouhal numbers from 1.0 to 5.0, the average reduction is 5 db for 20 ppm, 3.5 db

for 100 ppm, and 5.5 db for 200 ppm. These are much less than the 9 db average reductions obtained in this frequency range for the higher speed. However, the reductions at low frequencies are at least as great at the low speed as they were for the high speed. In the Strouhal number range from .1 to .5, we obtain average reductions of about 2.5 db for both 200 ppm polyox and 300 ppm guar gum.

Data for U_w = 171 cm/sec, x = 154.5 cm are shown in figures 25 and 26. Again the 200 ppm polyox and 300 ppm guar gum solutions yield average reductions of about 2.5 db in the low frequency range. The high frequency behavior in this case is about the same as at x = 51.5 cm.

The slight reductions in spectrum level at low frequencies for the higher solution concentrations may be an effect of increased viscosity. The empirical equation for the relative viscosity of a dilute polymer solution is

$$\nu/\nu_o = 1 + Nc + kN^2c^2 ,$$

where c is polymer concentration, N is the intrinsic viscosity (approximately 20 for WSR-301 polyox), and k is an empirical constant with a value of about .4. This formula predicts a relative viscosity of 1.22 for the 100 ppm solution, and 1.46 for the 200 ppm solution.

If we assume that the normalization of the wall pressure spectrum used above is valid, the only parameter affected by viscosity is δ^*. If we further assume that δ^* is

proportional to $\nu^{1/5}$, then we predict that δ^* is increased by the factor 1.08 for the 200 ppm polyox solution. This will shift the normalized spectrum to the right on the frequency scale by the same factor, while lowering the spectrum levels by .5 db. This correction reduces the low frequency reductions at this concentration by only about 1 db. Thus we cannot conclude that the low frequency spectrum level reductions at high concentrations are due entirely to increased viscosity.

We have seen that the reductions in wall pressure spectrum at high frequencies are greater at the high speed than at the low speed. This implies that the polymer solution spectra have a different speed dependence from that of the pure water spectra. Figure 27 shows the unnormalized wall pressure spectra for 100 ppm polyox at x = 154.5 cm for both speeds. Comparing this with figure 14 we see that the speed dependence at low frequencies is nearly the same for the polymer solution as for pure water, with spectrum level being proportional to $U_w^{3.5}$. However, at the high frequencies the speed dependence is quite different. Whereas the pure water spectrum varies as U_w^5 in the frequency range from 1 kHz to 3.15 kHz, the polymer solution spectrum varies as U_w^2 in this range. While the high frequencies are more sensitive to speed changes than the low frequencies in pure water, they are actually less sensitive in the polymer solutions. The normalization which nearly eliminated the speed

dependence of the spectrum in pure water obviously does not work for the polymer spectra.

It should be mentioned that effects of polymer shear degradation or aging were not observed in the polymer wall pressure spectra. Spectra which were measured after the experiment had been running for 30 minutes and those measured after the solution had been left in the experiment for 24 hours were essentially the same as the spectra measured when the experiment was initially started up.

In summary, the pure water wall pressure data of the present experiment are in reasonable agreement with data from other experiments. The chief difference is that the spectra of the present experiment have a more constant slope than usual, with spectral density varying nearly as $1/f^2$ throughout the measured spectrum. The polymer additives cause large reductions in the pressure spectrum at high frequencies and high speed, with up to 9 db average reduction in the high frequency band. The high frequency reductions at the lower speed are less, averaging about 5 db. There is evidently a slight low frequency reduction for the more concentrated solutions, particularly at the lower speed. The most obvious effect of polymer concentration is that increasing concentration lowers the lowest frequency at which the large spectrum level reductions occur.

V. RADIATED NOISE MEASUREMENTS

A. Measurements with an Omnidirectional Transducer.

Measurements of the noise radiated from the boundary layer of the scroll wall are made with a piezoelectric transducer located 20 cm inward from the wall, on the vertical center of length. This transducer is attached to the stationary plexiglass shaft which runs along the central axis of the scroll. Since it is far outside of the boundary layer, the only fluid flow over the surface of the transducer is the slow outward movement of fluid toward the wall. This radial flow has a maximum velocity of 5 cm/sec and is not sufficient to set up a measurable fluctuating pressure field on the surface of the transducer. The transducer is designed to be omnidirectional in its receiving characteristics; that is, it is equally sensitive to sound coming from any direction. It therefore measures the radiated sound from the entire scroll boundary layer, from the leading to the trailing edge.

The signal from the transducer follows a coaxial cable down the inside of the stationary vertical shaft. At the bottom of the shaft the signal is amplified 20 db by a low noise, high impedance pre-amplifier. The signal is then amplified an additional 40 db and recorded on the Ampex SP-300 tape recorder along with the wall pressure data. The radiated noise tapes are analyzed in the same way as the

the wall pressure, using an audio spectrometer and level recorder to obtain the 1/3 octave band levels of the signal. These band levels are again converted to acoustic power spectral density in db referred to 1 dyne/cm^2 by applying the appropriate corrections for gain, bandwidth, and transducer sensitivity.

Because of the extremely low intensity of the radiated noise from the boundary layer, several precautions had to be taken to insure that other noise sources were not contributing significantly to the measured spectrum. As mentioned above, the drive motor of the experiment was surrounded by a glass-lined box and fully isolated from the floor and the tank by shock mounts and flexible drive couplings. In addition, air bubbles under the plexiglass top of the tank were carefully eliminated before each run. If this was not done, these surface bubbles made a noticeable contribution to the measured noise spectrum.

In spite of all precautions, one unforeseen difficulty was encountered. It was found in the first radiated noise measurements that the stator vanes on the outsides of the two honeycomb assemblies were vibrating when the tank was running at maximum speed, thus radiating a considerable noise field of their own. This problem was solved by cutting slots in the trailing edges of the stator vanes in the direction parallel to the flow. These slots ran half the chord length of the vanes and they were filled with silicone rubber. This

process had the effect of decoupling and damping the various parts of the trailing edge of each vane, and was quite effective in eliminating the vibration. Other minor difficulties were also encountered, including vibrating electrical cables and squeaky seals, but these were easily remedied.

To determine the background noise level due to mechanical sources, spectra were measured with the scroll out of the tank. The transducer and the honeycomb assemblies were in their usual places, but there was no scroll and thus no turbulent boundary layer. The noise measured in this configuration is that caused by the drive motor, bearings, and any surface bubbles which were not removed. It was found that this noise level is at least 20 db below the measured radiated noise spectrum at all frequencies below 4 kHz. At higher frequencies the signal to noise ratio becomes progressively poorer, but data up to 16 kHz have been retained for comparisons between water and polymer spectra.

The measured background noise spectrum has one fairly sharp peak at 400 Hz. This peak appears in all of the radiated noise spectra, and it is quite repeatable in both amplitude and frequency. The peak is also noticeable in some of the wall pressure spectra, but is less pronounced there because the wall pressure field is of higher intensity than the radiated noise. It is obviously of mechanical origin, but it could not be eliminated.

Due to the high speed dependence of the radiated noise intensity (U^6 or U^8) the signal to noise ratio was adequate

only at the highest attainable speed of the experiment, U_w = 238 cm/sec. Figures 28 through 32 show the radiated noise spectrum of water compared with the spectra of 20, 50, 100, and 200 ppm polyox solutions, and a 300 ppm guar gum solution. We see that like the wall pressure spectrum, the slope of the radiated noise spectrum for pure water is nearly constant throughout the measured frequency range. However, the average slope of the radiated noise spectrum for pure water is 8.5 db/octave, while that of the wall pressure spectrum is only 6 db/octave. This implies that the radiated noise spectrum level behaves as $1/f^{2.8}$, while the wall pressure spectrum behaves as $1/f^2$.

It is seen in these figures that the polymer additives have a very significant effect upon the high frequency end of the radiated noise spectrum, as it did in the case of the wall pressure. It appears to have little or no effect upon the low frequency end. In the frequency band from 1 to 10 kHz, we obtain an average reduction of 4.5 db for 20 ppm polyox, 6.5 db for 50 ppm, and 8 db for 100 ppm. When the concentration is increased to 200 ppm polyox, however, the average reduction in the same frequency band is only 3.5 db, and the spectrum level for the polymer solution is actually higher than that for pure water in the band from 2 to 2.5 kHz. The cause of this 2 kHz peak in the 200 ppm polyox spectrum is unknown. It may be due to increased viscosity, or molecular agglomerations of the polymer. In any case,

this result is quite repeatable. We see the same effect in the spectrum for the 300 ppm guar gum solution (Fig. 32), but here it is even more pronounced. The 2 kHz peak in the polymer spectrum is now 6 db above the pure water spectrum at the same frequency, and another peak in the polymer spectrum has appeared at 8 kHz, thus eliminating most of the noise reduction at the high end of the spectrum. These runs were not made in order of increasing concentration, so this phenomenon could not represent a progressive deterioration of the experimental apparatus. Note that for both the 200 ppm polyox and the 300 ppm guar gum the low frequency half of the spectrum is quite close to that of pure water.

Comparing the spectrum for 50 ppm polyox (Fig. 29) with that of 100 ppm (Fig. 30), we see that the significant reductions in spectrum level begin at a slightly lower frequency for the higher concentration, as they did in the case of the wall pressure spectra. The 100 ppm solution yields large noise reductions starting at about 800 Hz, while the 50 ppm solution produces its first significant reduction at 1,250 Hz. In addition, the 100 and 200 ppm polyox solutions give measurable reductions (2 or 3 db) in the frequency band from 200 to 315 Hz, while the 20 and 50 ppm solutions show no reduction at all in this band. We may conclude from these results that higher concentrations will affect lower frequencies of both the wall pressure and the radiated noise spectrum.

The mean square sound pressure, $\overline{p^2}$, can be expressed in terms of the power spectral density, E(f), by the equation

$$\overline{p^2} = 2\pi \int_0^\infty E(f')\, df' \ .$$

From the shape of the present radiated noise spectra we can see that components at frequencies greater than 500 Hz make a very small contribution to this integral, even if we neglect the unknown part of the spectrum below 40 Hz. Thus the reductions in the high frequency part of the spectrum by the polymer additives will have almost no effect upon the value of $\overline{p^2}$.

As was done in the wall pressure measurements, radiated noise spectra were measured for a polymer solution which had been run in the experiment for 30 minutes continuously, and for one which had been in the tank for 24 hours. No effects of aging or shear degradation were observed.

B. Near Field Radiated Noise Spectrum as a Function of Distance from the Leading Edge.

Measurements of the radiated noise spectrum as a function of position on the scroll wall are made with a 1 cm diameter cylindrical transducer. This transducer is mounted on the stationary central shaft as was the larger omnidirectional transducer, but it is located much closer to the boundary layer. Whereas the omnidirectional transducer was

positioned 20 cm from the scroll wall for all measurements, the smaller transducer is located as close as 2.5 cm from the wall at the leading edge. As the scroll wall moves past the transducer, this distance increases to 7 cm at the trailing edge. In terms of the measured boundary layer displacement thickness, the transducer is 10 thicknesses from the wall at the leading edge, and 12 thicknesses from it at the trailing edge. Measurements are also made with the small transducer located at 7.6 cm and 12.7 cm from the wall at the leading edge.

These measurements are all taken in the acoustic near field, since the transducer is less than one wavelength from the wall at all frequencies of interest. However, the transducer is still located well outside of the boundary layer in a region of relatively slow moving fluid, so that the measured pressure field is that which is radiated from the boundary layer and wall, rather than one generated by a turbulent flow over the face of the transducer. The transducer Reynolds number, based upon the 5 cm/sec outward radial velocity of the flow in the scroll interior, is 500.

The signal from the transducer is amplified 60 db by low noise, high impedance amplifiers. After the first stage amplification, the signal goes through a high pass filter, which has a 6 db down point at 80 Hz and a slope of 6 db/octave. This filter has no effect upon frequencies above 200 Hz. It is required because of the relative high intensity of the

very low frequency end of the spectrum measured close to the wall. This high intensity is due chiefly to the fact that as the leading edge of the scroll passes the transducer a large pressure jump occurs, having high spectral content at frequencies below 40 Hz. The high pass filter keeps this pressure jump within the dynamic range of the instrumentation.

The amplified and filtered signal is recorded on a CEC Datatape recorder, which runs at a tape speed of 120 inches/second in the FM mode. FM recording is necessary to obtain information about the very low frequency end of the spectrum. The recorder frequency response is from 0 to 15,000 Hz.

In addition to the radiated noise signal, there is recorded on another channel of the tape a series of pulses, each 1 millisecond in length. Each pulse indicates a passage of the leading edge of the scroll wall across the face of the transducer. The pulses are generated by a small electric coil mounted on the external framework of the experiment about 2 cm from the outside wall of the rotating tank. A magnet attached to the outside of the tank induces a current in this coil each time it goes by. This current signal is then amplified and recorded. These fiducial pulses permit us to establish the position of the leading edge on the radiated noise record. Using the known velocity of the scroll wall we can relate any position on the wall to a fixed time delay from the leading edge fiducial pulse.

When the tank rotates at 70 rpm, the fiducial pulses

occur at intervals of about 0.86 second. During this time period the entire 205 cm of the scroll wall moves past the transducer. We wish to divide the length of the wall into about ten regions and estimate the radiated power spectrum from each region. This requires the measurement of a complete power spectrum in a real time period of .086 second. Even though we may slow down the tape recorder considerably on playback, this requirement makes digital analysis almost mandatory. Using a digital computer, the power spectrum of each of the .086 second sections can be calculated by the fast-Fourier transform method, and these spectra can then be ensemble averaged over many revolutions of the tank.

The first step in the digital analysis is the conversion of the analog radiated noise tapes to digital tapes which can be fed into the computer. The analog signal voltage is sampled and converted to twelve binary bit digital numbers by a Raytheon "Multiverter". The resulting digital data are then recorded on a Kennedy model 3110 synchronous digital tape recorder. The Multiverter and digital recorder are controlled and coordinated by a coupler designed at CIT. The Kennedy recorder is a nine-track, IBM compatible unit which writes data at a rate of 30,000 bytes of tape per second. This writing speed cannot be varied. The CIT coupler allows the data to be formatted in one of two ways. In the first mode, all twelve binary bits from the Multiverter are written on two successive bytes of tape, and the Multiverter

is commanded to make 15,000 conversions per second. In the second mode, eight of the Multiverter bits are written on one byte of tape, the other four are discarded, and the Multiverter then makes 30,000 conversions per second. In the present experiment the system was used in the second mode, sacrificing some resolution for the higher digitizing rate. The resolution in this mode is one part in 256, which is adequate considering that the analog recordings are limited to a 40 db dynamic range.

The analog tapes are played back into the digitizer at one half speed, which makes the digitizing rate in real time equal to 60 kHz. The period between samples is thus 1.67×10^{-5} second. The data are sampled in blocks, or records, of 4096 words. Each word is one digital conversion and one byte of tape. Each record requires 136.4 milliseconds to be written. Due to the two to one slowdown of the analog tape, a record will occupy 68.2 milliseconds in real time, which then becomes the time length of the sections into which we divide the length of the wall. It is assumed that the radiated power spectrum remains essentially constant during each record. During one record the scroll wall moves 16 cm. Consecutive data records are separated by an inter-record gap of 21.2 milliseconds. Thus the wall moves 18.5 cm from the beginning of one record to the beginning of the next, and it takes about eleven records to cover the length of the scroll wall.

The digital records are related to positions on the wall in the following way. The fiducial pulse recorded on the analog tape at each passage of the leading edge is used to start the digitizer. The digitizer then converts and writes eighteen records, after which it stops. Sometime during the twelfth record a second fiducial pulse occurs, but it has no effect while the digitizer is still running. Thus one complete tank revolution and part of the next are covered by the cycle of eighteen records. The next fiducial pulse arriving after the digitizer has stopped will start it up again, and the process is repeated. Fifty of these record cycles are written for each data run, encompassing 100 revolutions of the tank. Since each cycle starts precisely when the leading edge passes the transducer, the position assigned to each of the eighteen records will be the same for all cycles. This position will be the average of the positions at the beginning and the end of the record. The assumption that the power spectrum is nearly constant during the length of a record may not be valid near the leading edge of the scroll.

Once written on the digital tape in this manner, the data are analyzed by a Univac 1108 computer. The computer Fourier analyzes every data record using the fast-Fourier transform algorithm. It then ensemble averages coefficients corresponding to the same position on the wall. The results are plotted as eighteen different power spectra for the

eighteen different wall positions. The ensemble averaging process gives stability to the results, particularly at the two ends of the spectrum. This can be seen in figures 33 and 34. The first of these figures is a typical power spectrum for pure water with the ensemble average taken over fifty records. The second figure shows the same spectrum with no ensemble averaging -- only one record is analyzed. It is clear that with one data record little information can be obtained about the power spectrum.

Figure 35 shows the power spectrum of a 400 Hz sine wave, digitized and processed in the same way as the radiated noise data. The broadening of the fundamental peak is a result of the rectangular data window used by the computer in the Fourier analysis. This type of window sets the time function to be fast-Fourier analyzed abruptly equal to zero at the two ends of the time domain. There are other window functions better suited to the analysis of a periodic time function, but the rectangular window gives better results in the analysis of random noise and so was chosen in this case. The harmonic peaks shown in figure 35 are genuine; the sine wave is one that has been synthesized from straight line segments.

As a further check on the digital analysis technique, some of the wall pressure data were processed in this way and the results compared with the analog spectra obtained above. The wall pressure spectra produced by the digital analysis

are in excellent agreement with the analog spectra.

Radiated noise power spectra for pure water with the transducer located 2.5 cm from the wall are shown in figures 36 to 40. Comparisons are made between power spectra for different distances from the leading edge. The spectrum for x = 7.8 cm is higher than any of the others at practically all frequencies. This is the location closest to the leading edge of the scroll wall. The difference between the spectrum at this position and the others is greatest at the low frequencies, from 10 to 60 Hz. The low frequency end of the spectrum is sharply peaked here because of the large pressure jump created by the passage of the leading edge across the transducer face, as noted above. We shall see below that the effect of this pressure jump is felt most strongly near the wall, and it decays rapidly as the transducer is moved away from the wall.

The power spectrum of each position on the wall has its own characteristic shape or signature. If we compare spectra of two positions which are very close together, such as x = 7.8 cm and x = 9.3 cm, we should expect them to have similar signatures. (x = 7.8 cm is the twelfth record of the eighteen record cycle, while x = 9.3 cm is the first record.) Figure 36 shows that this is indeed the case. Although the spectrum closer to the leading edge is slightly higher, the signatures of the two spectra are almost identical. On the other hand, if we turn to figure 37 we see that the signa-

tures at x = 7.8 cm and x = 46 cm are quite different from one another.

Power spectra for two positions not near the leading edge are compared in figure 40. The two positions are x = 28 cm and x = 157 cm. The differences between these two spectra are not very great, although the spectrum for 28 cm is slightly higher at most frequencies. If the sources of noise are thought of as being located on the wall, then the difference between these two spectra might be explained by the simple fact that the wall is further from the transducer when x = 157 cm than it is when x = 28 cm. It will be shown below that the spectrum level varies with distance from the wall as y^{-1} for most frequencies. Using this range dependence we obtain a 3 db correction to the spectrum level due to the difference in y for these two spectra. Once this correction is applied there is very little difference between the two spectra except for the differences in their signatures. Thus it appears that the noise spectra away from the leading edge are all roughly similar, while at the leading edge the spectrum level is considerably higher.

In 1955 Phillips (Ref. 12) demonstrated that the radiated noise from a flat plate boundary layer has a dipole component which varies as U^6 and is probably more significant at low Mach numbers than the quadrupole radiation of Lighthill, which varies as U^8. Phillips also showed that if the turbulence is statistically homogeneous in planes parallel to the

plate, then the dipole strength per unit area of source vanishes. Thus there should be a finite dipole strength near the leading edge of the plate where the turbulence is developing and the motion is not homogeneous in planes parallel to the plate. This dipole strength will approach zero further back from the leading edge as the condition of homogeneity becomes approximately satisfied. Phillips thus predicts that the radiated noise source strength per unit area will be greatest near the leading edge of the plate, and will decrease steadily further aft. This prediction is supported by the results of the present experiment as described above.

Unfortunately there is a possible ambiguity in this result due to the peculiar geometry of the experiment. The leading edge of the scroll wall is located very near to the trailing edge, and one might contend that the increase in noise level during the passage of the leading edge is actually caused by the trailing edge, which is only 9 cm behind (see Fig. 1). However, the trailing edge is 4.5 cm further from the transducer than the leading edge. In addition the trailing edge is separated from the transducer by part of the scroll wall; that is, there is no direct acoustic path from the trailing edge to the transducer. The stainless steel wall of the scroll provides a good acoustic miss-match with water, having a density 7.9 times that of water and a velocity of sound 3.9 times that of water. If sound from

the trailing edge were propagating through the wall in spite of this, we would not be able to explain the fact that the spectrum at x = 7.8 cm is slightly higher than that at x = 9.3 cm, which is almost exactly opposite the trailing edge. Thus the sound from the trailing edge can reach the transducer only by diffraction around the leading edge. We shall show below that this is also unlikely.

By comparing power spectra for the same distance from the leading edge but with the transducer at different distances from the wall, we can estimate the radiated noise dependence upon distance from the source. Data were obtained with the transducer at y = 2.5, 7.6, and 12.7 cm from the wall at the leading edge. Figure 41 shows pure water spectra for x = 9.3 cm, y = 2.5 cm and y = 12.7 cm. Note that the extreme low frequencies and the 40 Hz peak are the same for the two values of y, while the remainder of the spectrum is about 6 db lower for the greater distance from the wall. Figure 42 shows the same comparison for a position away from the leading edge, x = 83 cm. In this case the low frequency end of the spectrum actually increases with increasing distance from the wall, while the rest of the spectrum shifts downward as before. Note that the downward shift of the high frequencies is not altogether uniform; the signature of the spectrum tends to become smoother with increasing distance from the wall.

Figure 43 shows the spectrum level at several frequen-

cies plotted as a function of distance from the wall for $x = 9.3$ cm. The levels used here are averages over 1/3 octave bands. These levels are seen to vary roughly as y^{-1} from the frequencies shown. If the area of the wall which is contributing significantly to the noise spectrum at the transducer varies as y^2, then the y^{-1} behavior of the spectrum implies that the radiated sound energy per unit source area varies as y^{-3}. This result assumes that the noise sources are uncorrelated over distances comparable to the size of the wall region which is contributing significantly to the transducer spectrum. This being the case, the mean square sound pressure will be directly proportional to the source area.

The radiated sound intensity per unit source area must vary as y^{-2} in the far field by conservation of energy. The higher power dependence shown in these measurements is clearly a near field effect, to be expected since the receiver is less than one wavelength from the wall. However, if the sound measured near the leading edge were actually sound produced at the trailing edge and diffracted around the leading edge, as suggested above, we would not expect the range y-dependence of the spectrum to be as strong near the leading edge as it is at other positions. While the distance from the leading edge to the transducer is being varied by a factor of five, the distance from the trailing edge varies by a factor of only 2.5, since it is 4.5 cm further away to

start with. Thus it is highly improbable that the sound measured near the leading edge is originating at the trailing edge.

The strong dependence of the radiated noise spectrum upon distance from the scroll wall is further evidence that the sound measured in this experiment is indeed radiated from the wall boundary layer, and does not come from other sources in the tank. The exception to this is the sharp 400 Hz peak, which is present in all spectra. The amplitude of this peak is independent of distance from the wall, which supports the conclusion that the peak is of mechanical origin and should not be regarded as a part of the boundary layer radiated noise spectrum.

We shall now compare the power spectra for pure water with those obtained for the dilute polymer solutions. Figures 44 to 49 show spectra of pure water compared with those of 50 ppm polyox for several values of x with the transducer at y = 2.5 cm. There are substantial noise reductions caused by the additive at frequencies greater than 400 Hz for all values of x except x = 194 cm. At this position only, the power spectrum of the polymer solution is actually higher than that of pure water. At the other locations the signature of the spectrum is unchanged by the polymer at the low frequencies, but is considerably altered at the high frequencies. The extreme low frequency end of the spectrum is unaffected by the polymer except at x = 7.8 cm. Here the

low frequency peak caused by the passage of the leading edge is substantially reduced by the additive.

An interesting feature of the polymer spectra is the small peak at 2 to 3 kHz which occurs at several locations (e.g., in Fig. 46). In some cases the polymer spectrum level exceeds the pure water spectrum level in this frequency range. A similar peak was seen to occur in the data of the omnidirectional transducer as reported above, but only for the higher polymer concentrations.

Figures 50 to 52 compare water spectra with those of 20 ppm polyox for three values of x with the transducer 2.5 cm from the wall. The high frequency reductions are considerably less than for the 50 ppm solution, but the 2 to 3 kHz peak in the polymer spectrum is now absent. Again we find that at x = 194 cm the polymer spectrum is actually above the pure water spectrum. The upward shift of the polymer spectrum at this position is less for 20 ppm than it was for 50 ppm. The cause of this behavior is unknown.

Water and polymer noise spectra were also measured with the transducer located 7.6 cm from the wall, and comparisons of the two are shown in figures 53 to 58 for several values of x. If we compare these figures with figures 44 to 49, for y = 2.5 cm, we see some interesting differences. The very low frequency peak caused by the passage of the leading edge is much less pronounced for y = 7.6 cm than it was closer to the wall, and the polymer appears to have no effect

upon it. In addition to the high frequency reductions caused by the additive there are now significant reductions in the intermediate frequency range from 100 to 1,000 Hz (see Fig. 56). The greatest high frequency noise reductions for y = 7.6 cm occur at x = 157 cm, where there is more than 10 db reduction at some frequencies. These reductions show a tendency to increase with increasing distance from the leading edge. There is very little reduction at x = 9.3 cm or at x = 194 cm, both of which are close to the leading edge.

The spectrum for 50 ppm polyox at y = 7.6 cm, x = 194 cm shows a striking difference from the polymer spectra measured closer to the wall. Whereas the polymer spectra were consistently higher than the pure water spectra for this value of x at y = 2.5 cm, the 50 ppm polyox spectrum is now slightly below the water spectrum. In fact, the reduction caused by the additive is about the same at x = 9.3 cm and at x = 194 cm. These two positions are equidistant from the leading edge.

The signatures of the noise spectra are nearly the same at the low frequencies for both distances from the wall, but they are noticeably different at the higher frequencies. The 2 to 3 kHz peak in the polymer spectra measured at 2.5 cm from the wall is not present in the spectra measured at 7.6 cm. Instead there is a very broad peak centered at about 1 kHz in both the water and the polymer spectra. This peak was also present in the omnidirectional transducer data shown above.

V. SUMMARY AND CONCLUSIONS

The purpose of this experiment was to find out what effect polymer additives have upon radiated noise and wall pressure fluctuations in a turbulent boundary layer. Although the wall pressure aspect of this problem has been treated previously, there have been few if any measurements of the noise radiated from the boundary layer on a flat plate. The experimental geometry described in this paper was designed specifically to facilitate radiated noise measurements.

The series of measurements described in section III of this paper are intended to document the boundary layer of the experiment and to show that it resembles a turbulent boundary layer on a flat plate in a uniform free stream. It was demonstrated by these measurements that the mean vorticity of the flow is confined to a thin region near the wall, and that the mean velocity profile in this region agrees quite well with the law of the wall. The ratio of the measured displacement thickness to the momentum thickness was found to be about 1.4, which is in agreement with previous experimental data for boundary layers in wind tunnels.

The wall pressure spectra measured in this experiment, normalized in the usual way, are in good agreement with data of other experiments near the two ends of the measured spectrum. In the middle of the spectrum the present data are somewhat lower in spectrum level than those of previous

experiments. The power spectral density varies roughly as $1/f^2$ throughout the measured frequency range, while most of the previous data show a higher power law dependence at high frequencies than at low frequencies. There are at least two possible causes for this difference in the shape of the spectrum. One is the curvature of the wall, which has an inertially stabilizing effect upon the boundary layer. The other is the measured free stream turbulence level of about 1%, which is somewhat higher than that of most other experiments. The speed dependence of the wall pressure spectra measured in pure water in this experiment agrees well with theory.

The radiated noise spectra exhibit a power law dependence on frequency throughout the measured spectrum, as do the wall pressure spectra. However, the dependence of radiated noise on frequency is a stronger one, with spectral density proportional to $1/f^{2.8}$.

Both the wall pressure and radiated noise spectra are significantly affected by the polymer additives. Large reductions in spectrum level occur at frequencies greater than 500 Hz or at Strouhal numbers greater than one. The reductions in the high frequency end of the wall pressure spectrum are speed dependent, being typically 9 db for U_w = 238 cm/sec and 5 db for U_w = 171 cm/sec. There appear to be small reductions in the wall pressure spectrum at low frequencies, particularly at the lower wall speed. The radiated noise spectrum is reduced about 8 db at high frequencies

by the additives. With one exception, there were no measurable reductions at the low frequency end of the radiated noise spectrum. With the transducer positioned close to the wall, the low frequency peak caused by the passage of the leading edge is substantially reduced by the additives. At the highest polymer concentrations, new peaks appear in the high frequency end of both the wall pressure and radiated noise spectra. These peaks in the polymer spectra frequently exceed the pure water spectrum level.

Measurements of the radiated noise spectrum as a function of position on the wall show that the noise source strength is greatest near the leading edge, in agreement with the theoretical prediction of Phillips. Near the wall, the power spectrum falls off with increasing distance from the wall as y^{-1}, which implies that the radiated power per unit source area behaves as y^{-3}. Measurements made with the transducer located 7.6 cm from the wall show that the noise reductions caused by the polymer are greatest at positions away from the leading edge.

The fact that the polymer additives affect the radiated noise and wall pressure spectra primarily at the higher frequencies suggests that they influence the turbulent flow chiefly in a region close to the wall. If the mechanism responsible for the viscous drag reduction is related to that of the noise reduction, then these data lend support to drag reduction theories involving polymer effects upon

the viscous sublayer flow.

Although several of the proposed drag reduction mechanisms refer to the viscous sublayer, there is one which is more attractive on the basis of the present results. It has been stated by Lumley (Ref. 8) that the viscosity of a dilute polymer solution measured in an axisymmetric, irrotational stretching flow could be as much as 10^4 times greater than that of pure water, even though the ordinary shear viscosity is about the same as that of water. The work of Kline (Ref. 31) showed that there are periodic disturbances in the viscous sublayer which play an important role in generating the boundary layer turbulence near the wall. These "Kline eddies" have the appearance of small jets of fluid ejecting from the sublayer into the more turbulent region of the boundary layer. Partial suppression of the Kline eddies by the high viscosity of the polymer solution in axisymmetric strain could then have an effect upon the momentum transport of the boundary layer and thus upon the wall shear. The resulting stabilization of the sublayer could also lead to a reduction in the high frequency components of the radiated noise and wall pressure field. This mechanism for drag reduction has also been proposed by Walsh (Ref. 7).

REFERENCES

1. Wells, C. S. (ed.), "Viscous Drag Reduction," Plenum Press, New York, 1969.

2. Paterson, R. W., "Turbulent Flow Drag Reduction and Degradation with Dilute Polymer Solutions," Ph.D. thesis, Div. of Eng. and Appl. Sci., Harvard U., 1969.

3. Jackley, D. N., "Drag Reducing Fluids in a Free Turbulent Jet," NAVWEPS Report 9053, 1967.

4. White, D.A., "Velocity Measurements in Axisymmetric Jets of Dilute Polymer Solutions," J. of Fluid Mech., 28, 1967.

5. Fabula, A. G., "An Experimental Study of Grid Turbulence in Dilute High-Polymer Solutions," Ph.D, thesis, Dept. of Aero. Eng., Pennsylvania State U., 1966.

6. Deavours, C. A., "A Critical Survey of Literature Concerning the Toms' Effect," Div. of Appl. Math., Brown U., 1966.

7. Walsh, M., "On the Turbulent Flow of Dilute Polymer Solutions," Ph.D. thesis, Dept. of Aero. Eng., California Institute of Technology, 1967.

8. Lumley, J. L., "Drag Reduction by Additives," Dept. of Aero. Eng., Pennsylvania State U., 1968.

9. Lighthill, M. J., "On Sound Generated Aerodynamically, I," Proc. Roy. Soc. A, 211, 1952.

10. Curle, N., "The Influence of Solid Boundaries upon Aerodynamic Sound," Proc. Roy. Soc., A, 231, 1955.

11. Lighthill, M. J., "On Sound Generated Aerodynamically, II," Proc. Roy. Soc., A, 222, 1954.

12. Phillips, O. M., "On the Aerodynamic Surface Sound from a Plane Turbulent Boundary Layer," Proc. Roy. Soc., A, 234, 1956.

13. Liepmann, H. W., "On the Acoustic Radiation from Boundary Layers and Jets," unpublished, 1954.

14. Laufer, Ffowcs-Williams and Childress, "Mechanism of Noise Generation in the Turbulent Boundary Layer," NATO AGARDograph No. 90, 1964.

REFERENCES (cont.)

15. Haddle, G., and Skudrzyk, E., "The Physics of Flow Noise," J. Acous. Soc. Am., 46, 1969.

16. Killen, J. M., and Crist, S. D., "The Effect of Dilute Solutions of Drag Reducing Polymers on Radiated Flow Noise," St. Anthony Falls Hydro. Lab. Report No. 90, U. of Minnesota, 1967.

17. Willmarth, W., and Wooldridge, C., "Measurements of the Fluctuating Pressure at the Wall beneath a Thick Turbulent Boundary Layer," U. of Michigan Report No. 02920-1-T, 1962.

18. Bakewell, H. P.,"Turbulent Wall Pressure Fluctuations on a Body of Revolution," J. Acous. Soc. Am., 43, 1968.

19. Bull, M., "Properties of the Fluctuating Wall Pressure Field of a Turbulent Boundary Layer," NATO AGARD Report No. 455, 1963.

20. Corcos, G. M., "Pressure Fluctuations in Shear Flows," U. of California Inst. of Eng., Report No. 183.2, 1962.

21. Clinch, J. M., "Measurements of the Wall Pressure Field at the Surface of a Smooth-Walled Pipe Containing Turbulent Water Flow," J. Sound and Vib., 9, 1969.

22. Bradshaw, P., "The Turbulence Structure of Equilibrium Boundary Layers," NPL Aero. Report No. 1184, 1966.

23. Nisewanger, C. R., and Sperling, F. B., "Flow Noise Inside Boundary Layers of Buoyancy-Propelled Test Vehicles," USNOTS, China Lake, Calif., NOTSTp No. 3511.

24. Hoyt, J., and Fabula, A., "Effects of Additives on Fluid Friction," Proc. of the ONR 5th Sym. on Naval Hydrodynamics, 1965.

25. Patel, V. C., "Calibration of the Preston Tube and Limitations on Its Use in Pressure Gradients," J. Fluid Mech., 23, 1965.

26. Coles, D., "Law of the Wake in the Turbulent Boundary Layer," J. Fluid Mech.,1, 1956.

REFERENCES (cont.)

27. Weighardt, K., "Uber die Wandschubspannung in Turbulenten Reibungsschichten bei Veranderlichem Aussendruck," Zentrale fur wissenschaftliches Berichtwesen der Luftfahrtforschung der Generalluftzeugmeisters Untersuchunge und Mitteilunge No. 6603, Kaiser Wilhelm-Institut fur Stromungsforschung, Gottingen, 1943.

28. Freihe, C., and Schwartz, W., "The Use of Pitot-Static Tubes and Hot Film Anemometers in Dilute Polymer Solutions," Proc. of the 1968 Sym. on Viscous Drag Reduction, Plenum Press, New York, 1969.

29. Corcos, G. M., "Resolution of Pressure in Turbulence," J. Acous. Soc. Am., 35, 1963.

30. Chandiramani, K. L., "Interpretation of Wall Pressure Measurements Under a Turbulent Boundary Layer," Bolt, Beranek and Newman Report No. 1310, 1965.

31. Kline, S. J., and Runstadler, P. W., "Visual Studies on the Flow Model of the Wall Layers of the Turbulent Boundary Layer," Dept. of Mech. Eng. Report No. MD-3, Stanford U., 1958.

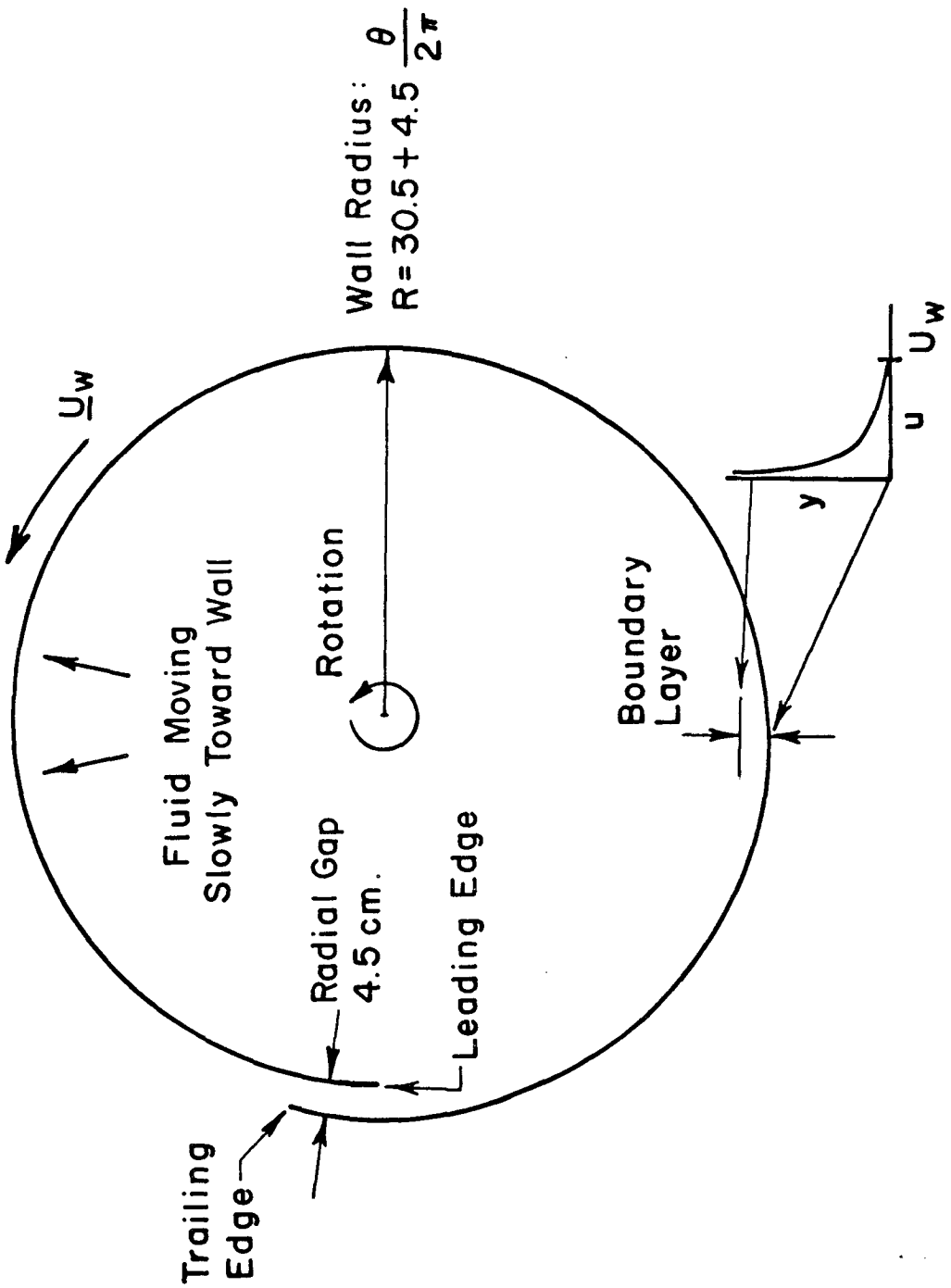

Figure 1. "Scroll" flow -- top view.

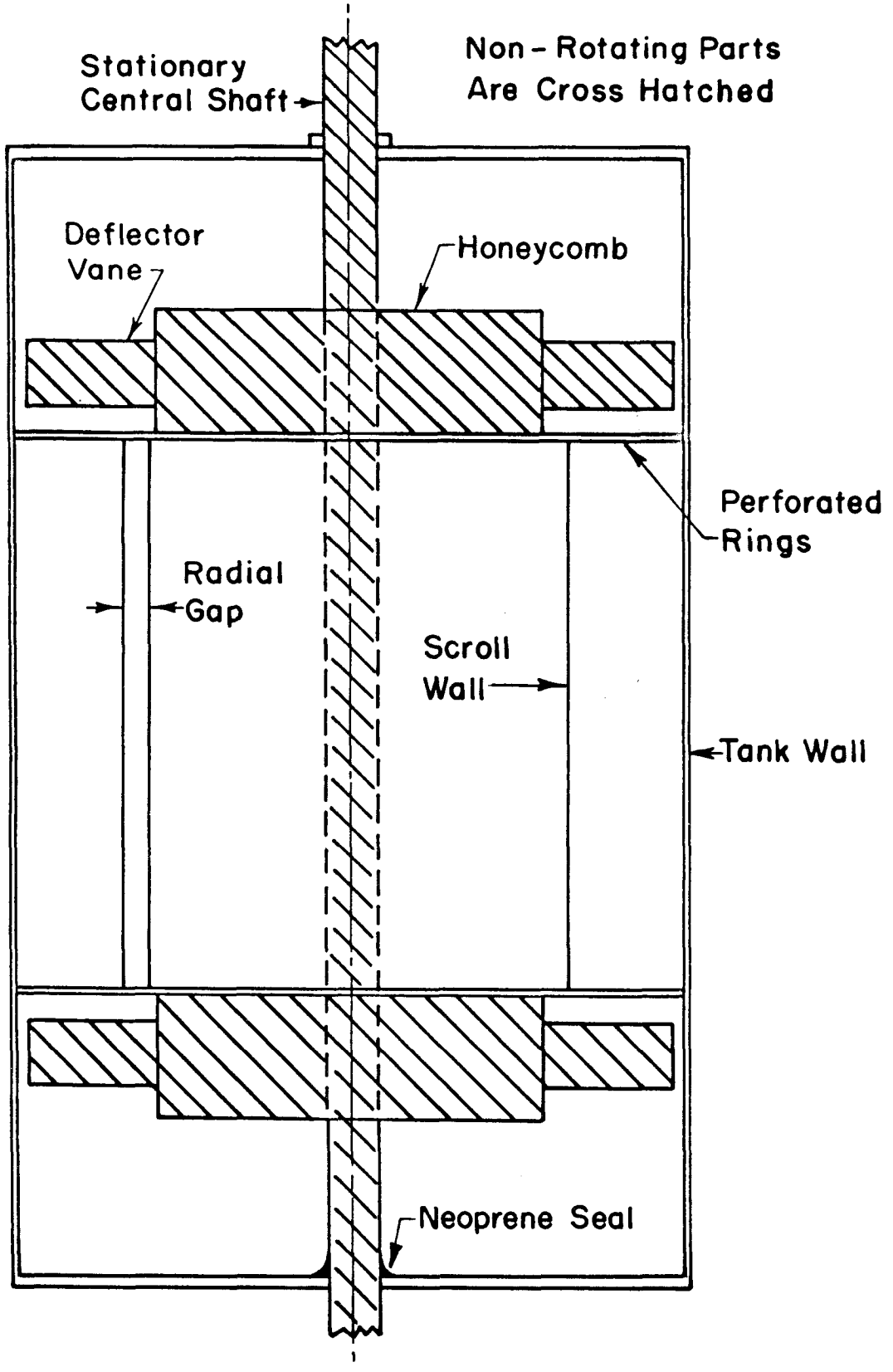

Figure 2. Side view of experiment.

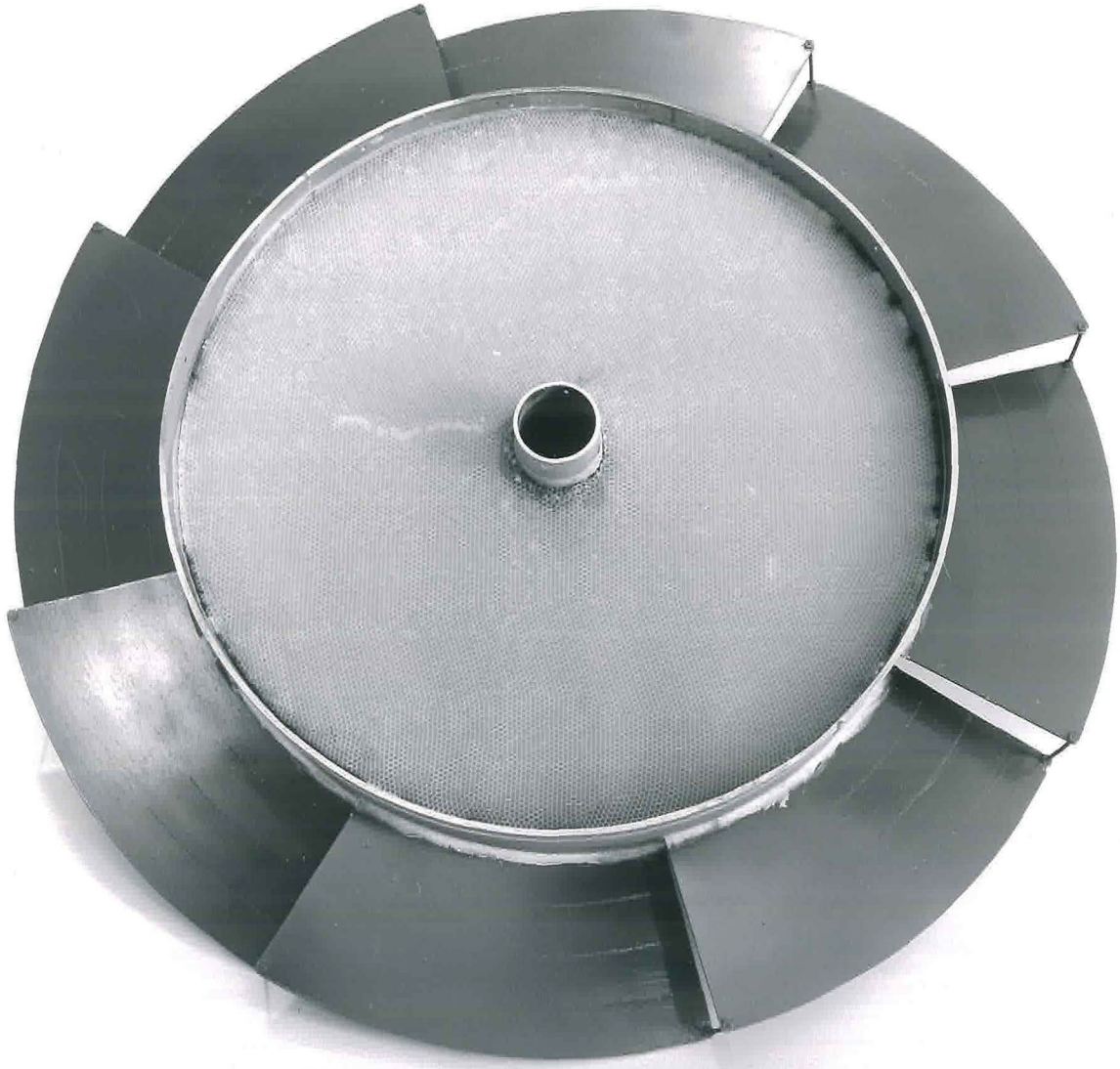

Figure 2a. Photograph of honeycomb assembly.

Figure 2b. Photograph of scroll.

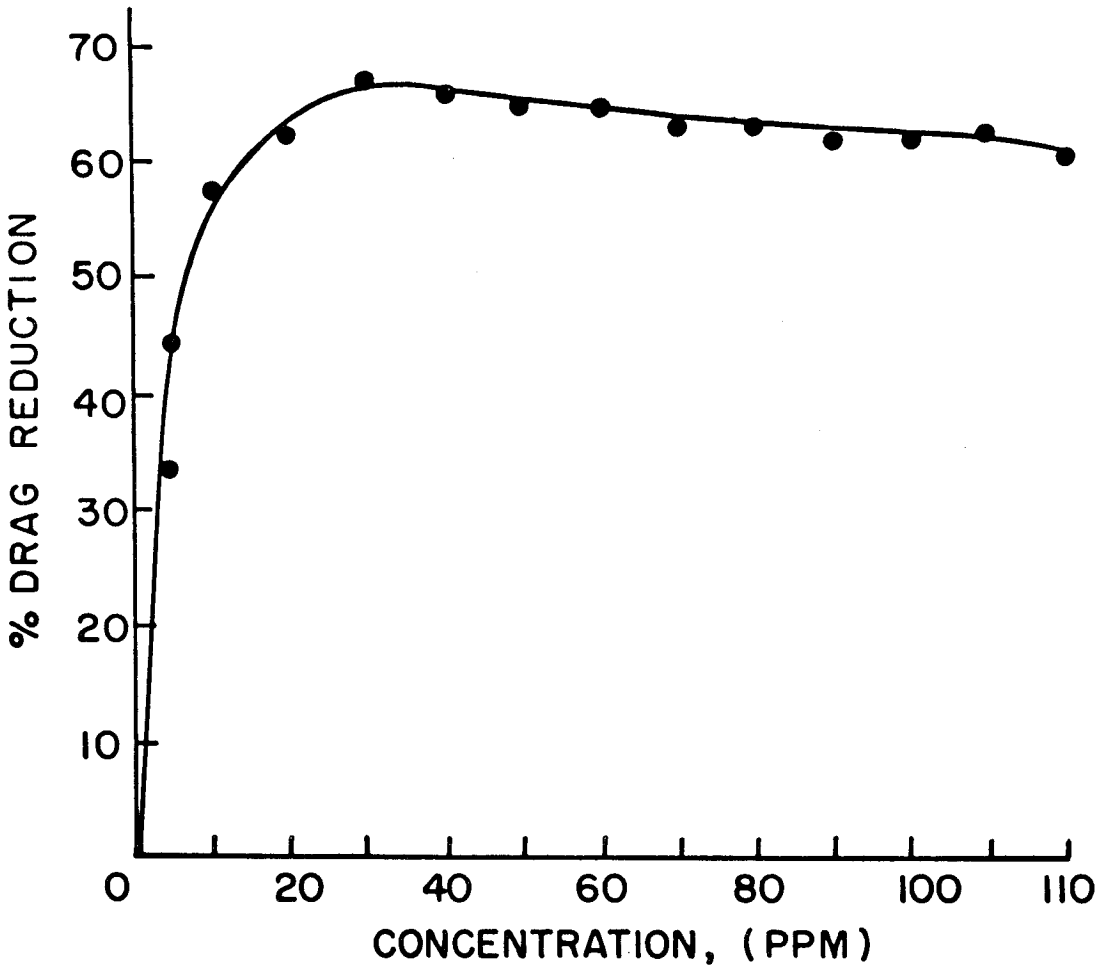

Figure 3. Drag reduction in pipe flow.

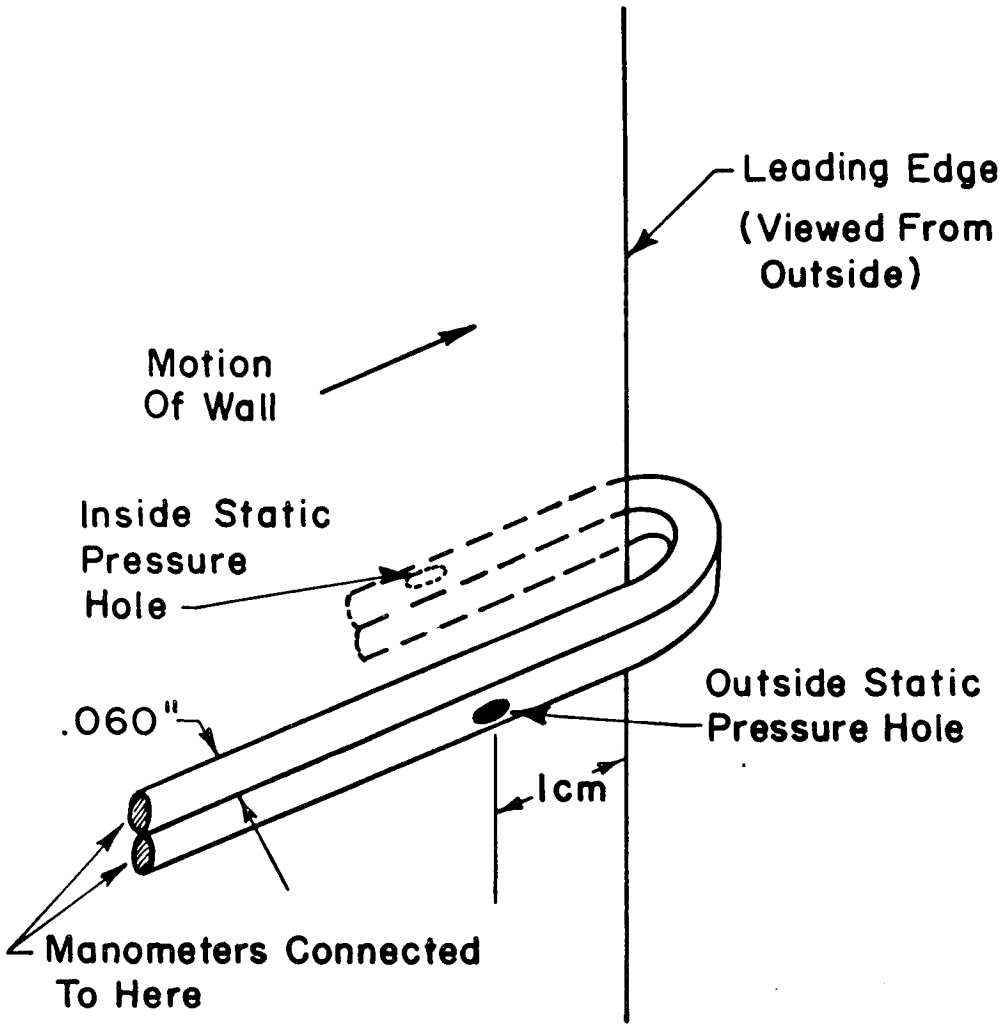

Figure 4. Leading edge probe configuration.

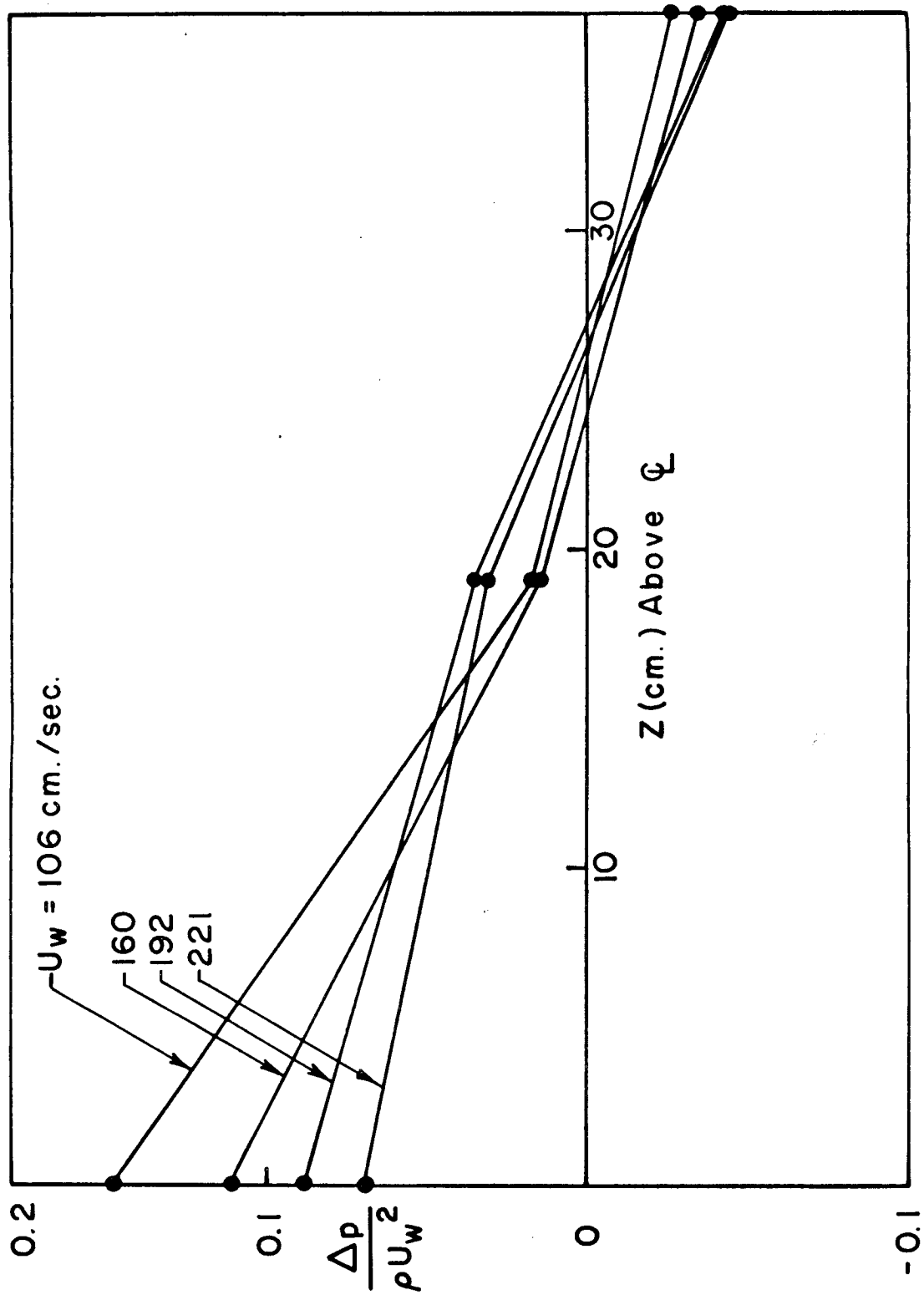

Figure 5. Leading edge probe results.

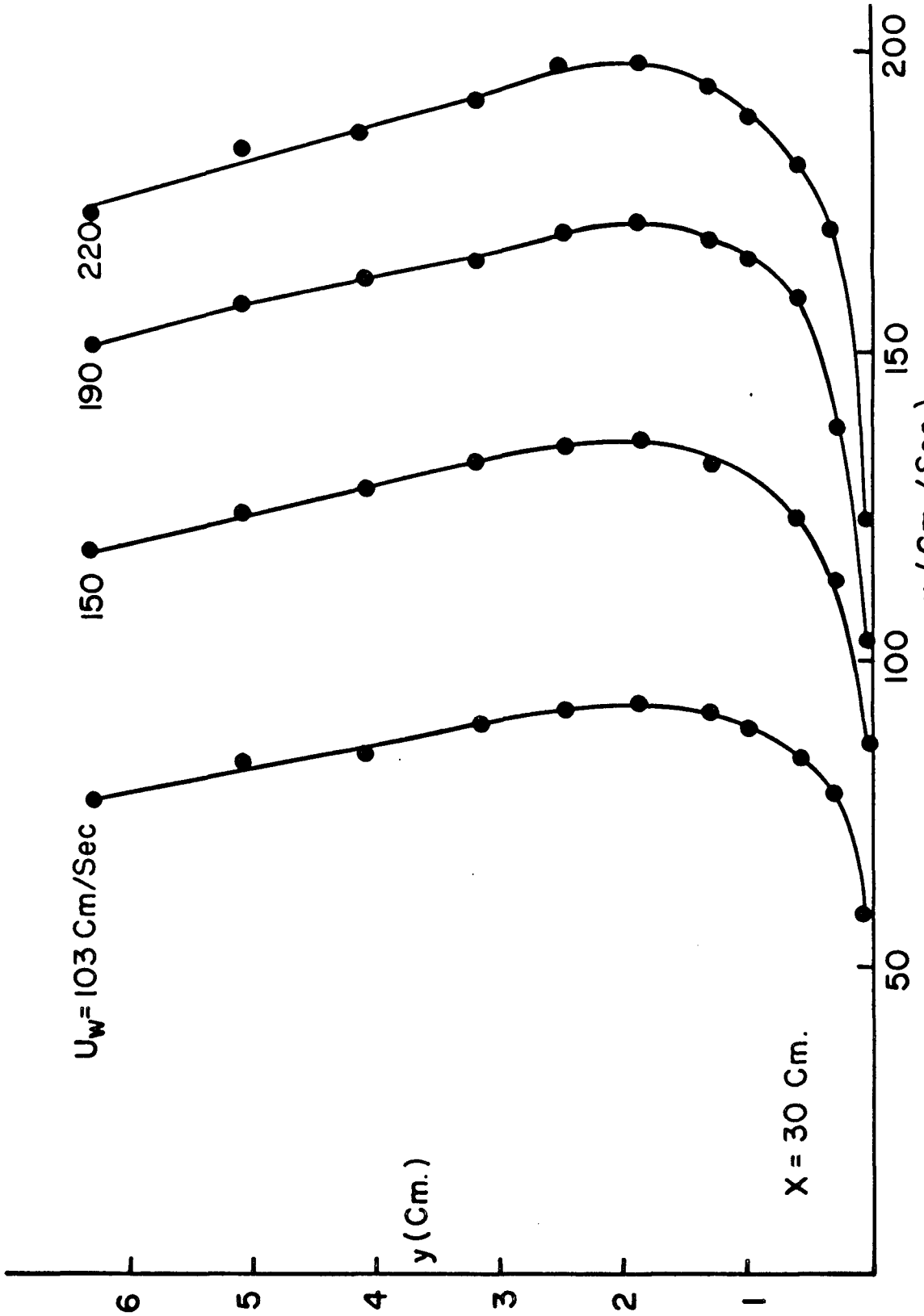

Figure 6. Mean velocity profiles.

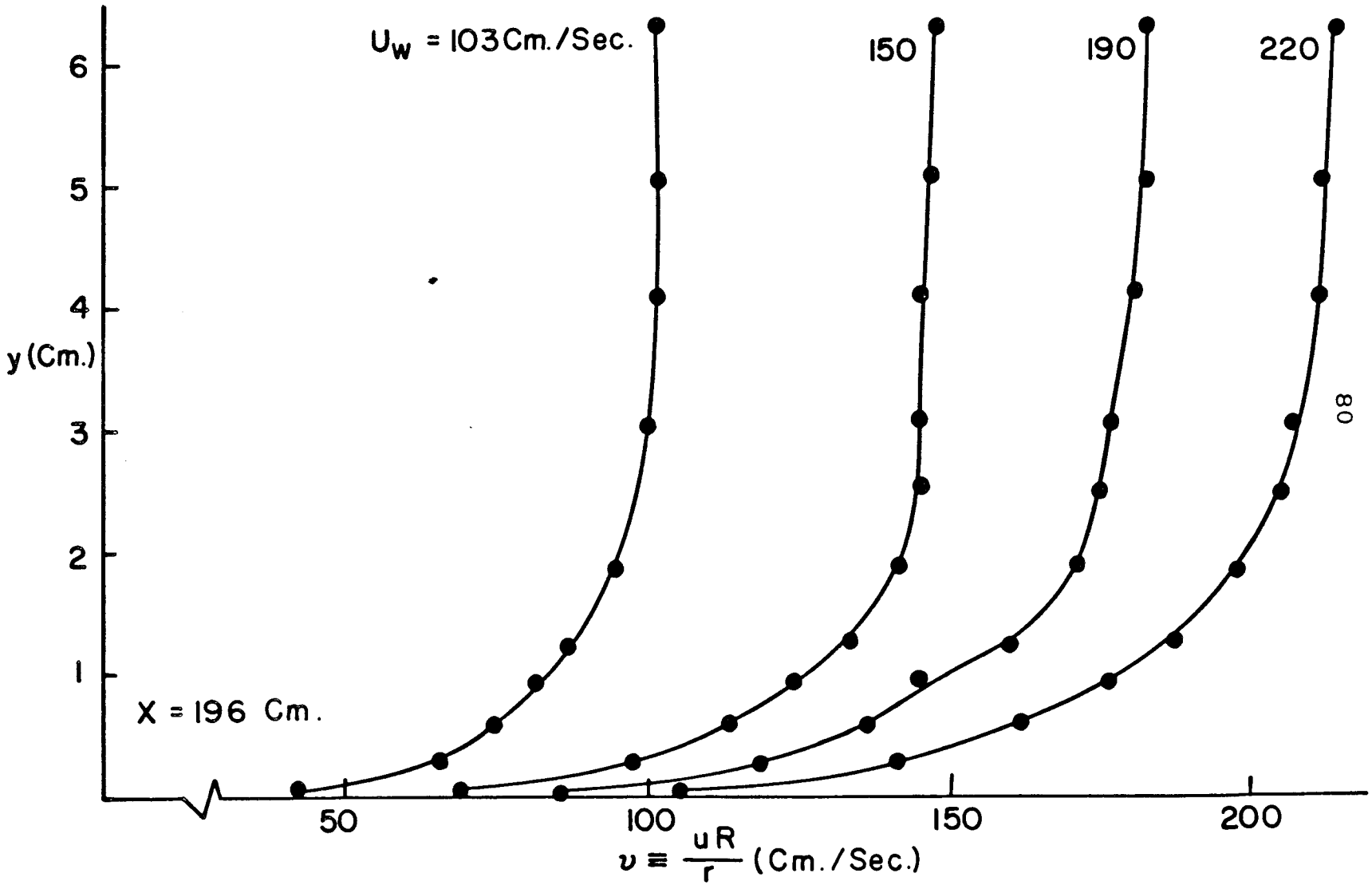

Figure 7. Mean angular velocity profiles.

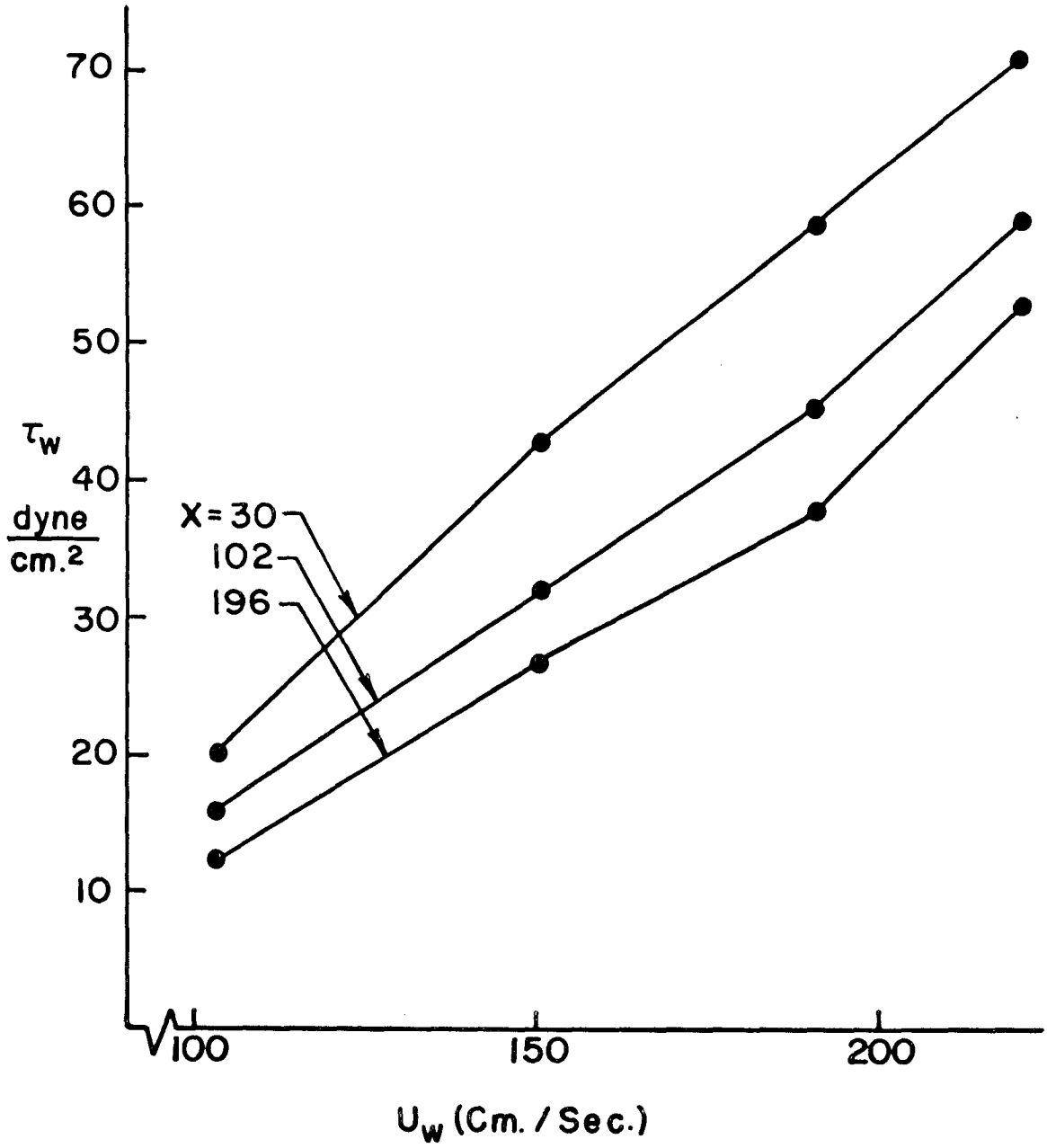

Figure 8. Wall shear stress from Preston tube.

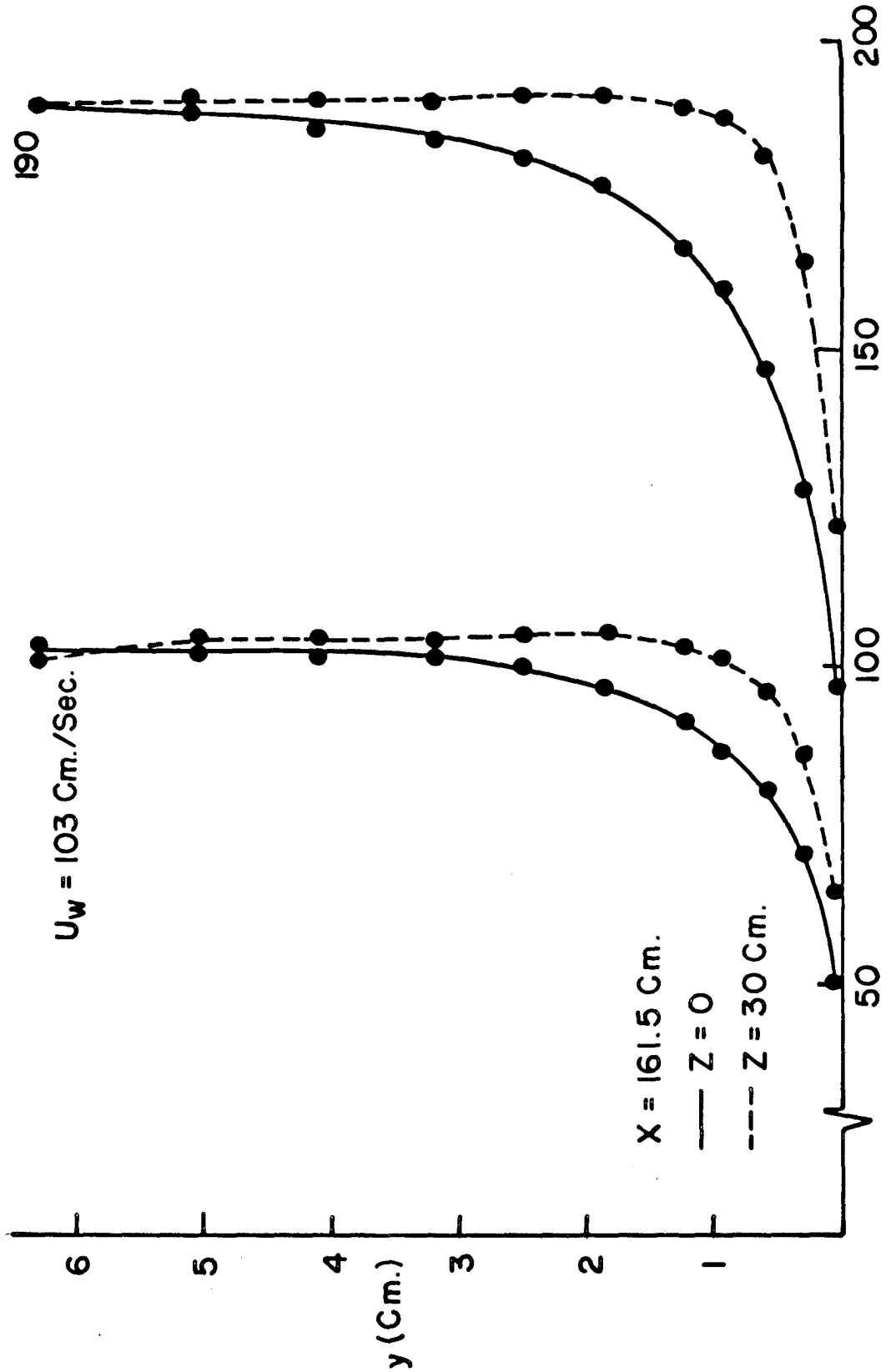

Figure 9. Velocity profile versus z-coordinate.

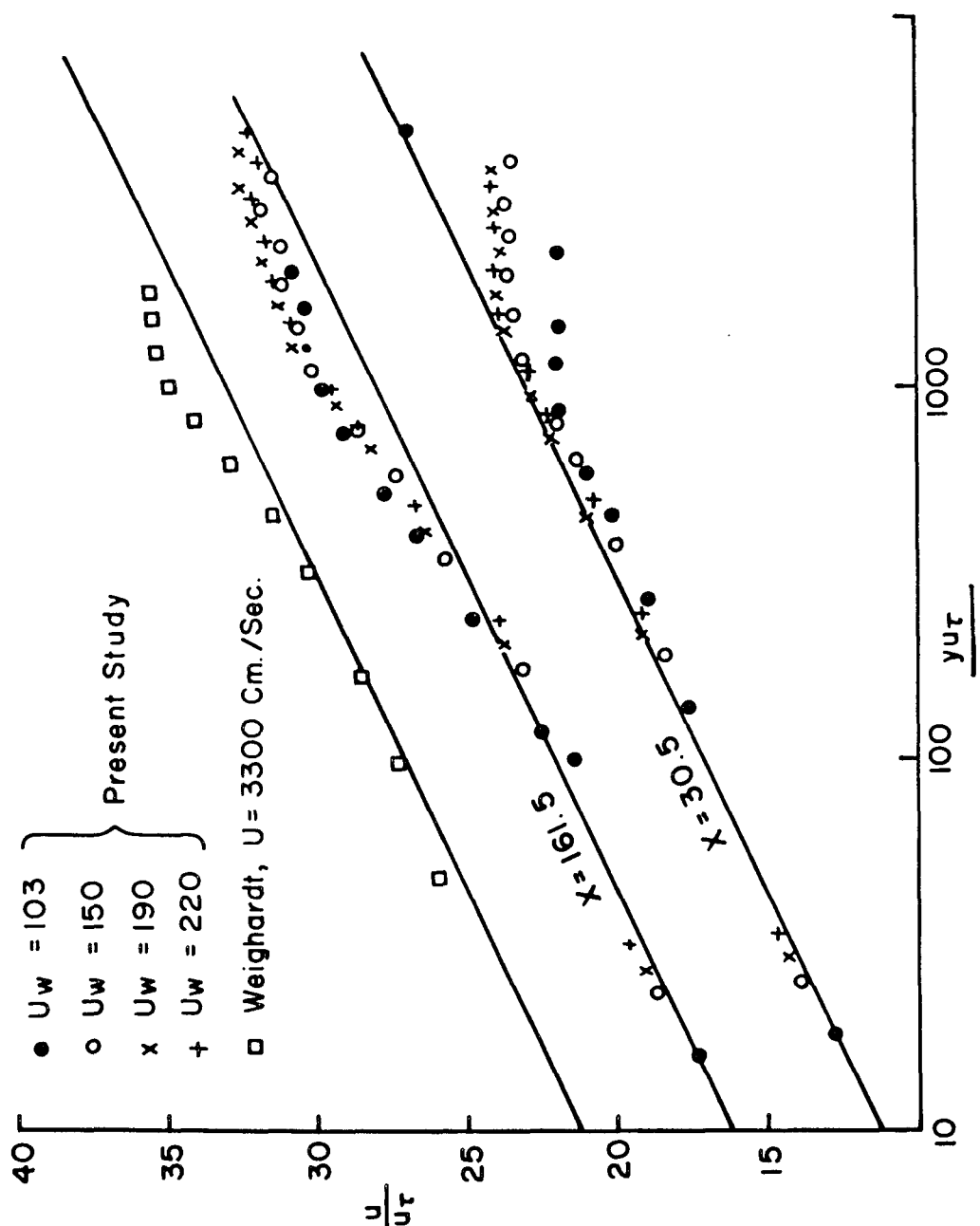

Figure 10. Law of the wall profiles: pure water

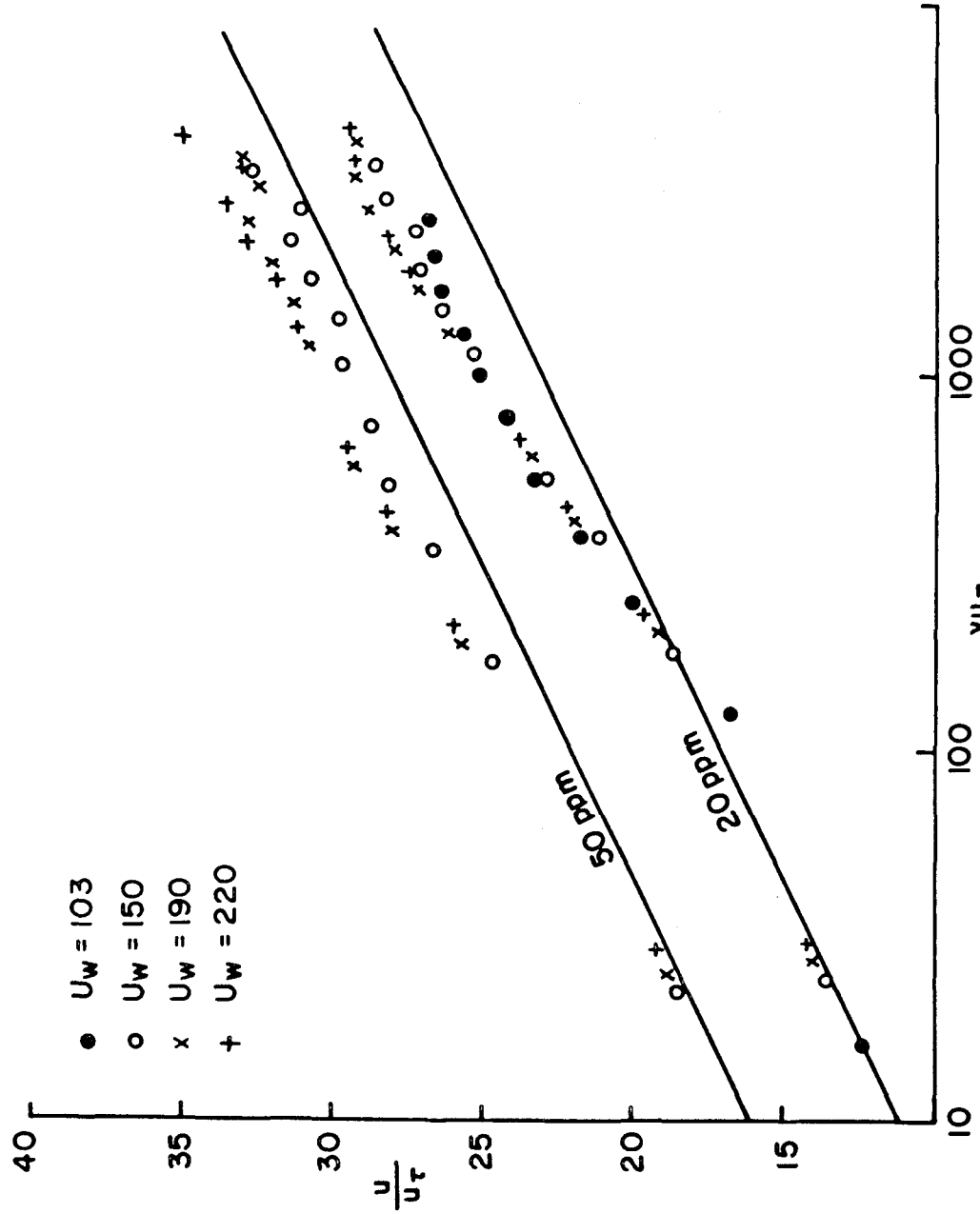

Figure 11. Law of the wall profiles: polymer solutions.

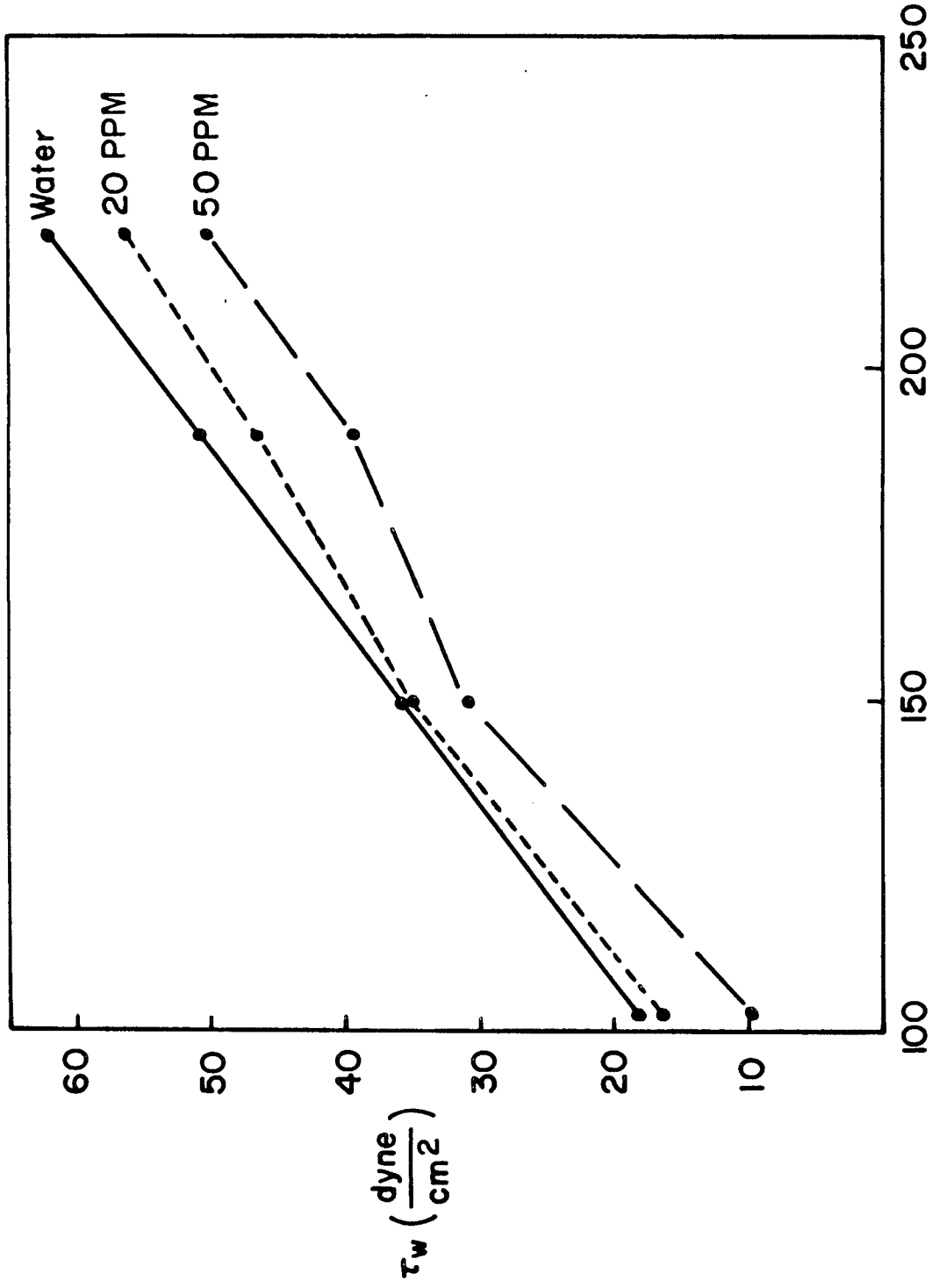

Figure 12. Wall shear stress for water and polymer.

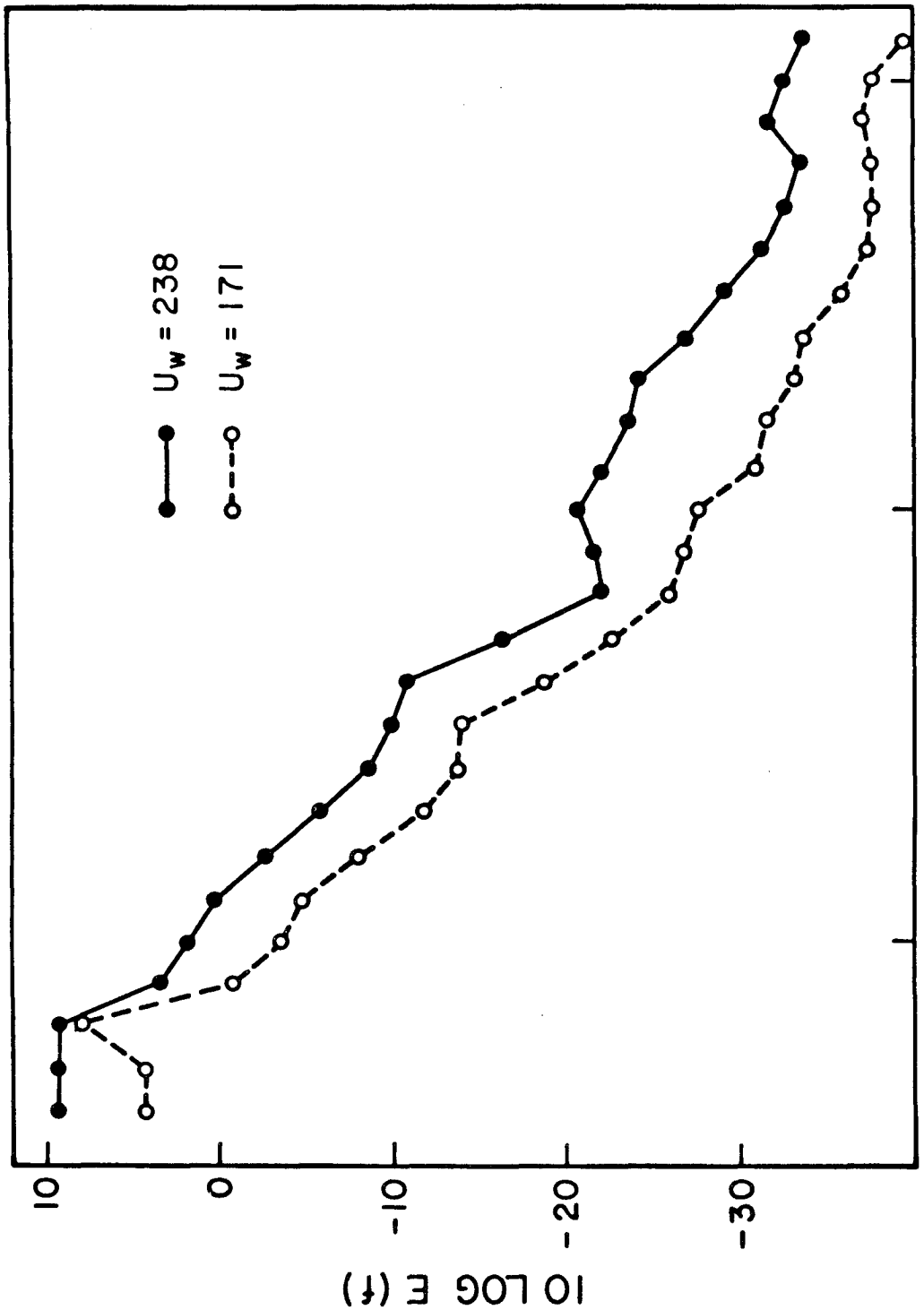

Figure 13. Wall pressure spectrum versus speed: water, x = 51.5 cm.

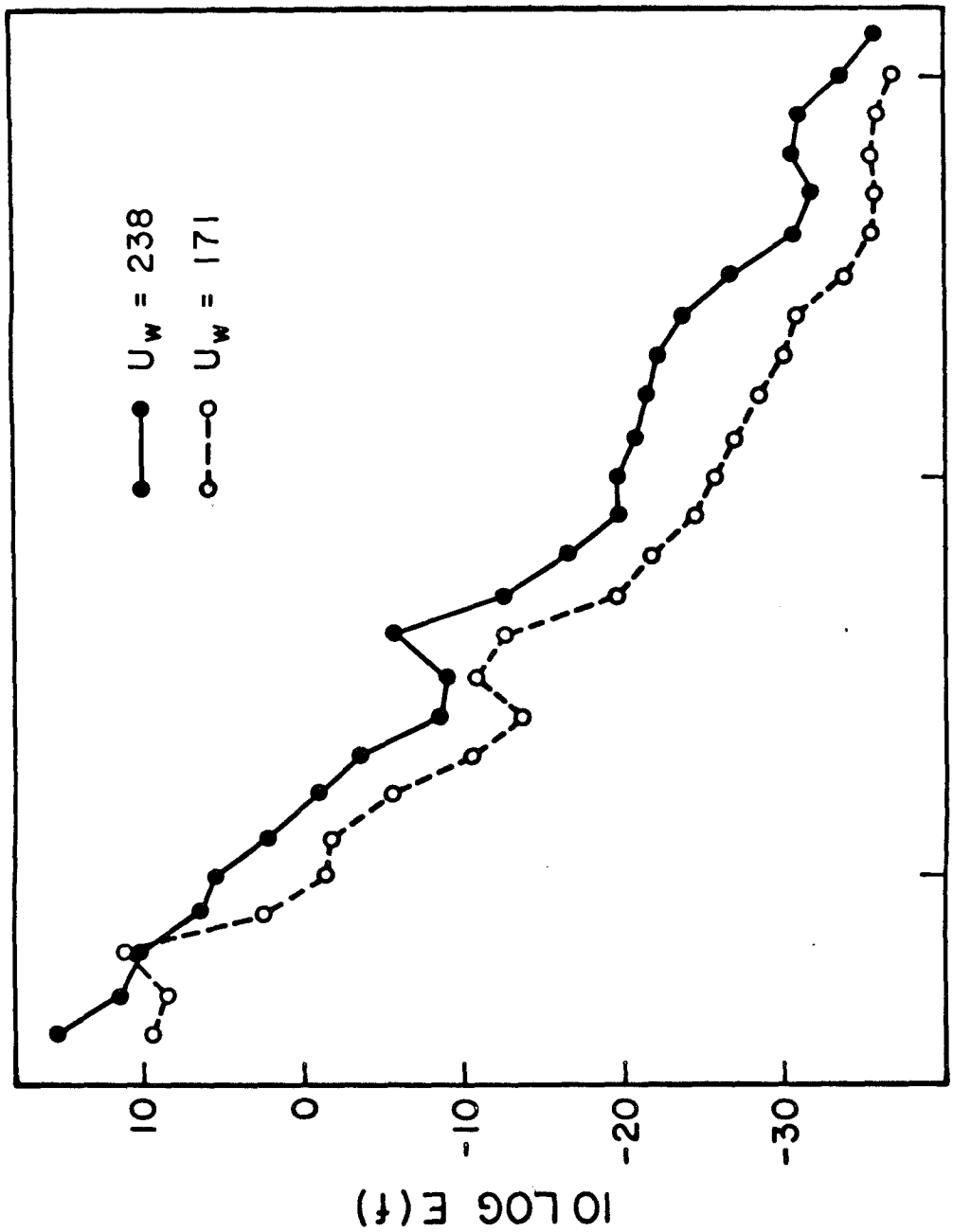

Figure 14. Wall pressure spectrum versus speed; water, x = 154.5 cm

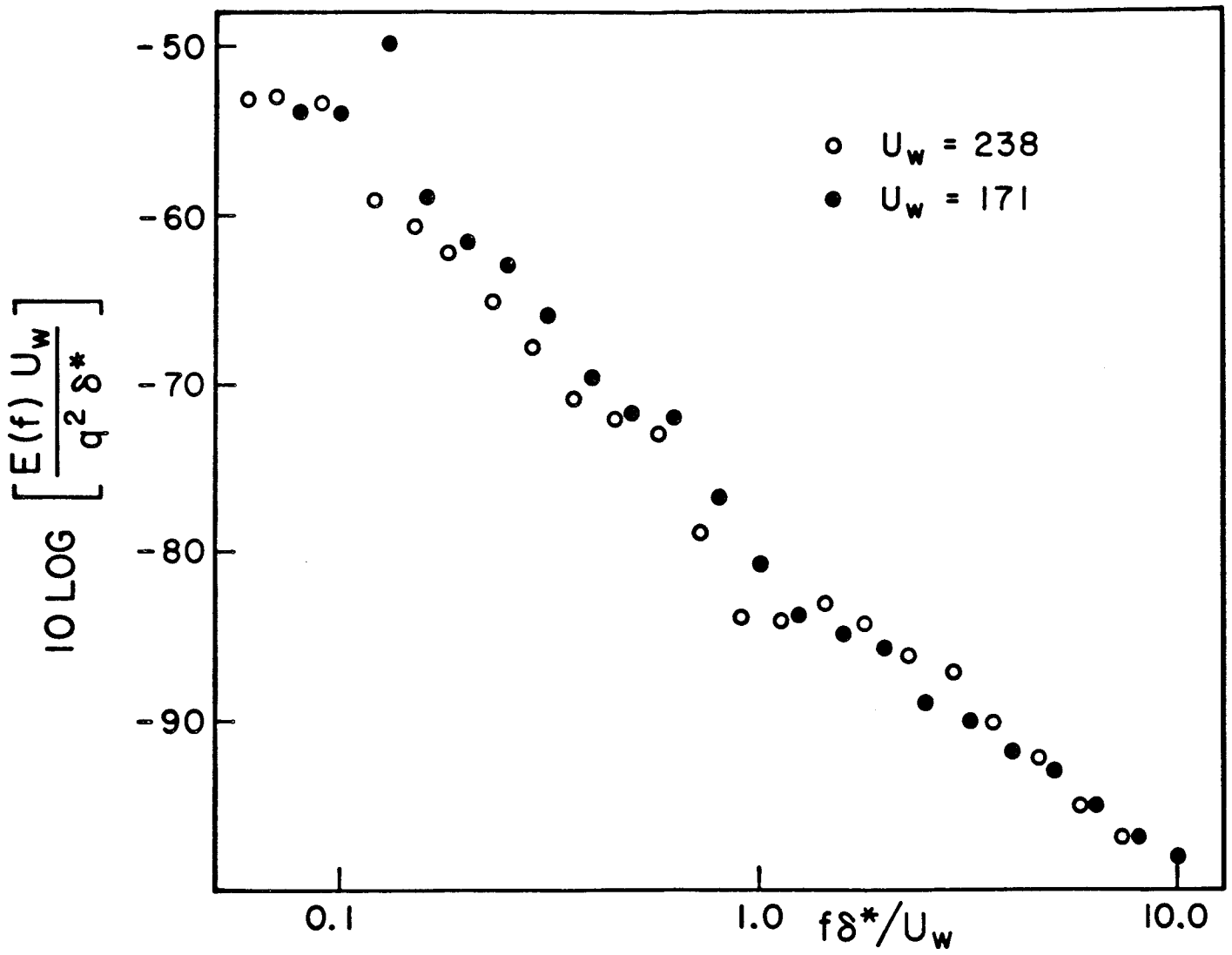

Figure 15. Dimensionless wall pressure spectrum: water, x = 51.5 cm.

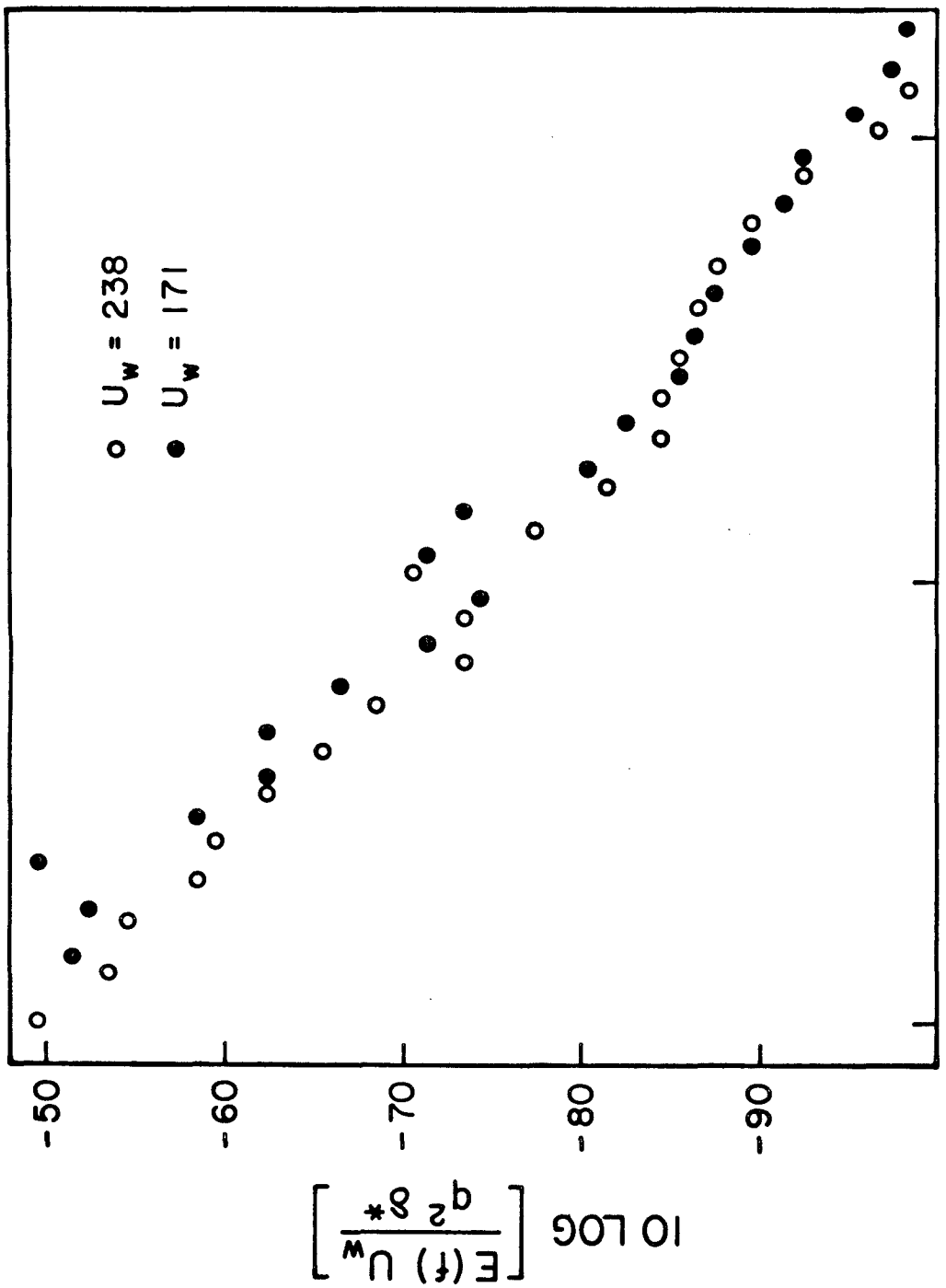

Figure 16. Dimensionless wall pressure spectrum: water, x = 154.5 cm.

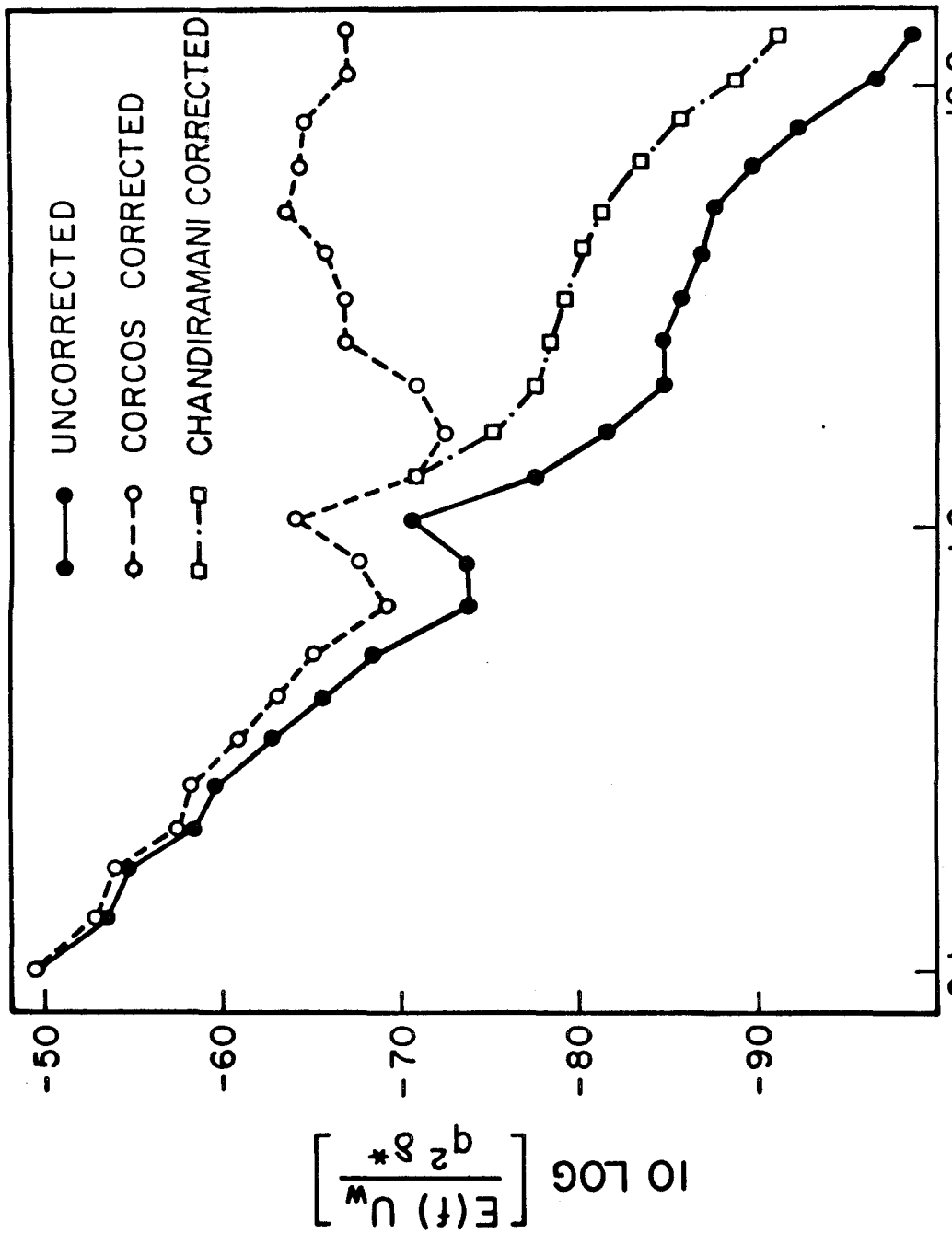

Figure 17. Wall pressure spectrum corrected for size effect.

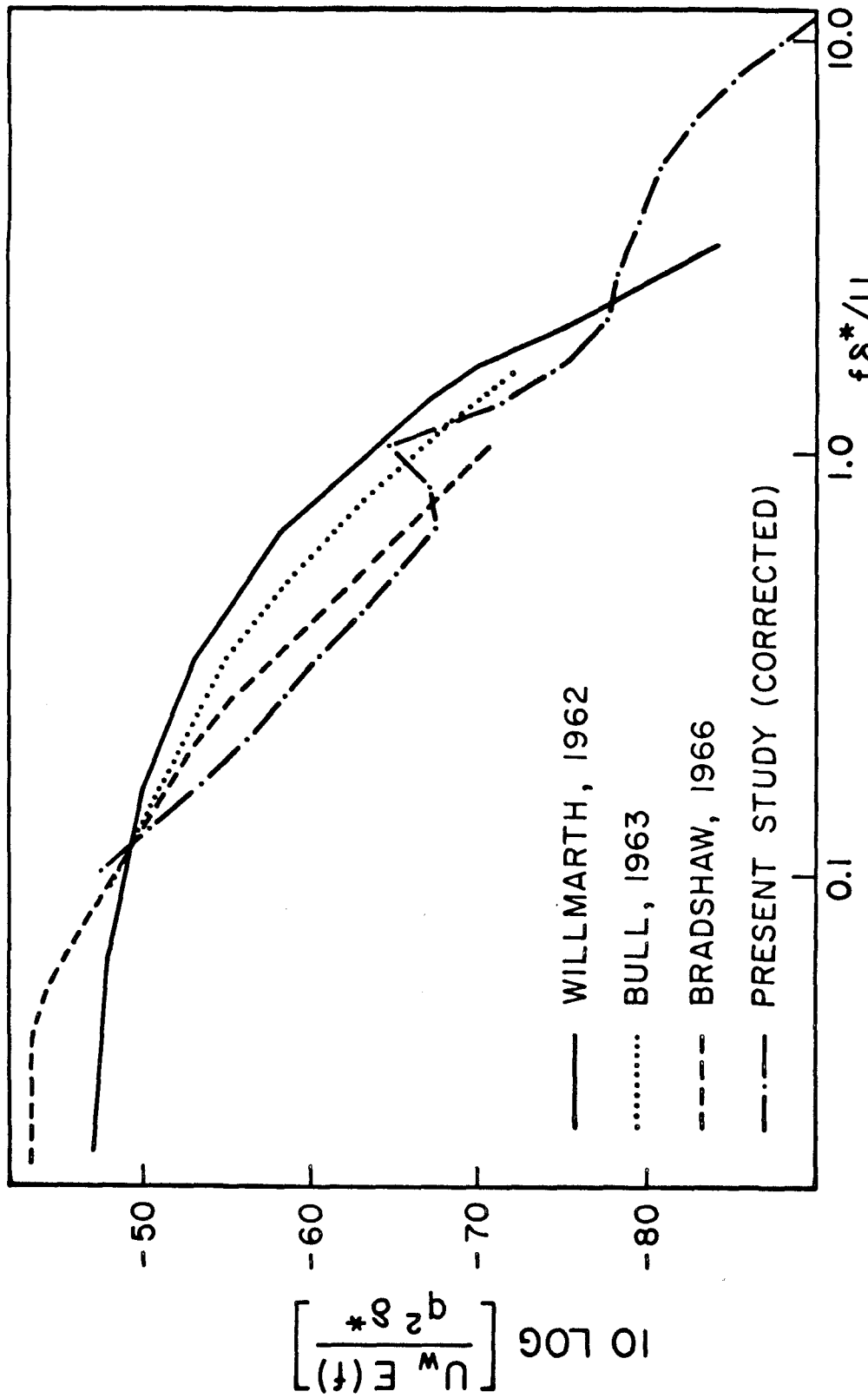

Figure 18. Wall pressure spectrum compared with previous experiments.

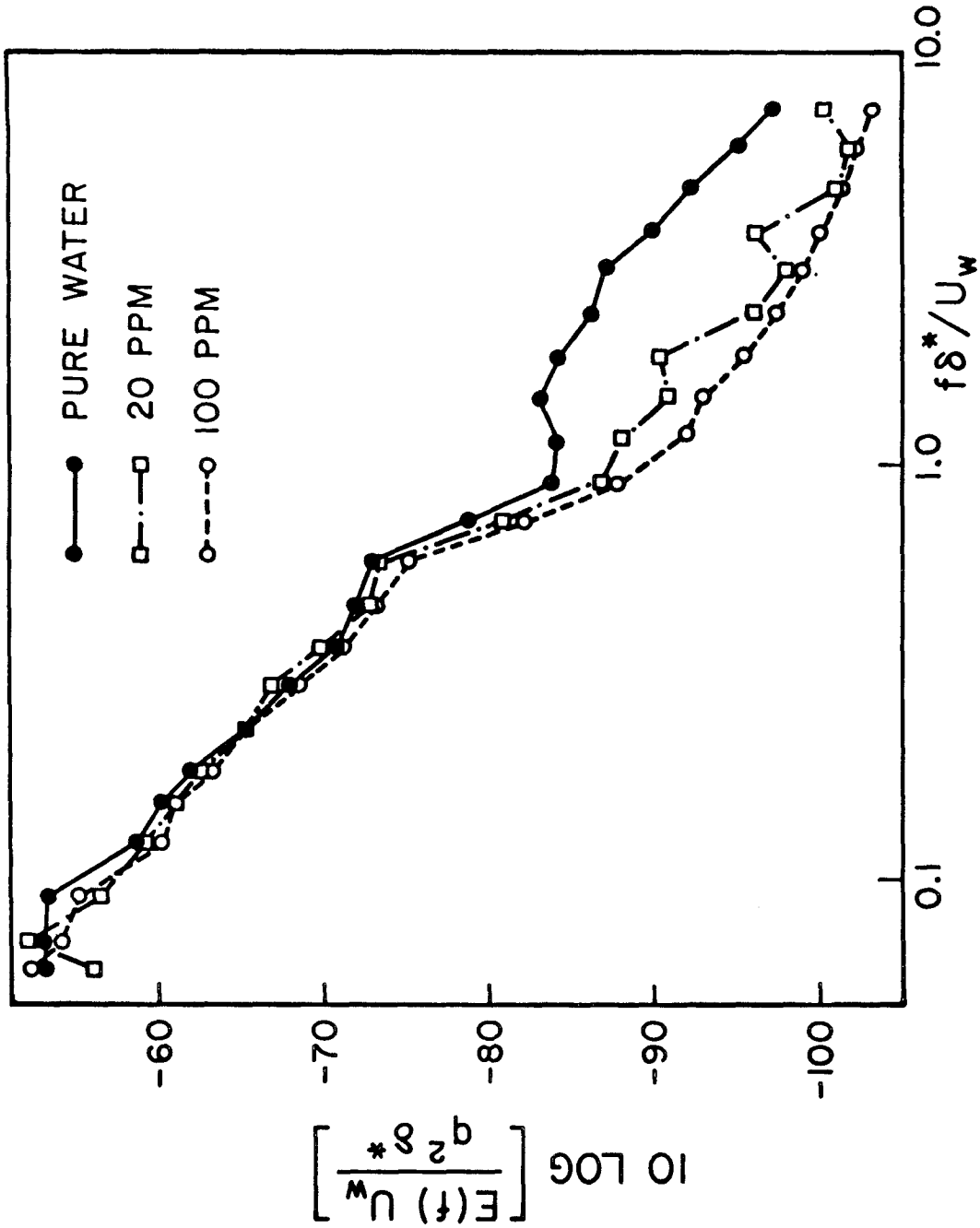

Figure 19. Wall pressure spectra of water, 20 and 100 ppm polyox: x = 51.5 cm, U_w = 238 cm/sec.

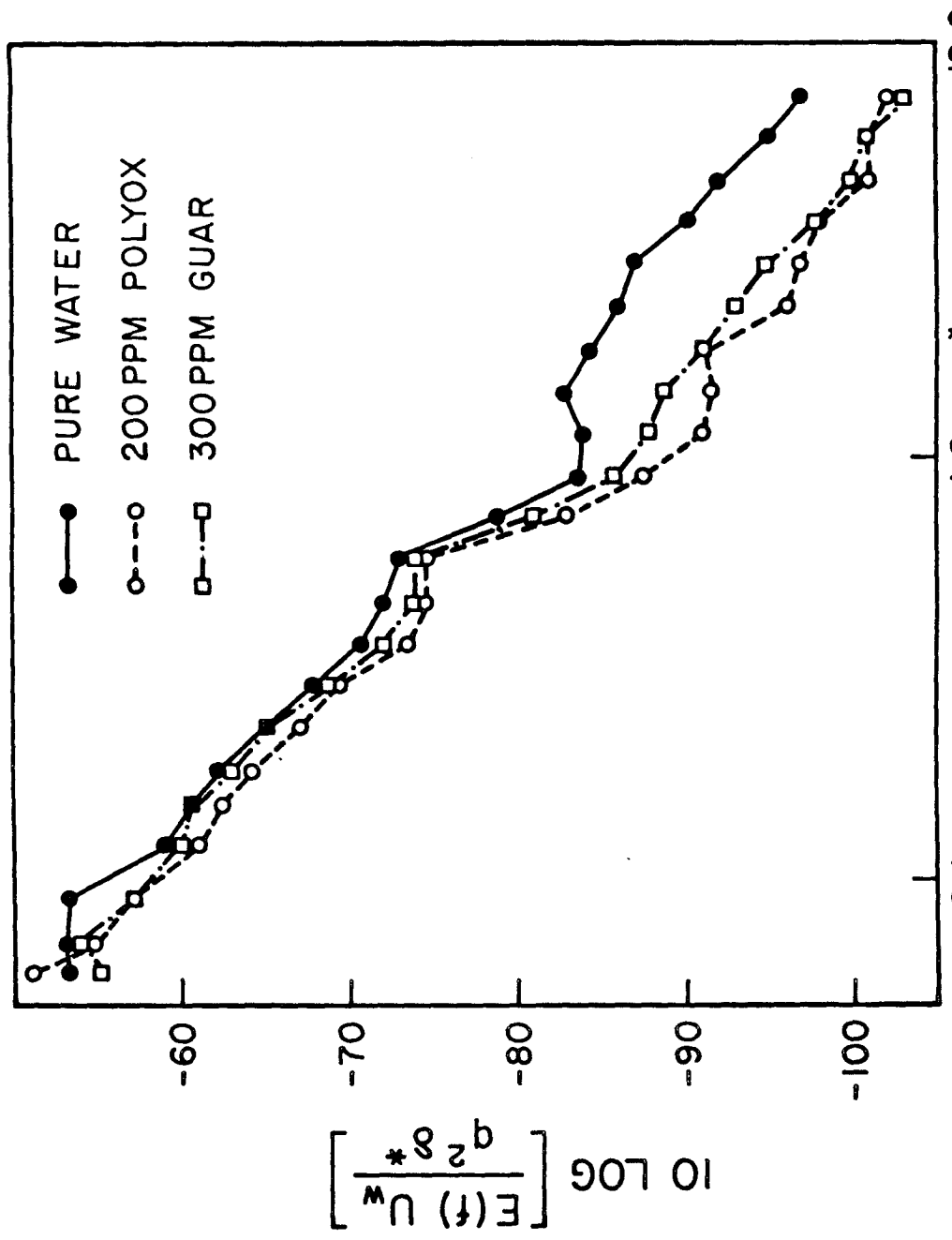

Figure 20. Wall pressure spectra of water, 200 ppm polyox and 300 ppm guar: x = 51.5 cm, U_w = 238 cm/sec.

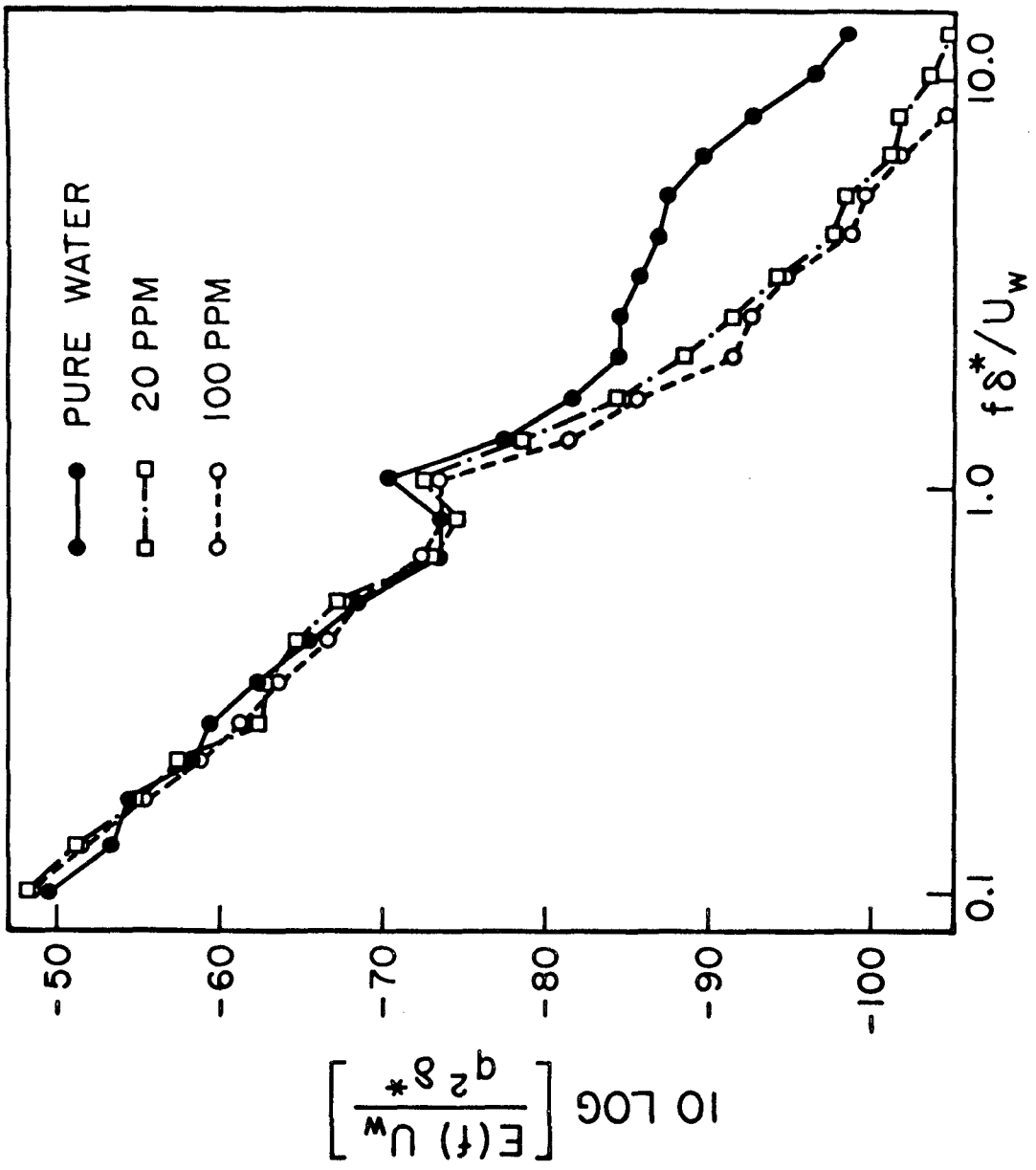

Figure 21. Wall pressure spectra of water, 20 and 100 ppm polyox: $x = 154.5$ cm, $U_w = 238$ cm/sec.

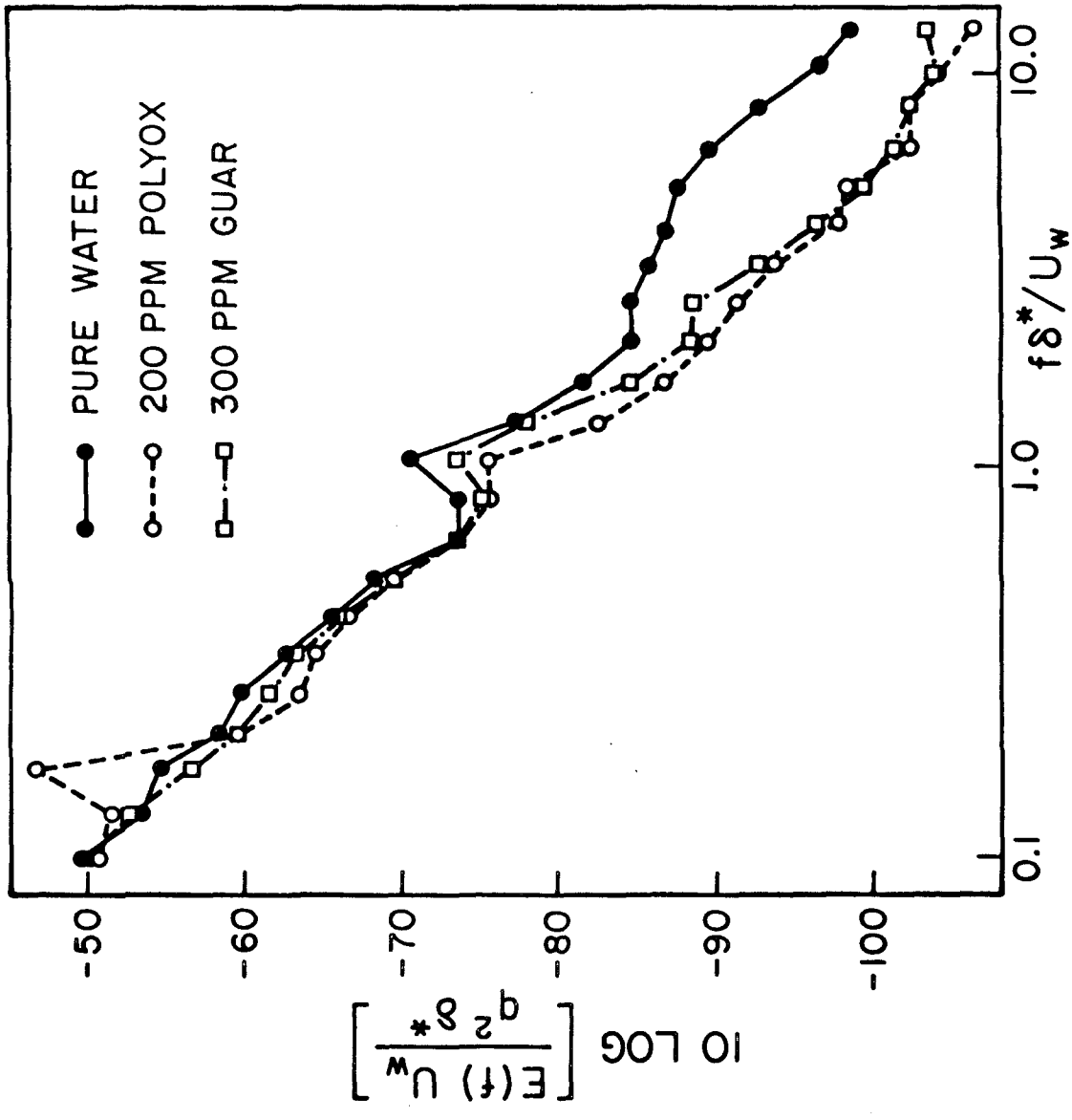

Figure 22. Wall pressure spectra of water, 200 ppm polyox and 300 ppm guar: x = 154.5 cm, U_w = 238 cm/sec.

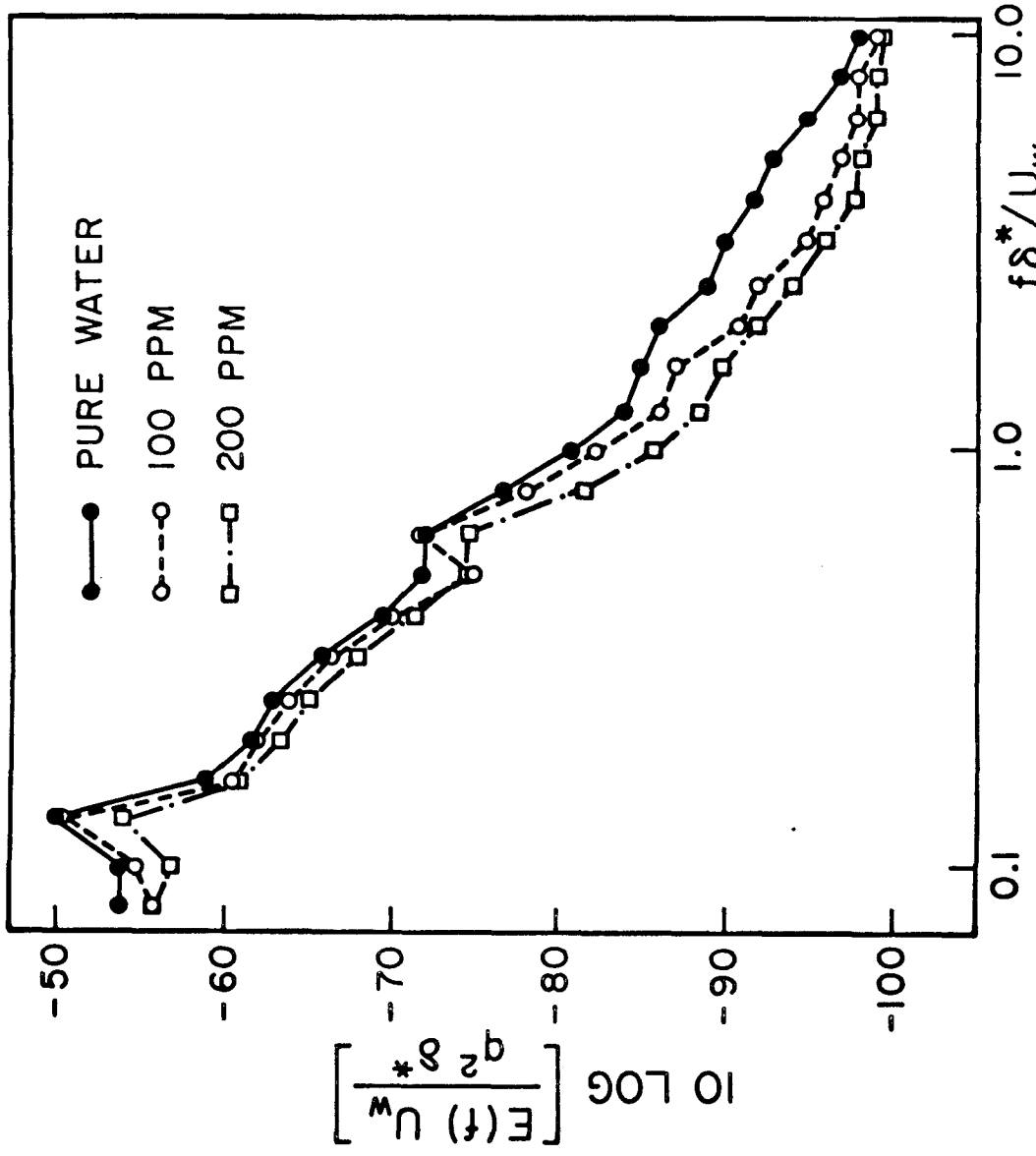

Figure 23. Wall pressure spectra of water, 100 and 200 ppm polyox: x = 51.5 cm, U_w = 171 cm/sec.

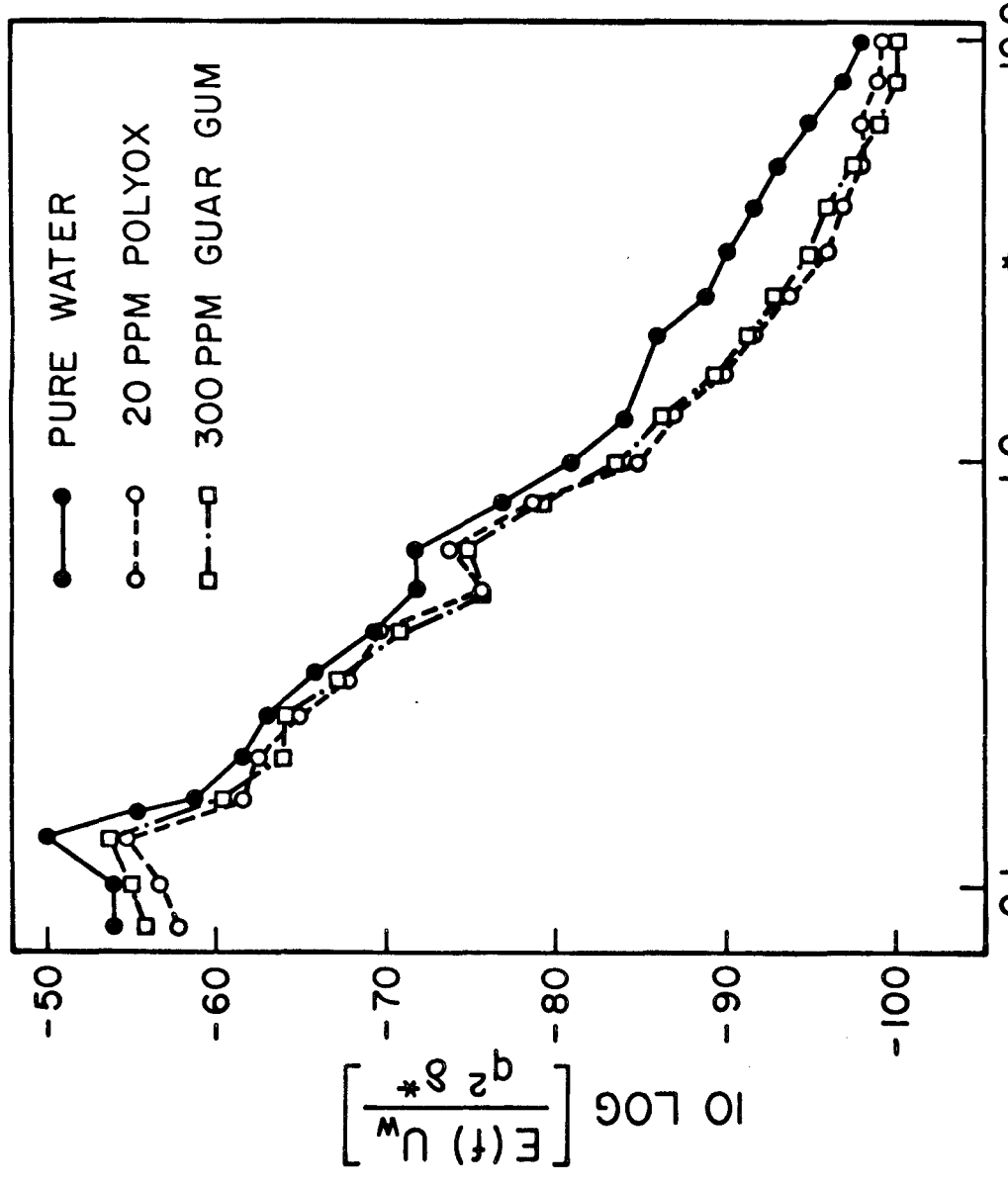

Figure 24. Wall pressure spectra of water, 20 ppm polyox and 300 ppm guar: x = 51.5 cm, U_w = 171 cm/sec.

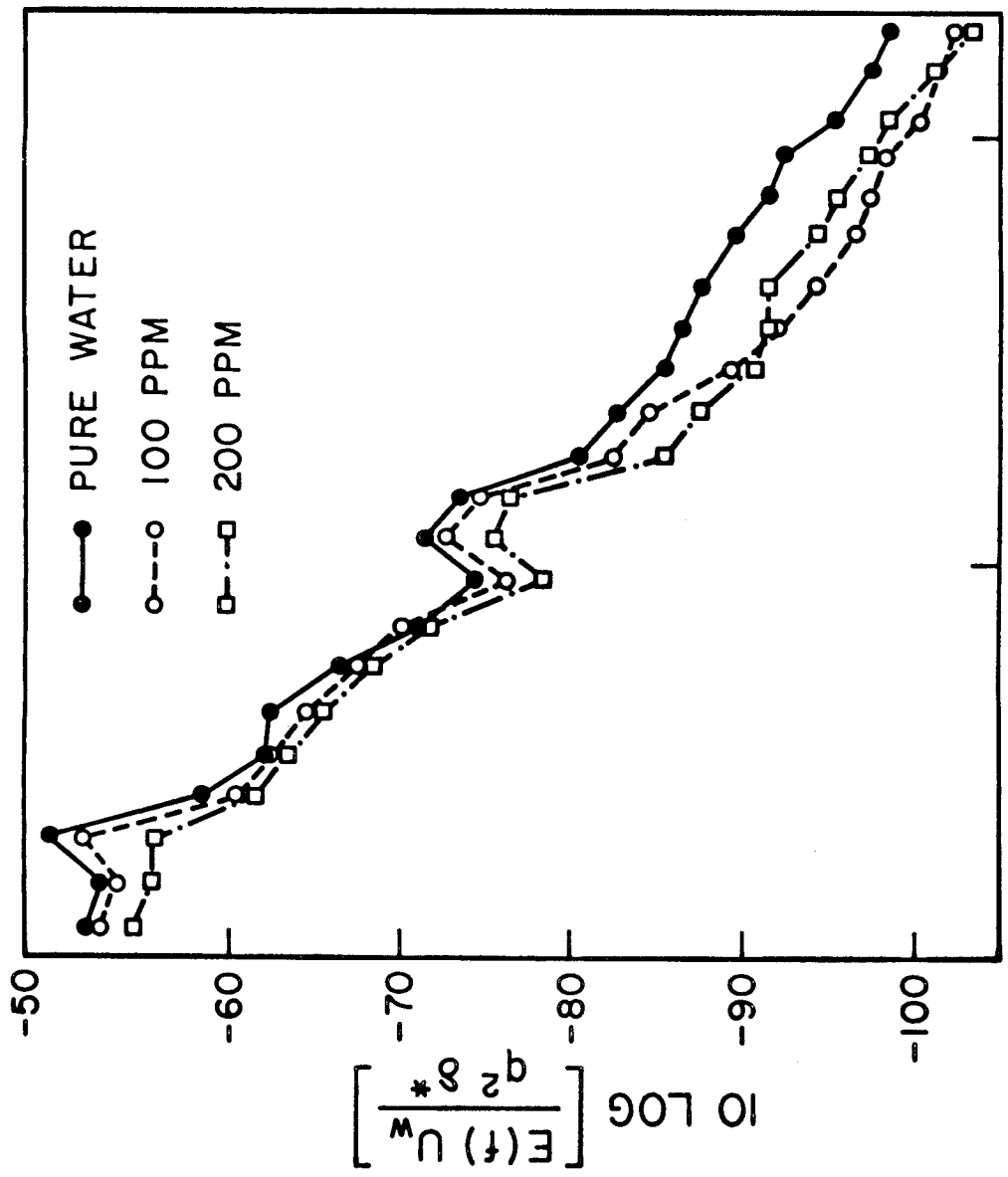

Figure 25. Wall pressure spectra of water, 100 and 200 ppm polyox: x = 154.5 cm, U_w = 171 cm/sec.

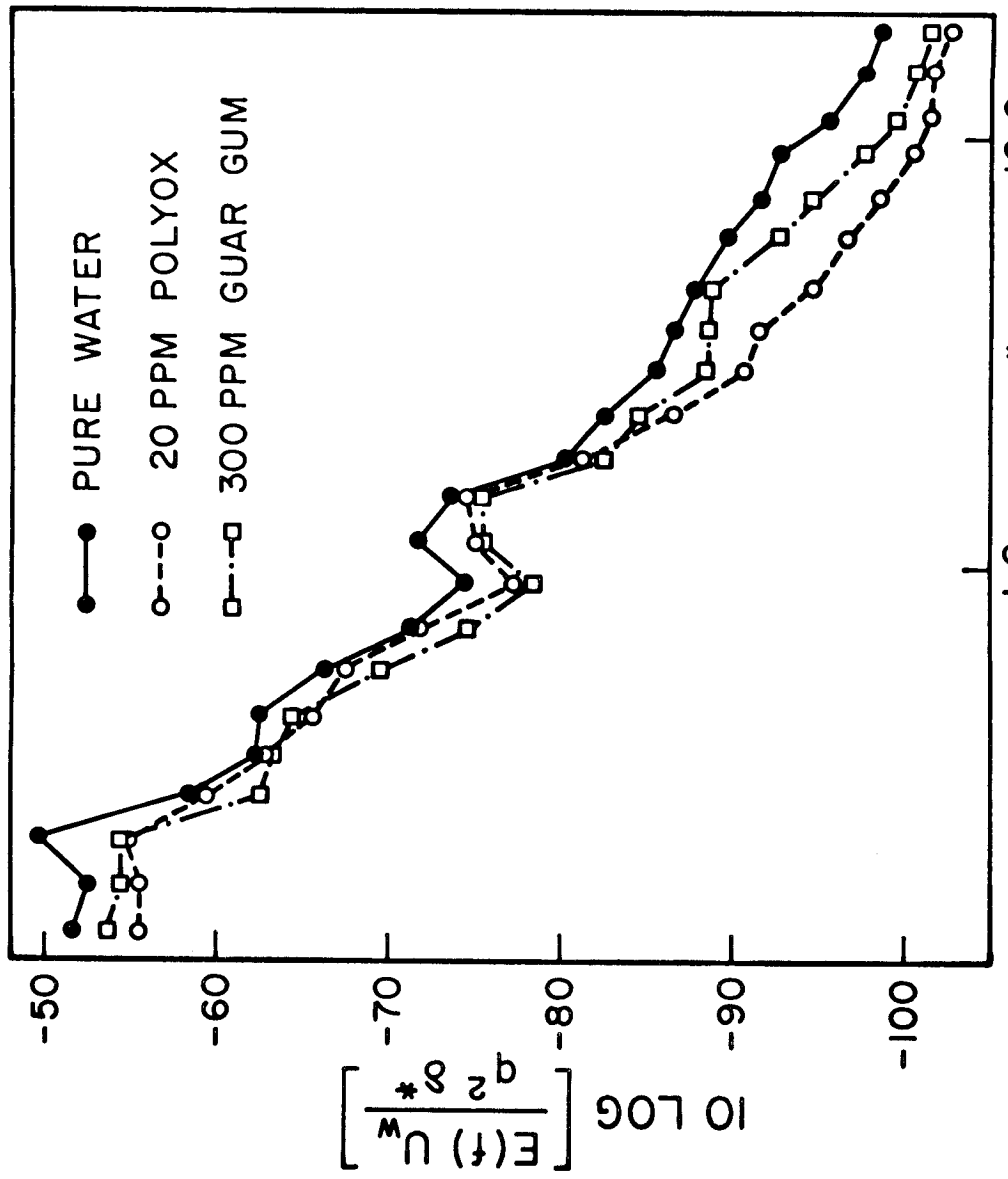

Figure 26. Wall pressure spectra of water, 20 ppm polyox and 300 ppm guar: x = 154.5 cm, U_w = 171 cm/sec.

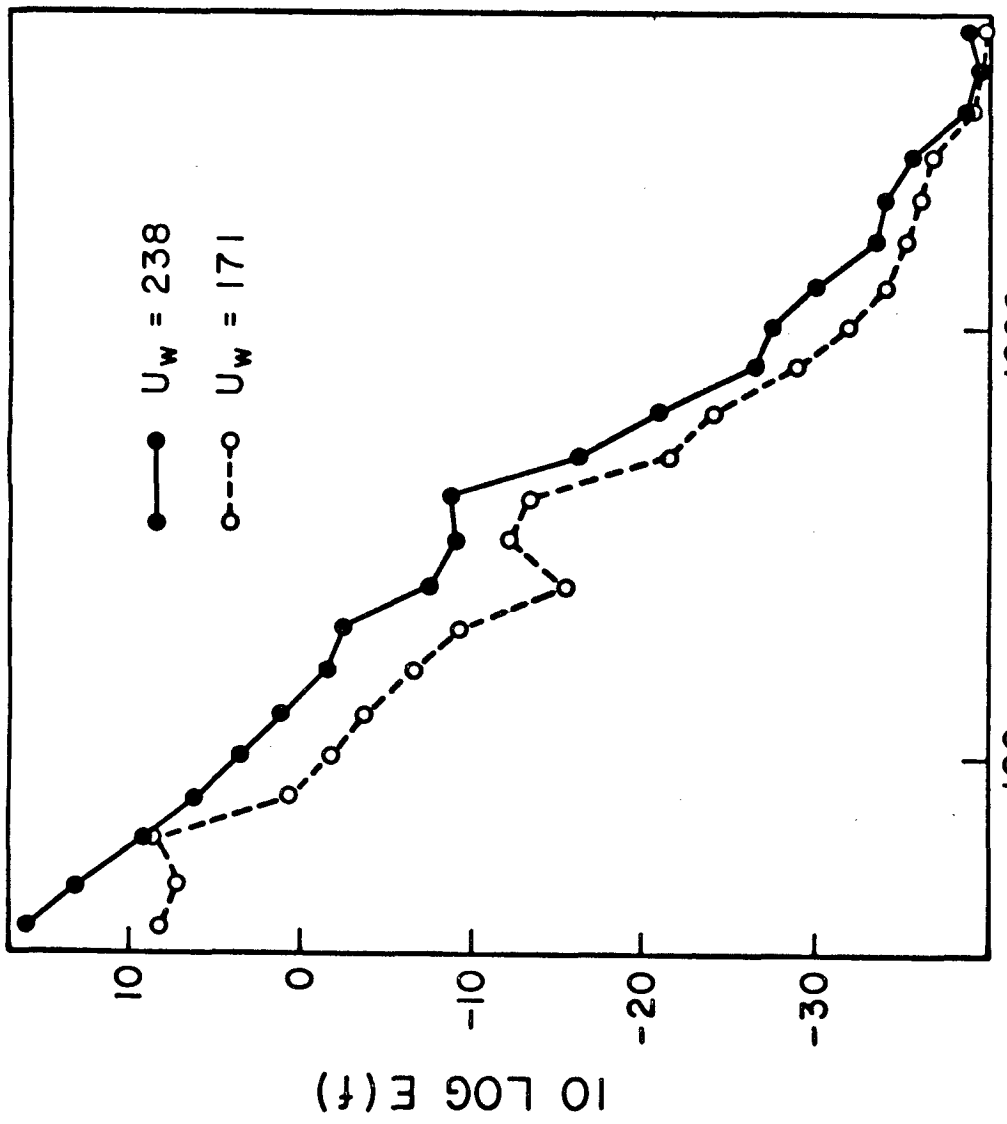

Figure 27. Wall pressure spectrum versus speed: 100 ppm polyox, x = 154.5 cm.

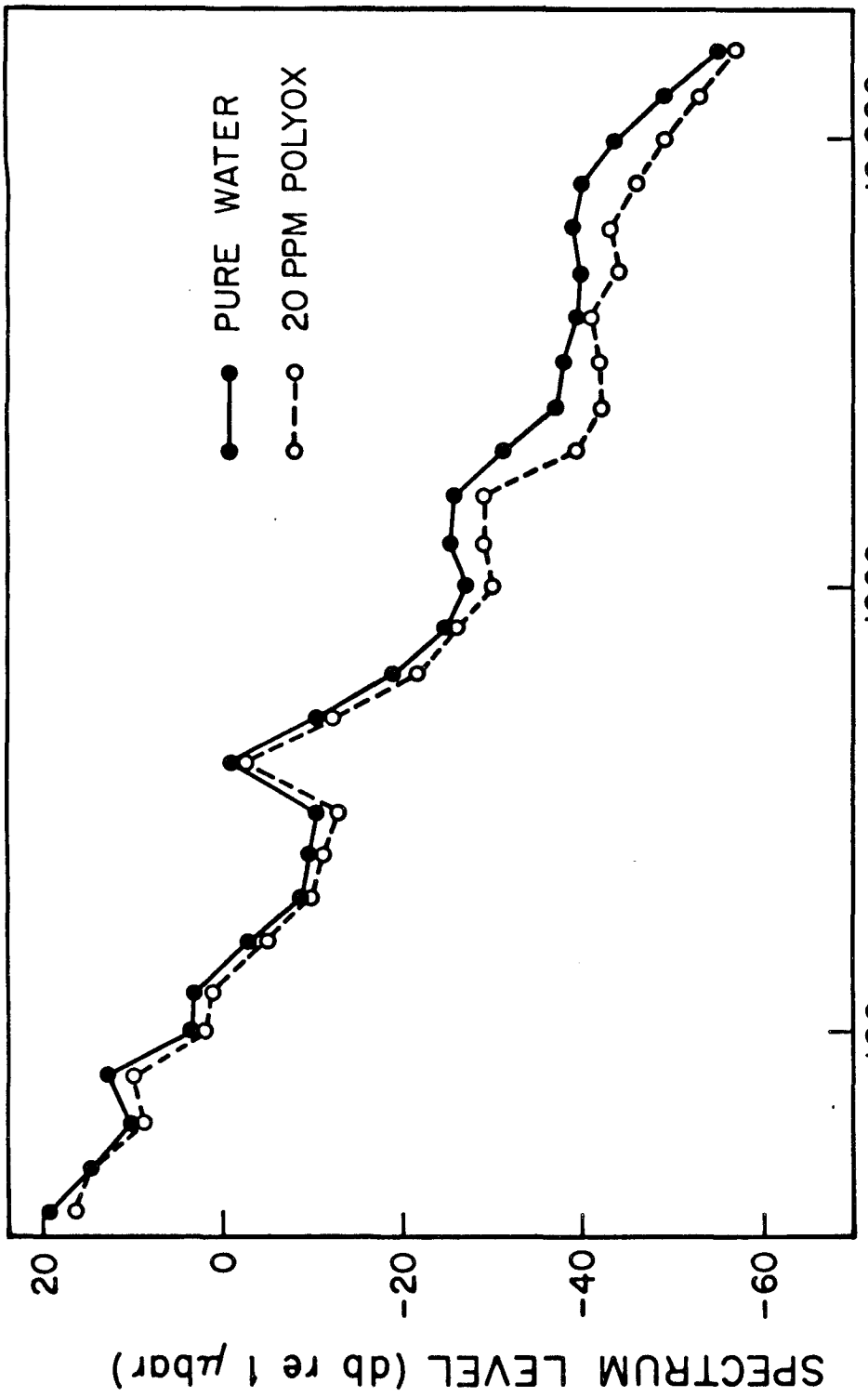

Figure 28. Radiated noise spectra of water and 20 ppm polyox.

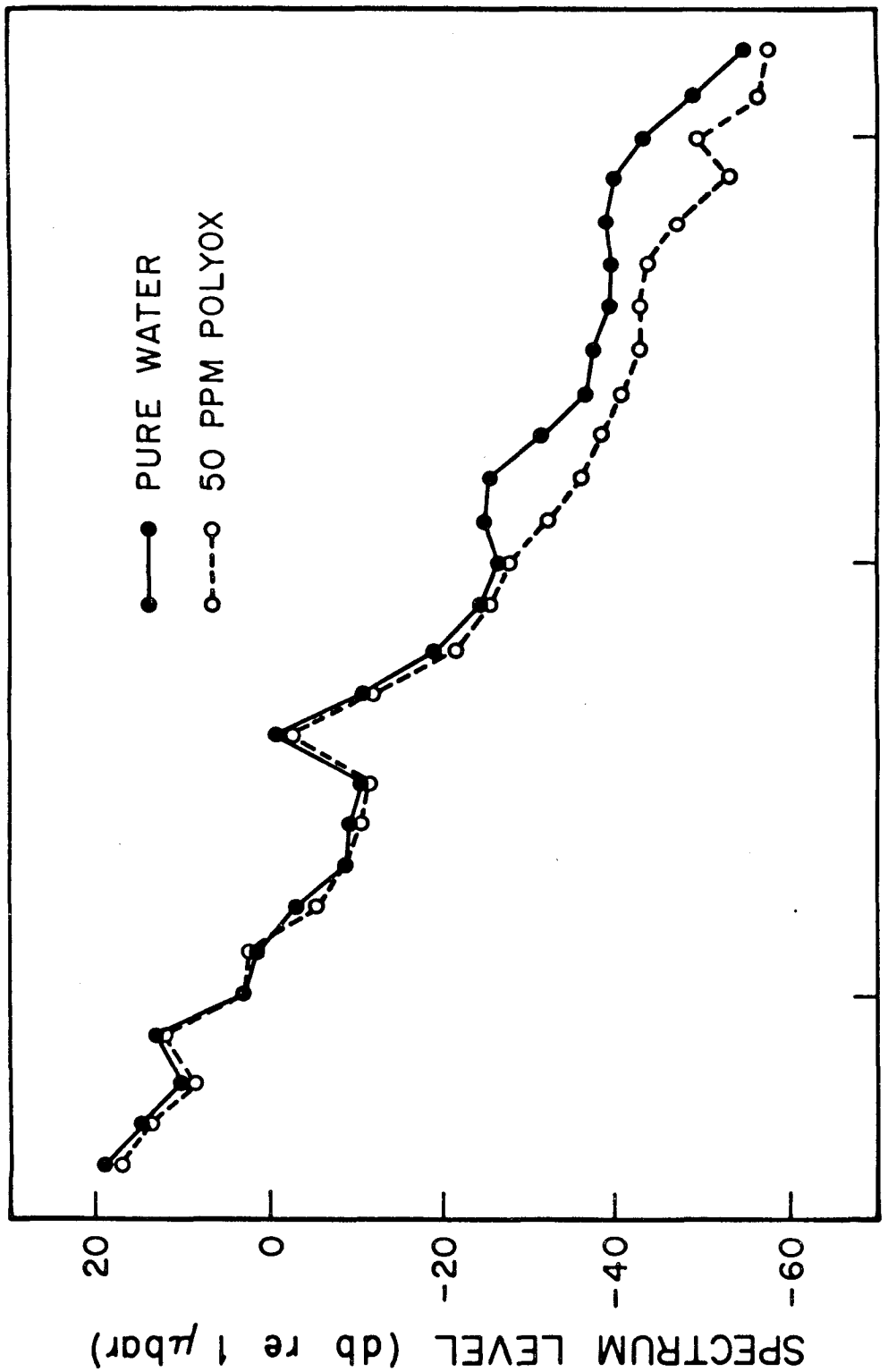

Figure 29. Radiated noise spectra of water and 50 ppm polyox.

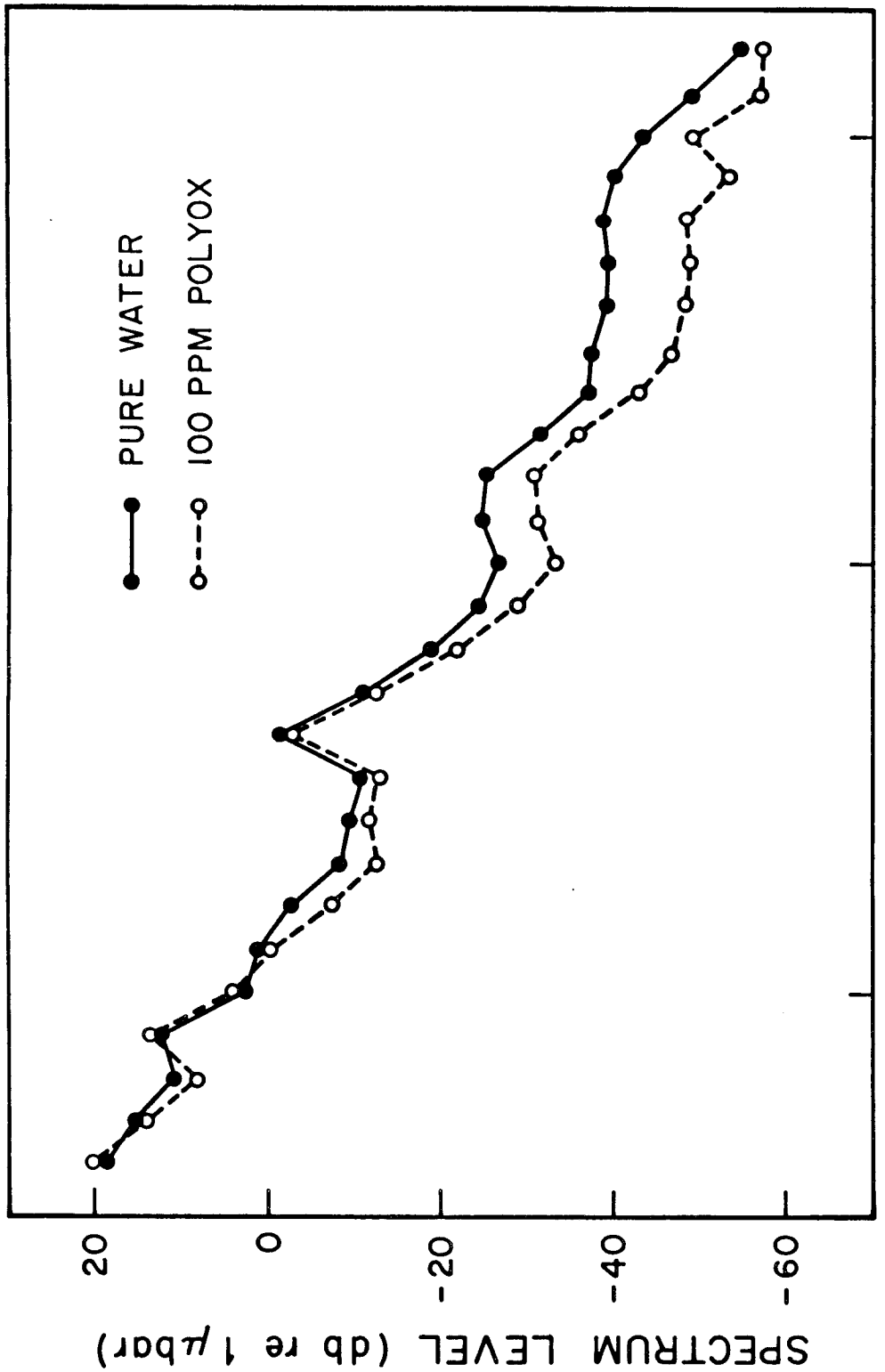

Figure 30. Radiated noise spectra of water and 100 ppm polyox.

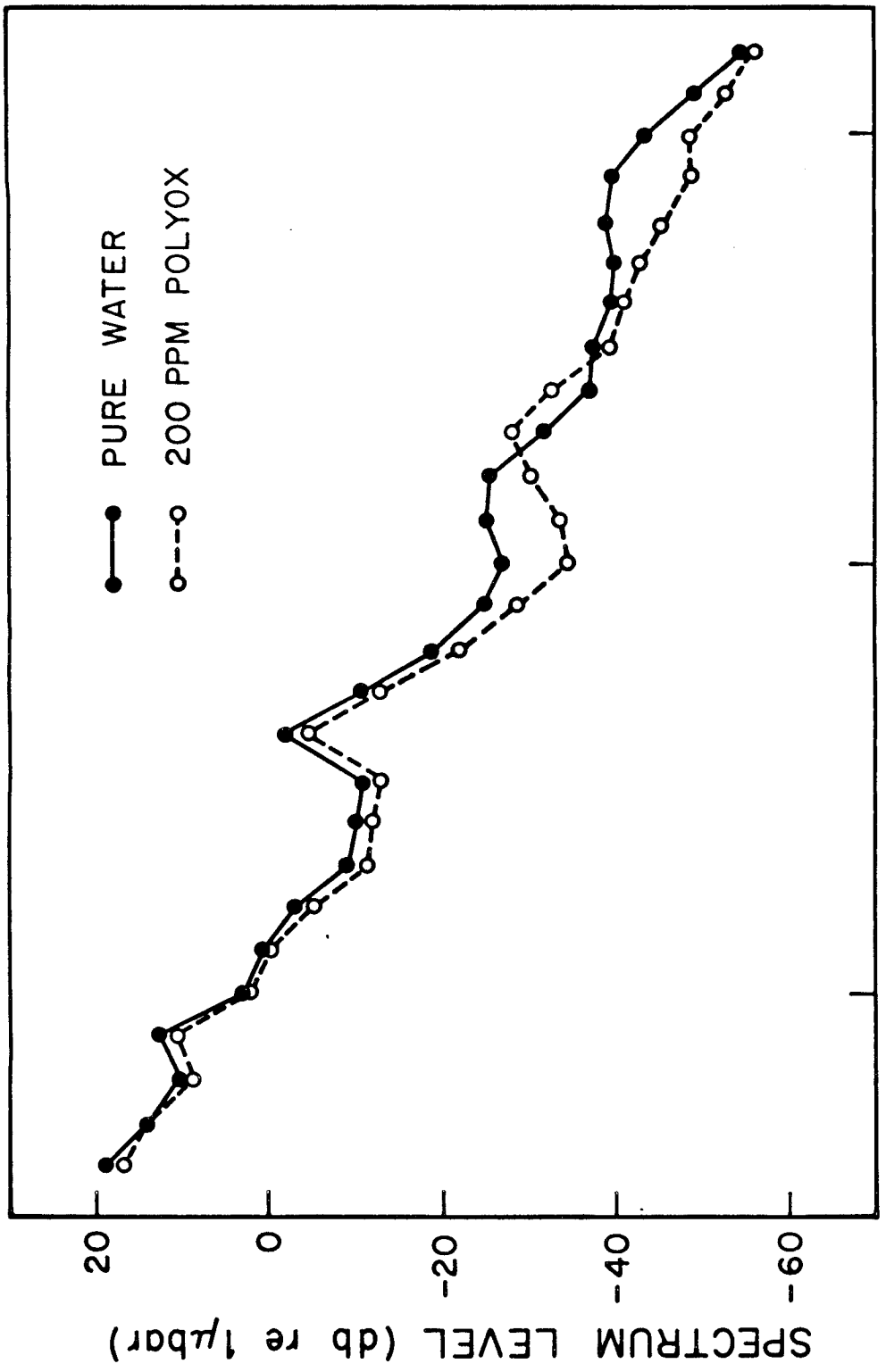

Figure 31. Radiated noise spectra of water and 200 ppm polyox.

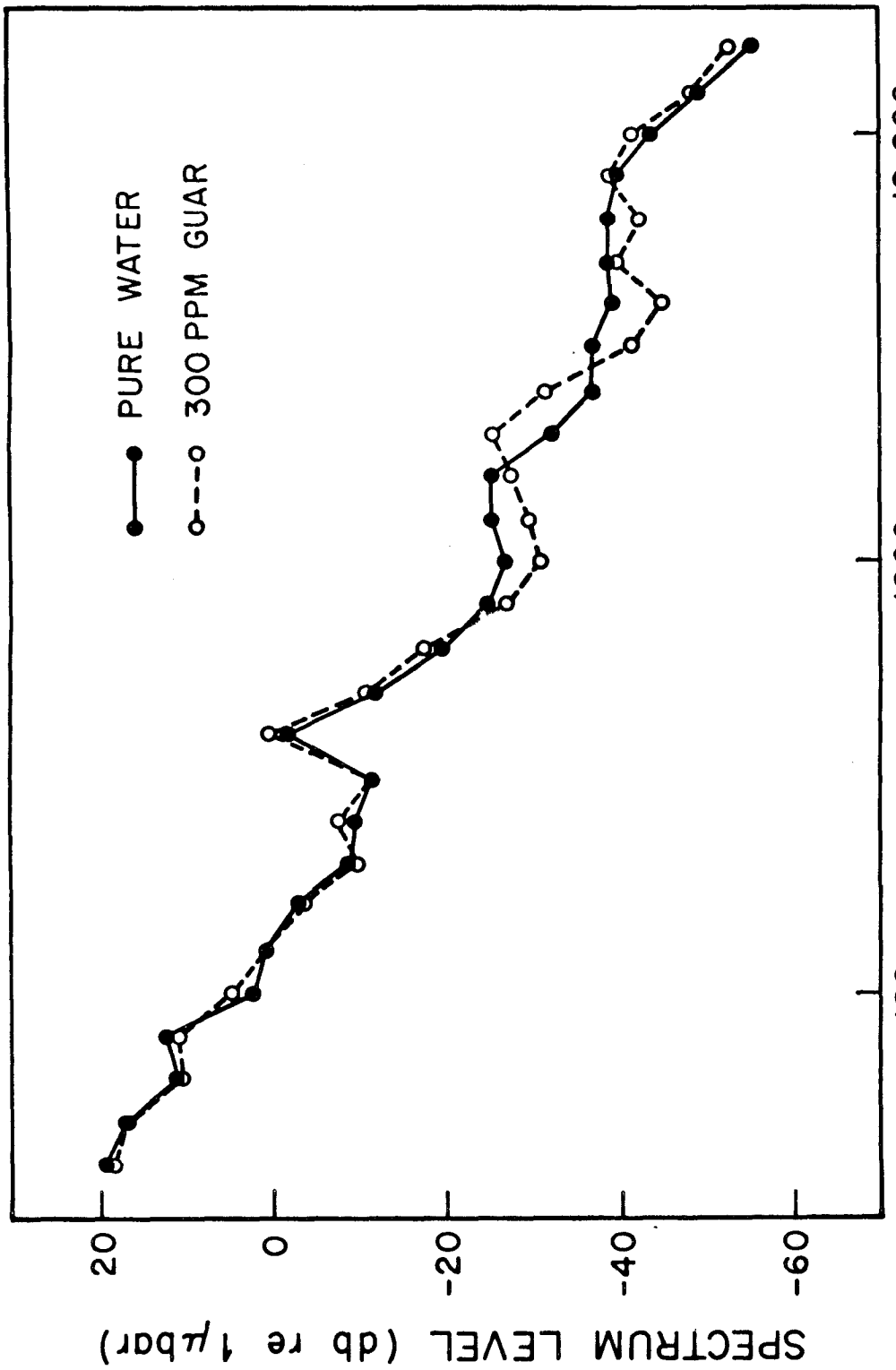

Figure 32. Radiated noise spectra of water and 300 ppm guar.

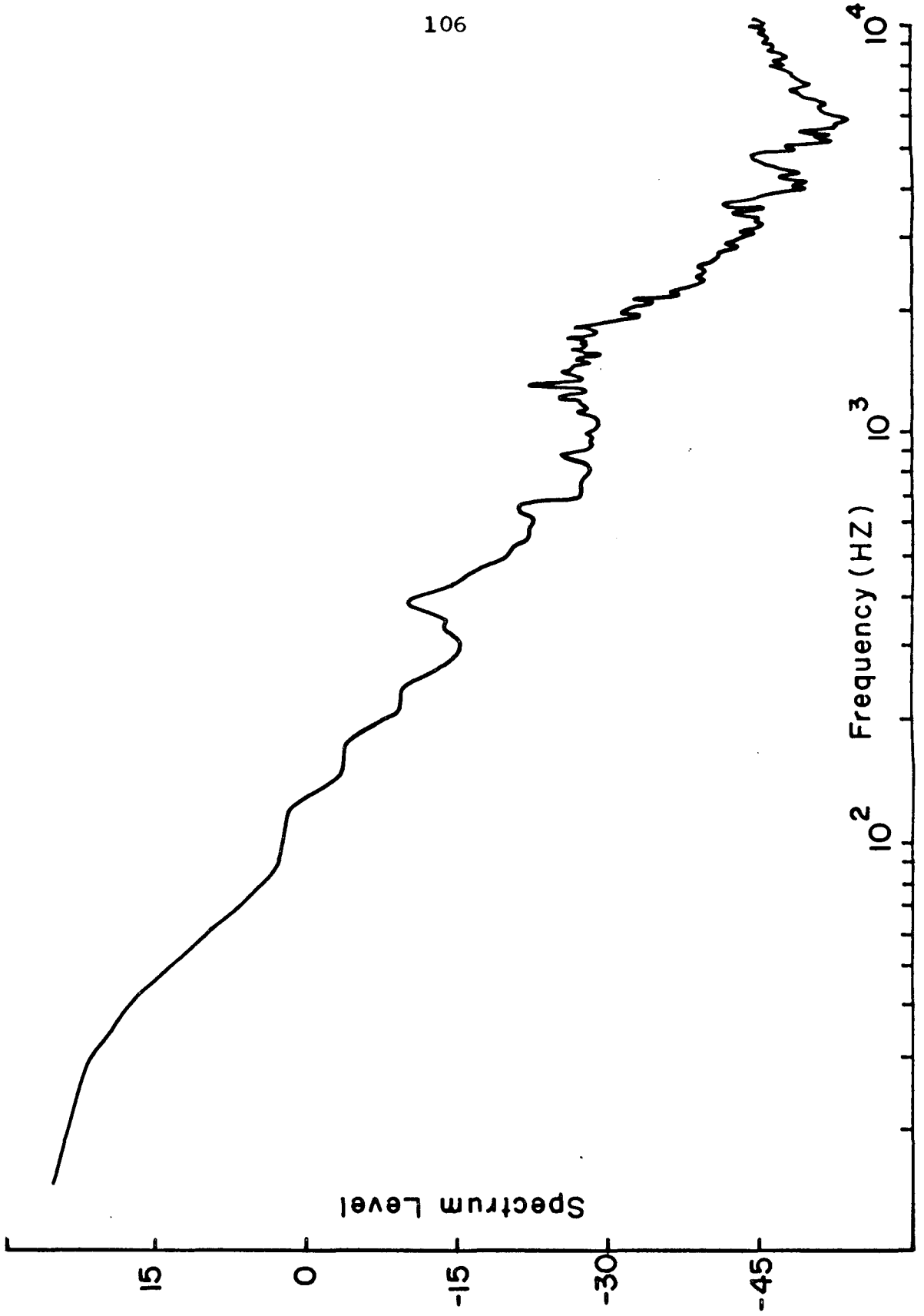

Figure 33. Typical digital noise spectrum with ensemble averaging.

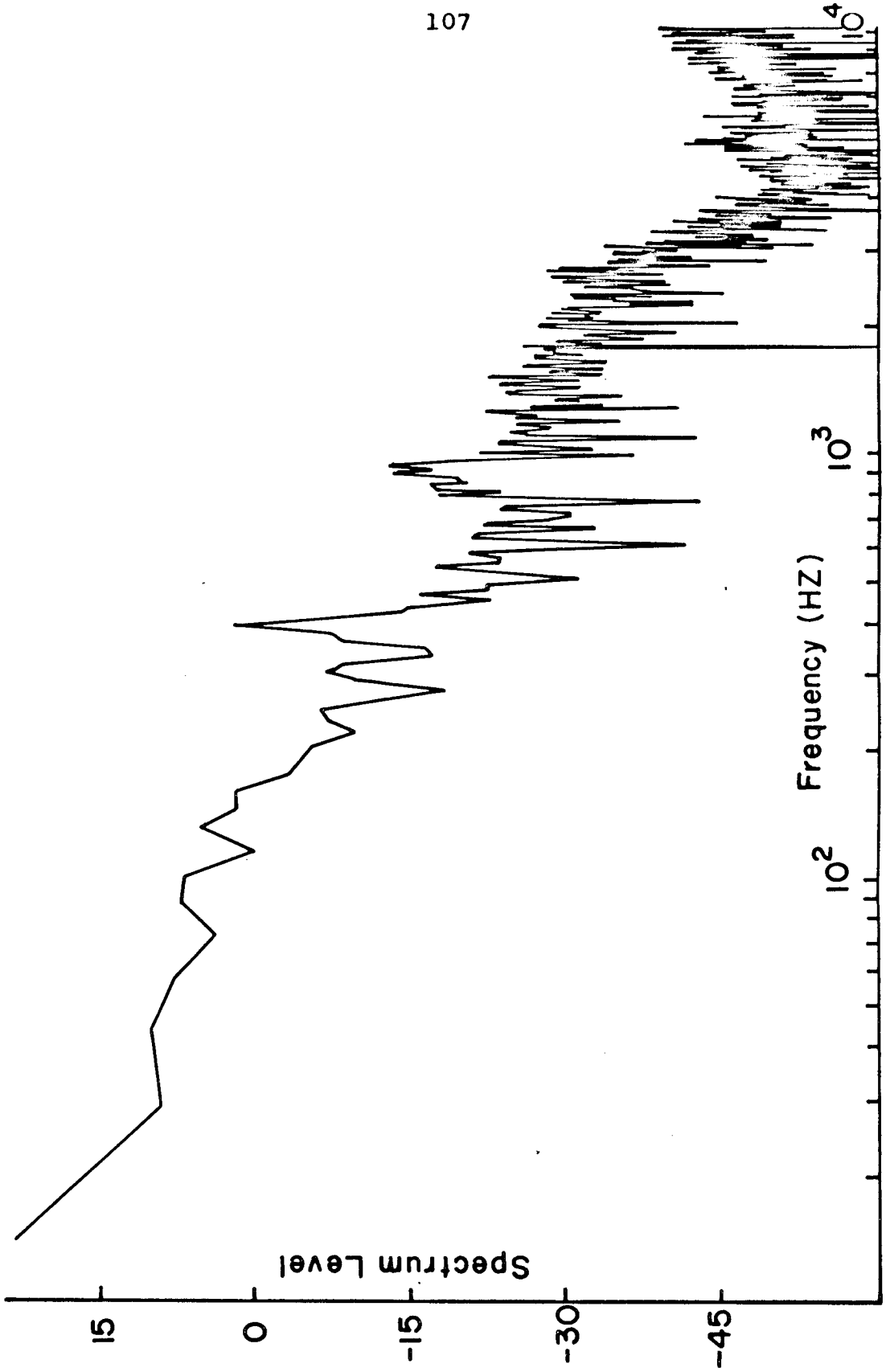

Figure 34. Digital noise spectrum without ensemble averaging.

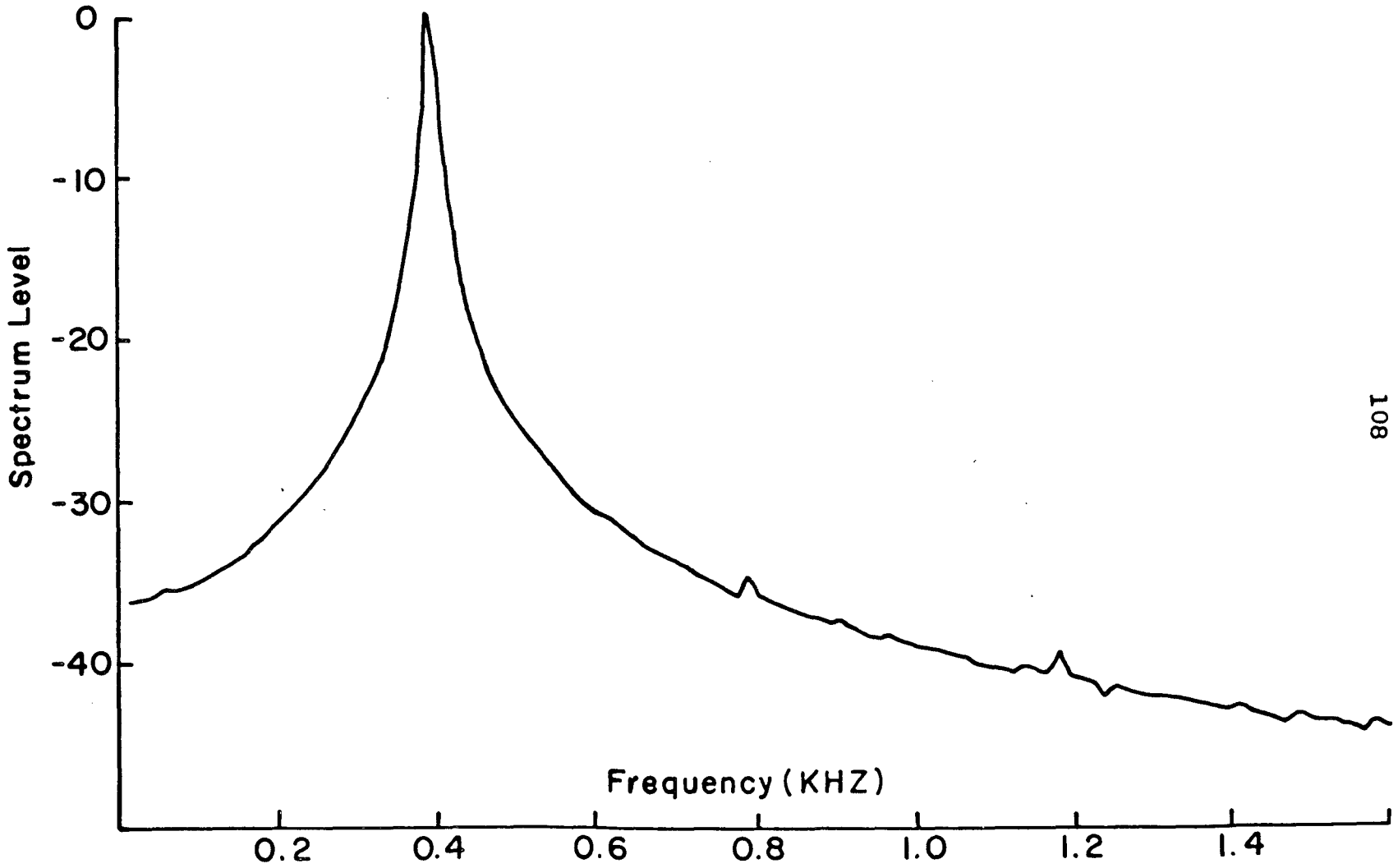

Figure 35. Digital spectrum of 400 Hz sine wave.

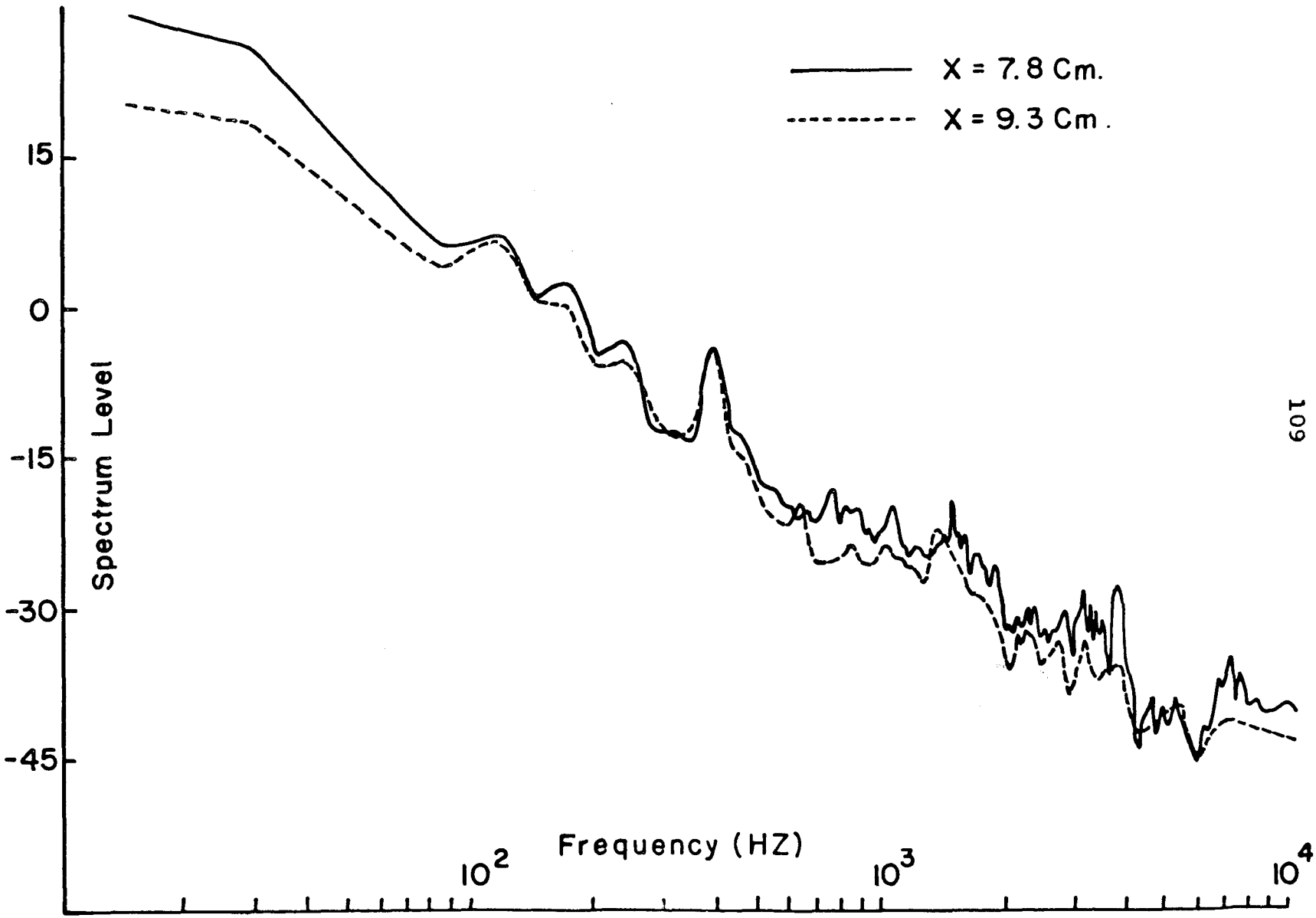

Figure 36. Pure water noise spectra: y = 2.5 cm; x = 7.8, 9.3 cm.

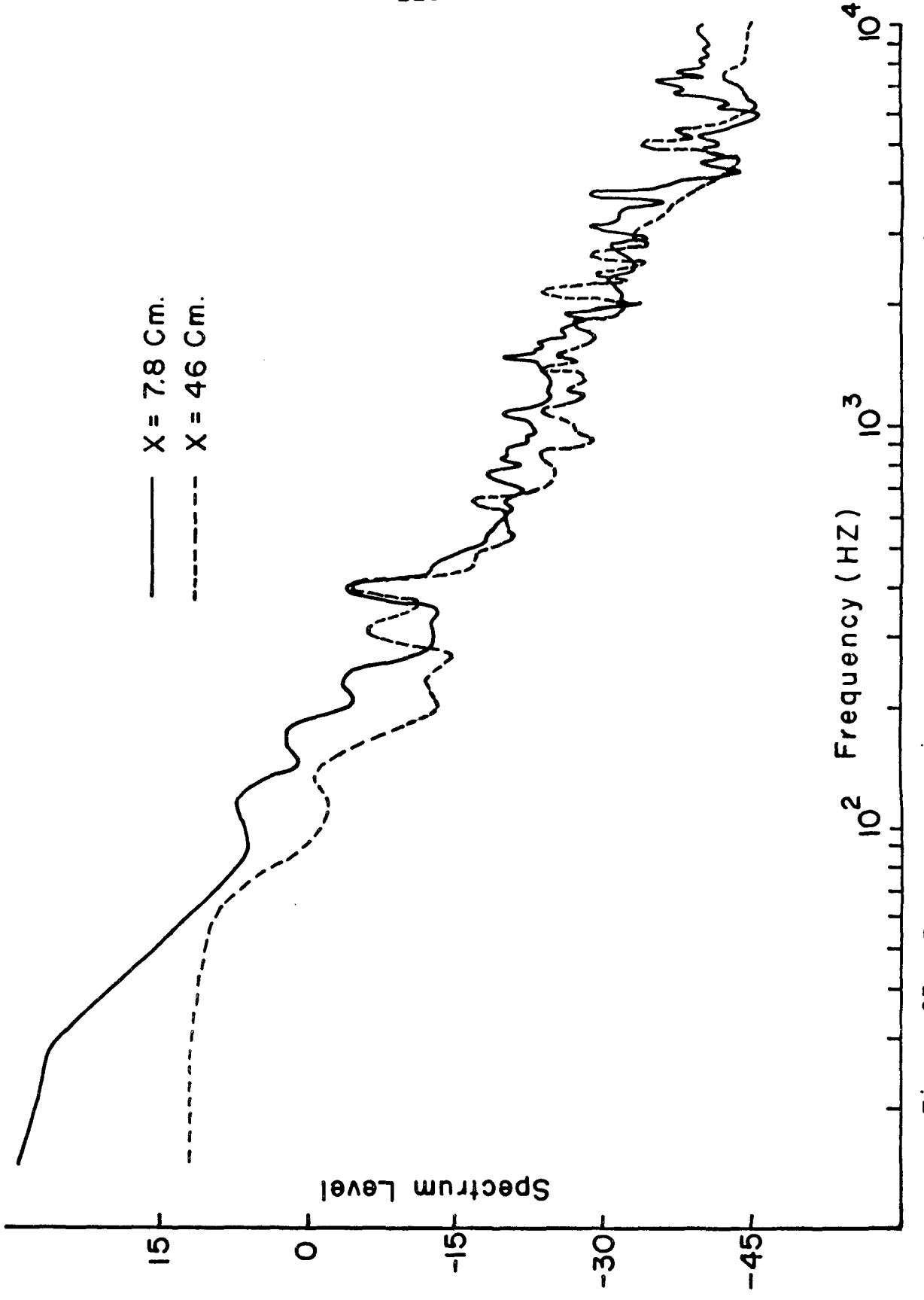

Figure 37. Pure water noise spectra: y = 2.5 cm; x = 7.8, 46 cm.

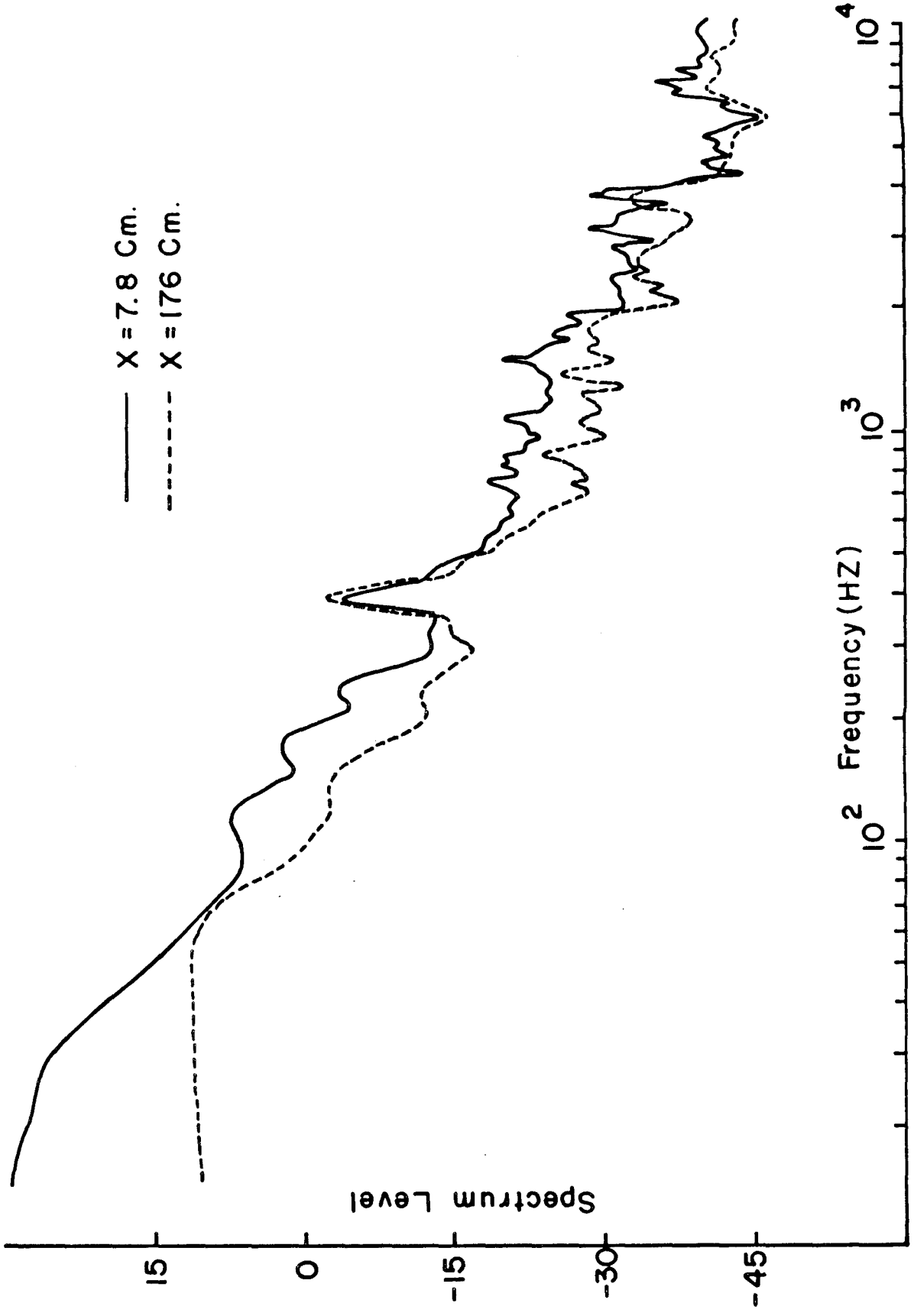

Figure 38. Pure water noise spectra: y = 2.5 cm; x = 7.8, 176 cm.

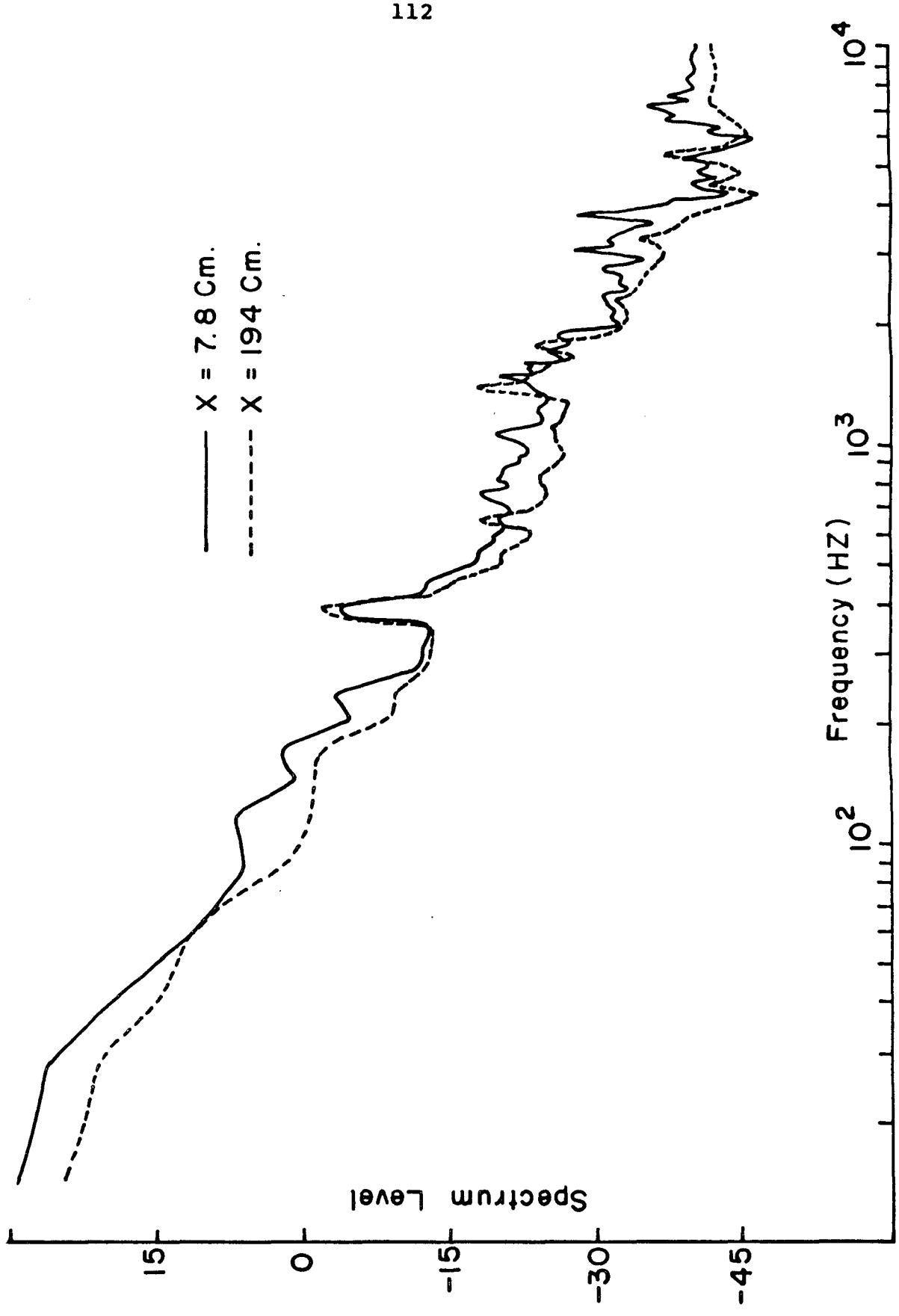

Figure 39. Pure water noise spectra: y = 2.5 cm; x = 7.8, 194 cm.

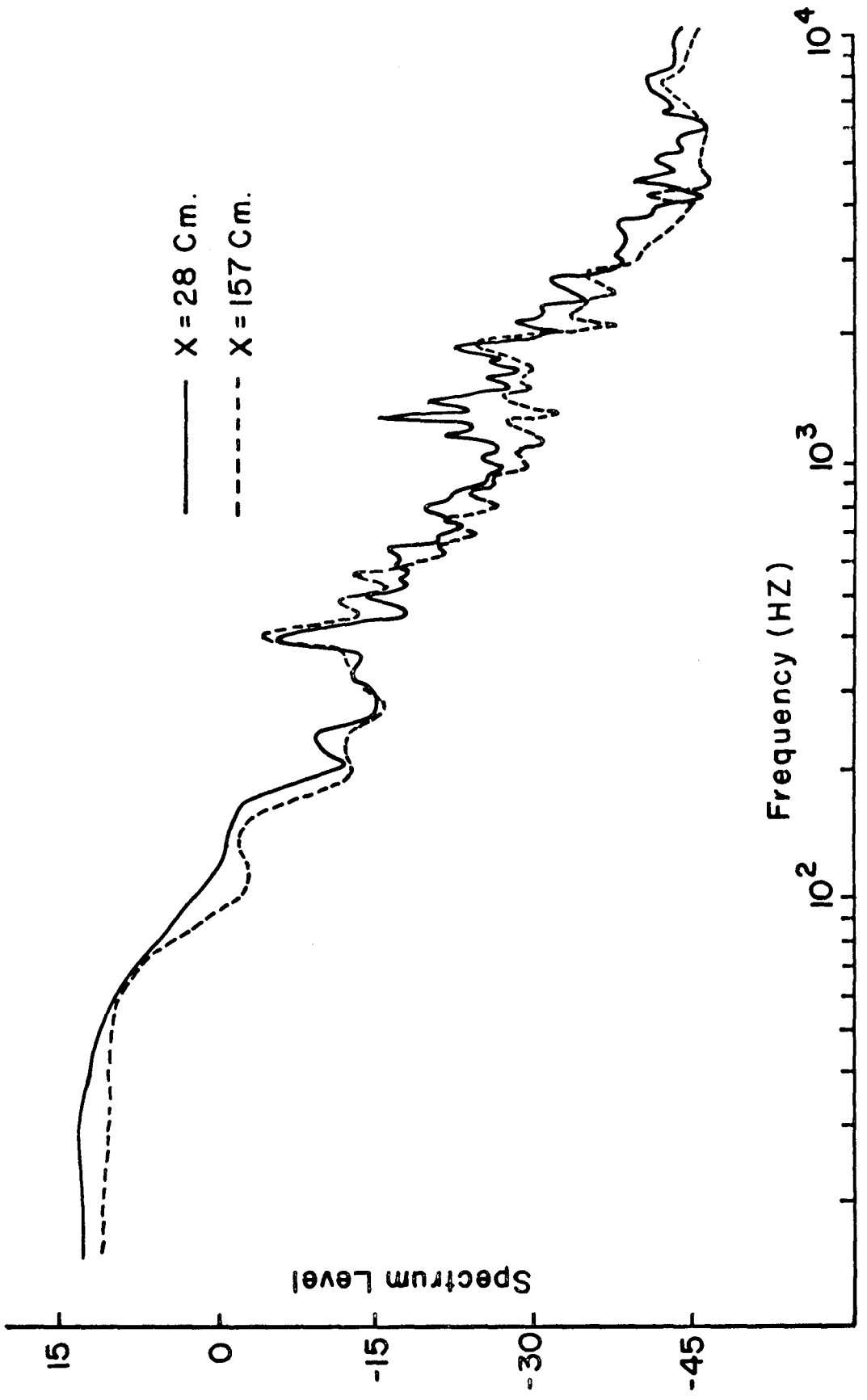

Figure 40. Pure water noise spectra: y = 2.5 cm; x = 28, 157 cm.

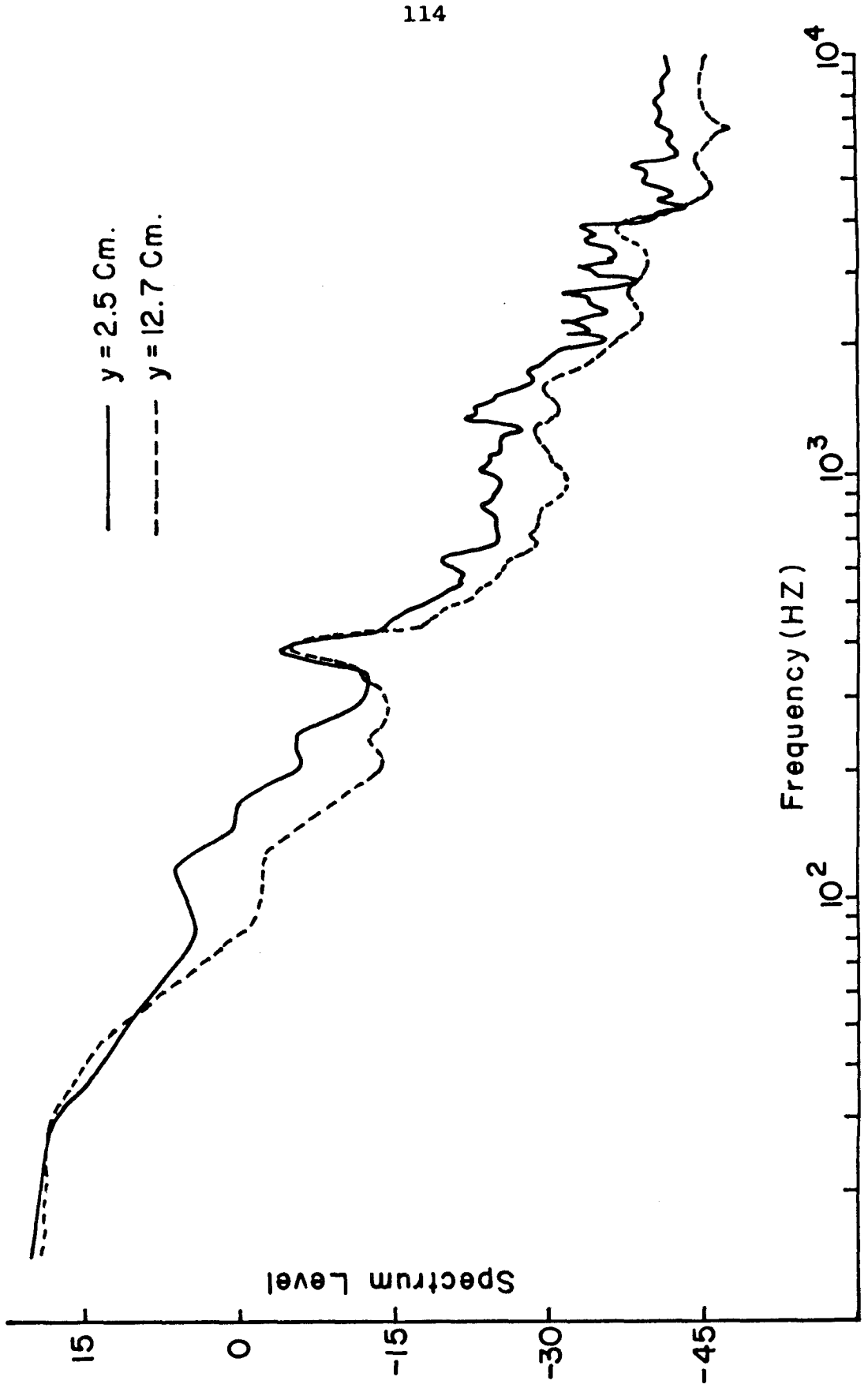

Figure 41. Pure water noise spectra: x = 9.3 cm; y = 2.5, 12.7 cm.

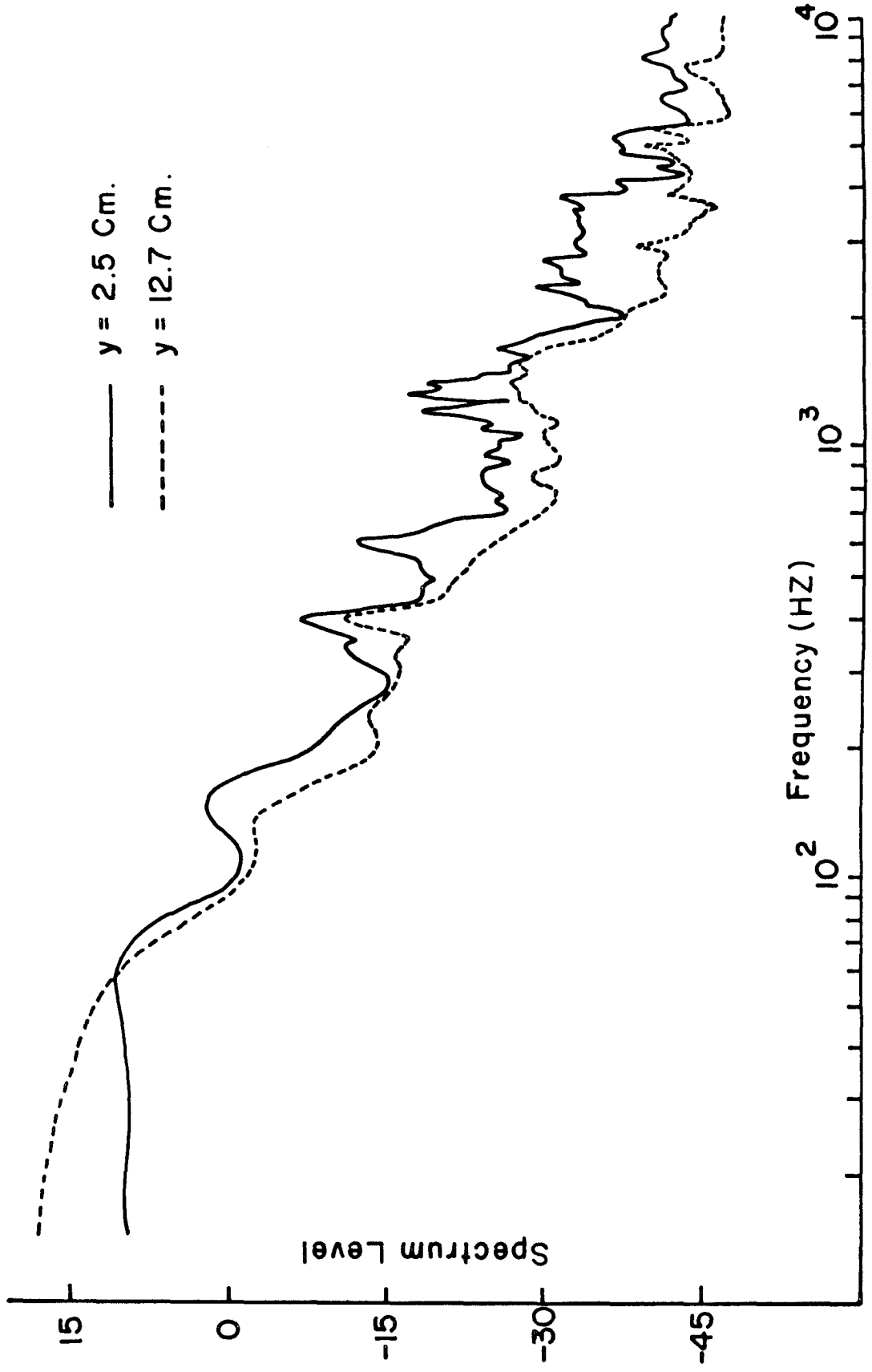

Figure 42. Pure water noise spectra: x = 83 cm; y = 2.5, 12.7 cm.

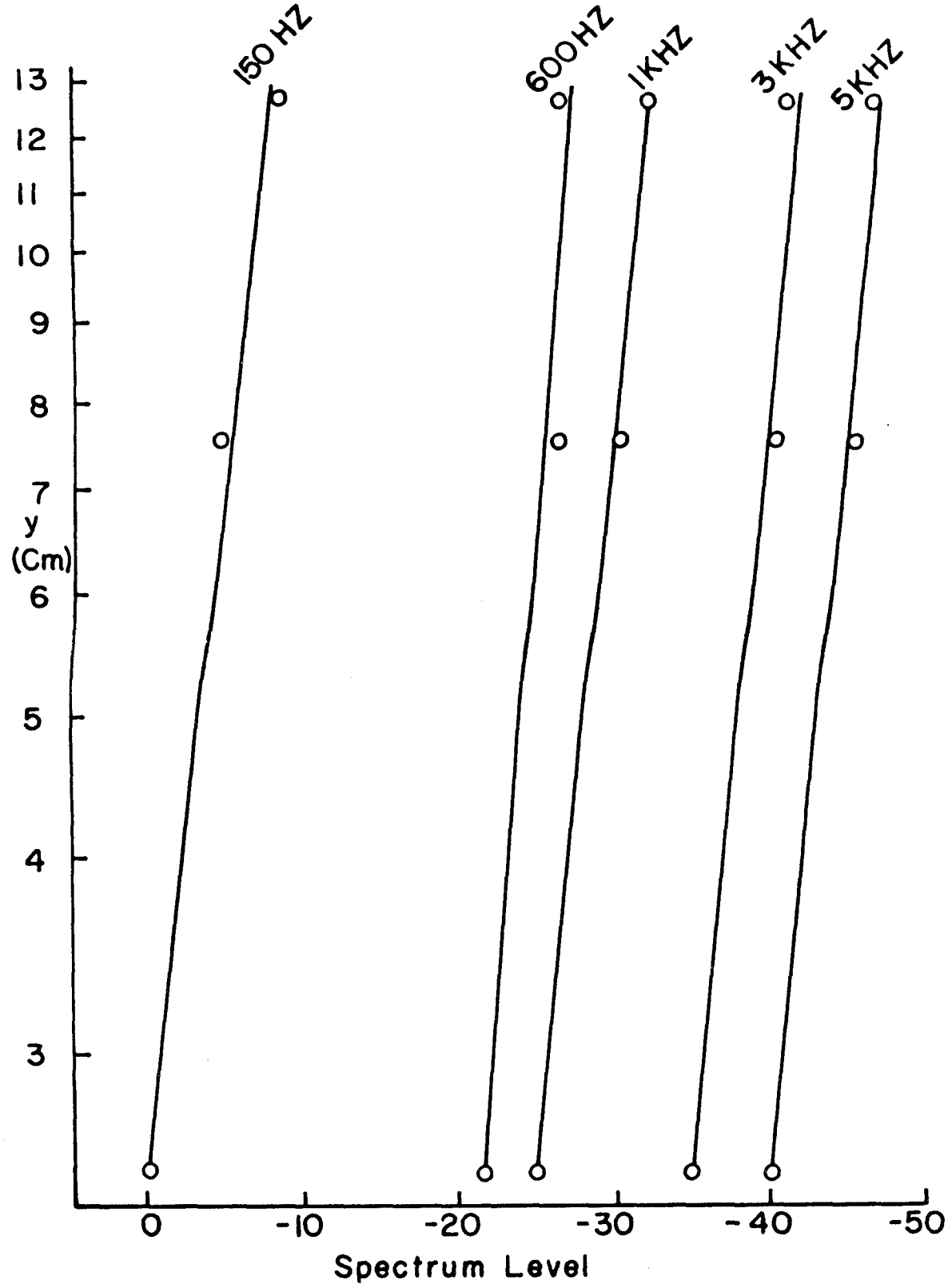

Figure 43. Noise spectrum level versus distance from wall.

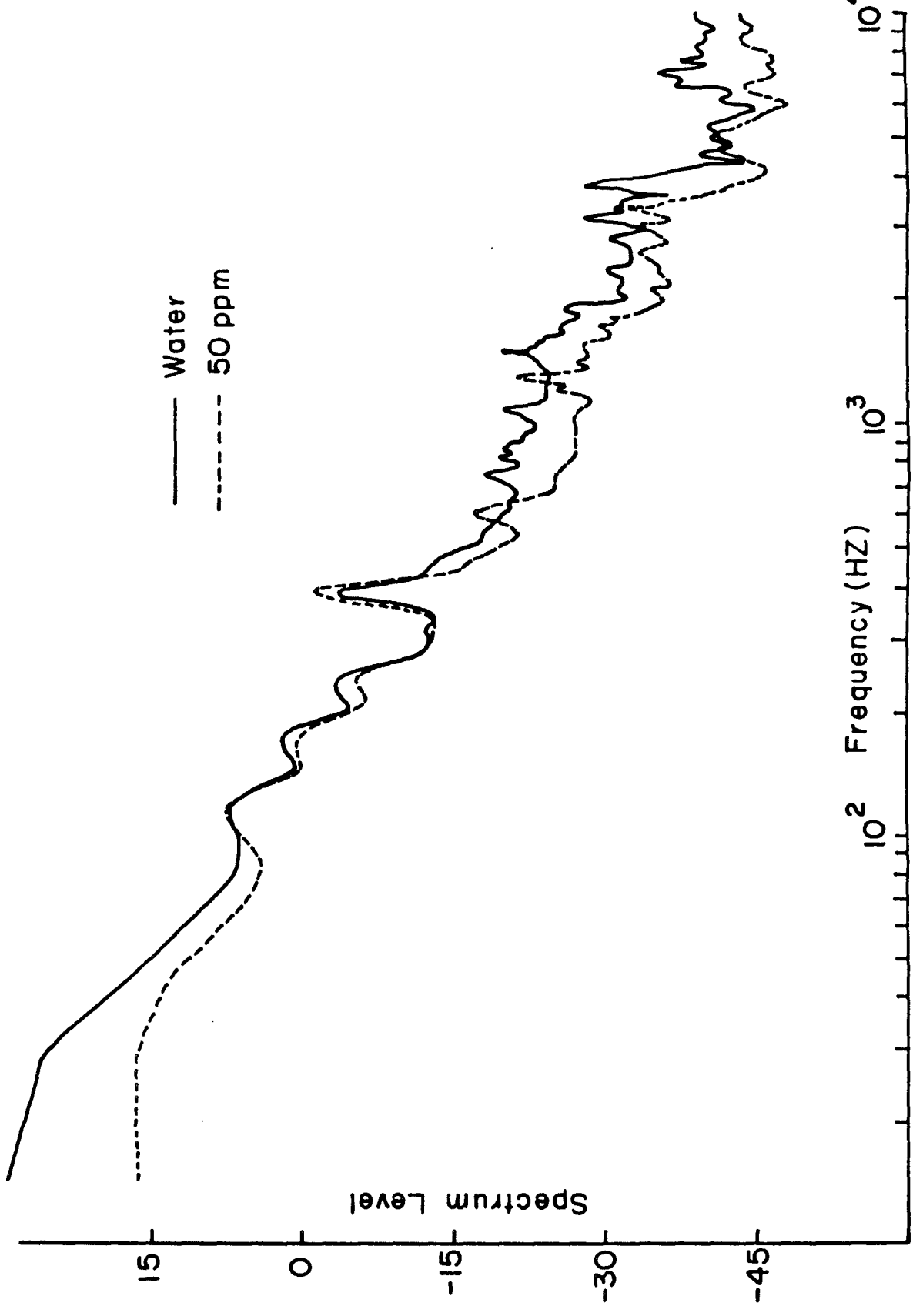

Figure 44. Noise spectra of water and 50 ppm polyox: y = 2.5 cm; x = 7.8 cm.

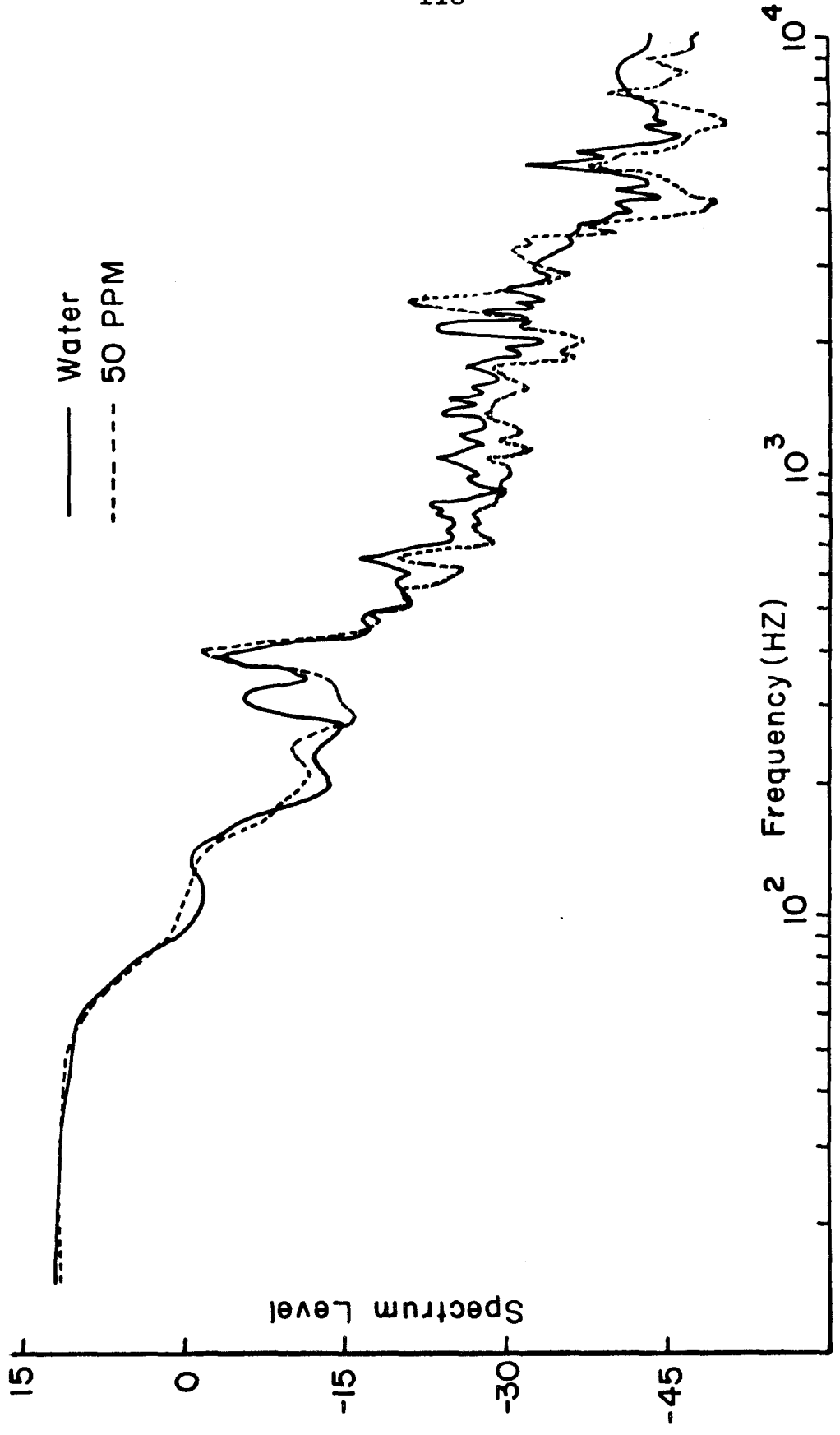

Figure 45. Noise spectra of water and 50 ppm polyox: y = 2.5 cm; x = 46 cm.

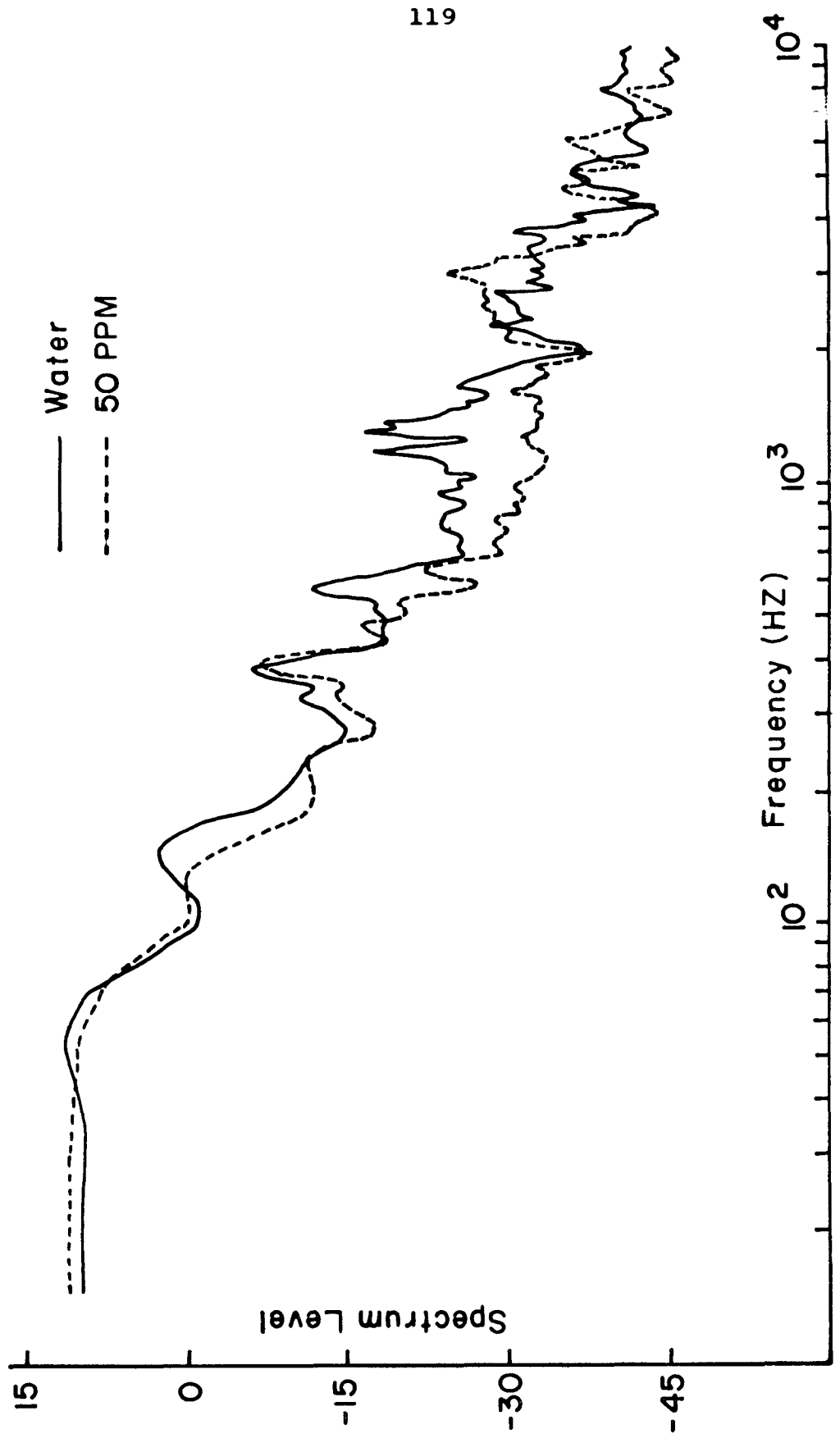

Figure 46. Noise spectra of water and 50 ppm polyox: y = 2.5 cm; x = 83 cm.

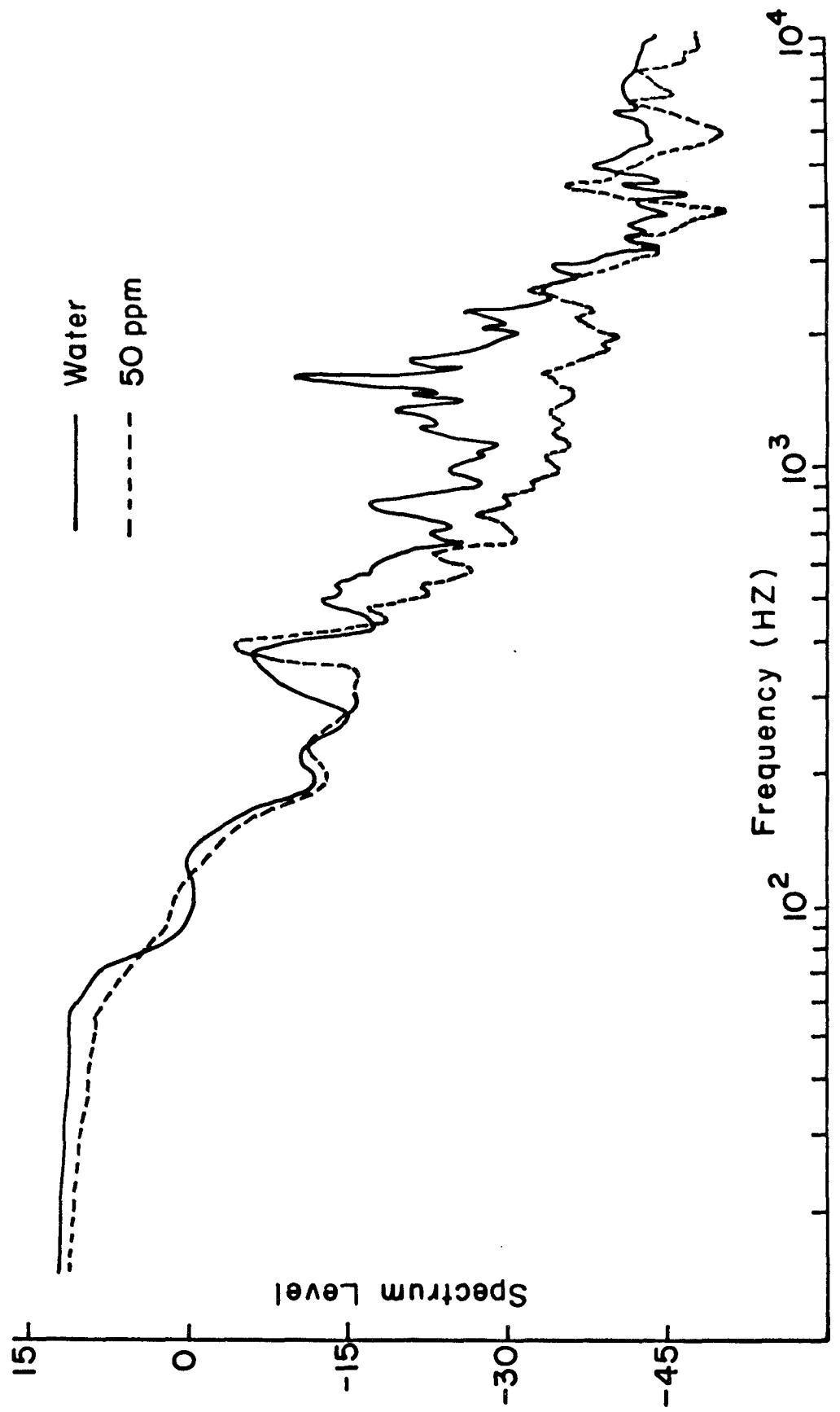

Figure 47. Noise spectra of water and 50 ppm polyox: y = 2.5 cm; x = 120 cm.

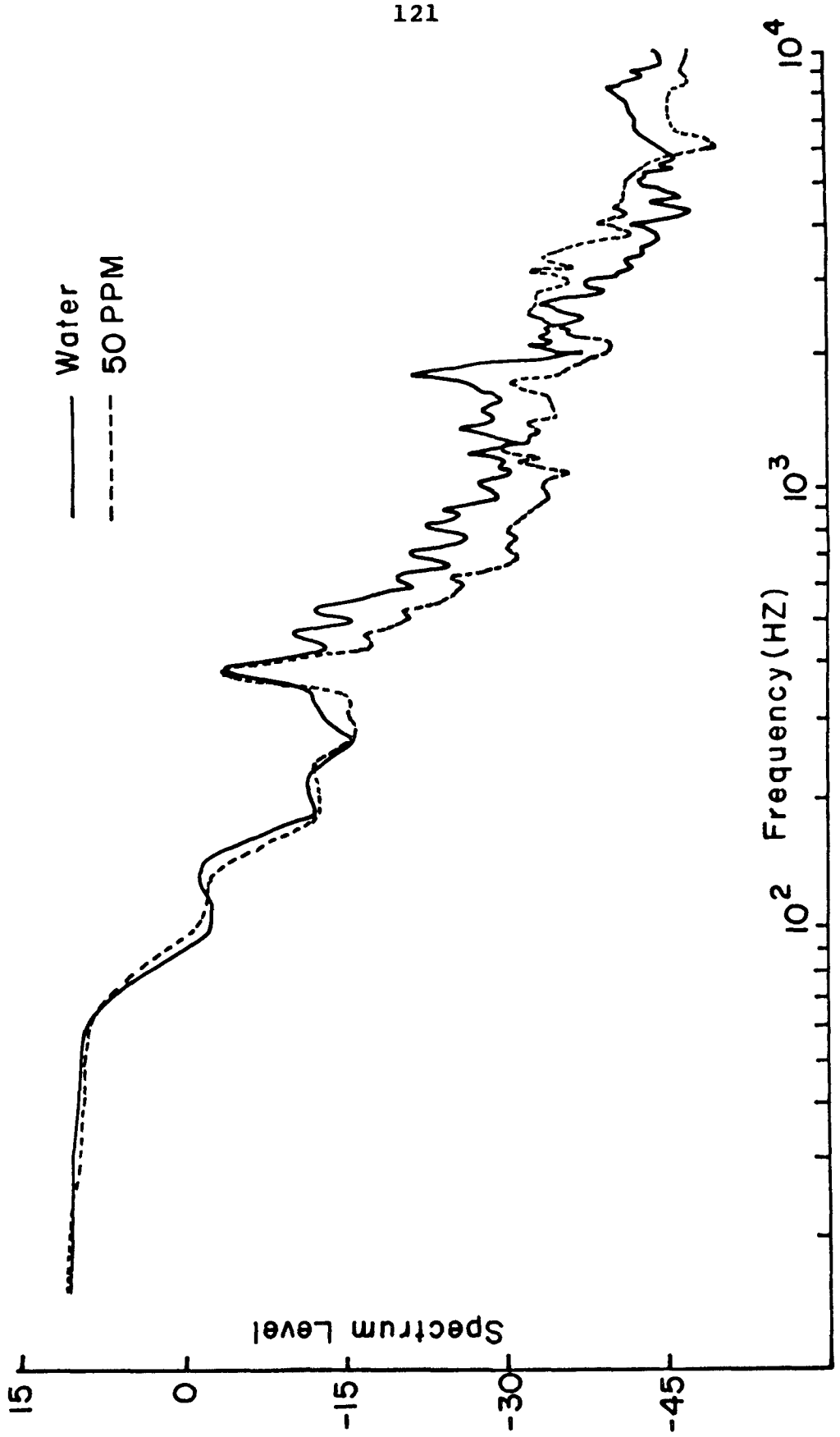

Figure 48. Noise spectra of water and 50 ppm polyox: y = 2.5 cm; x = 157 cm.

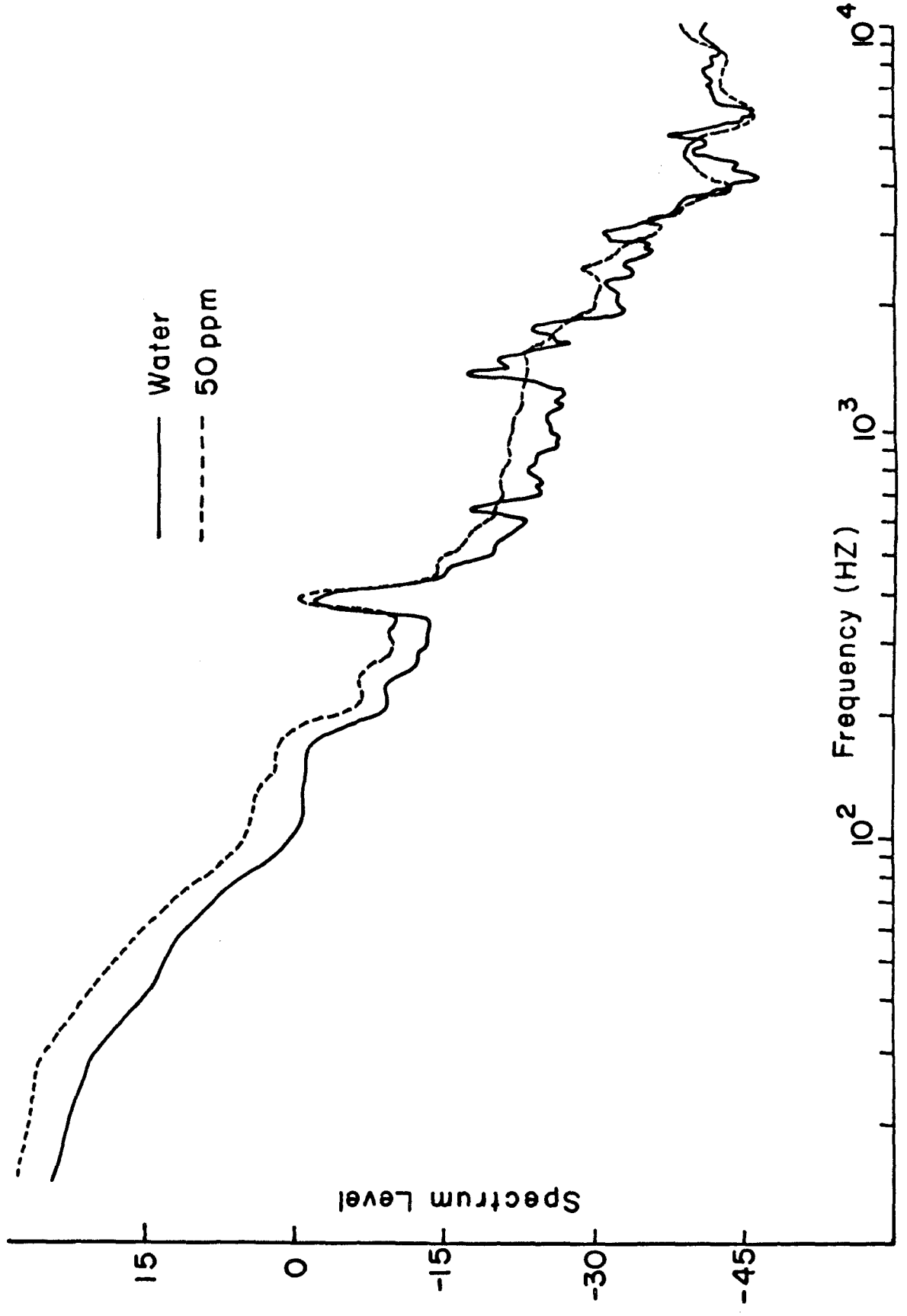

Figure 49. Noise spectra of water and 50 ppm polyox: y = 2.5 cm; x = 194 cm.

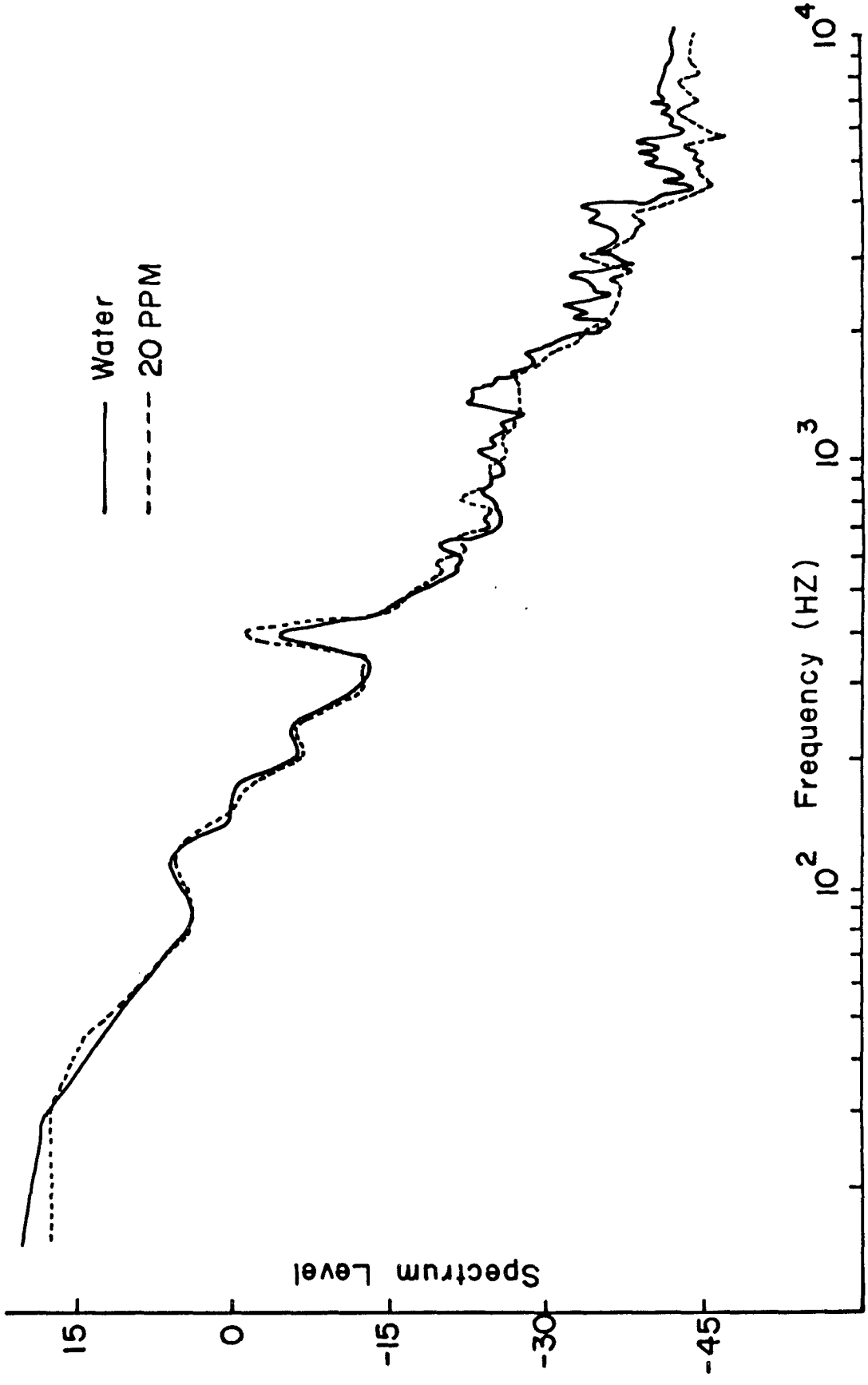

Figure 50. Noise spectra of water and 20 ppm polyox: y = 2.5 cm; x = 9.3 cm.

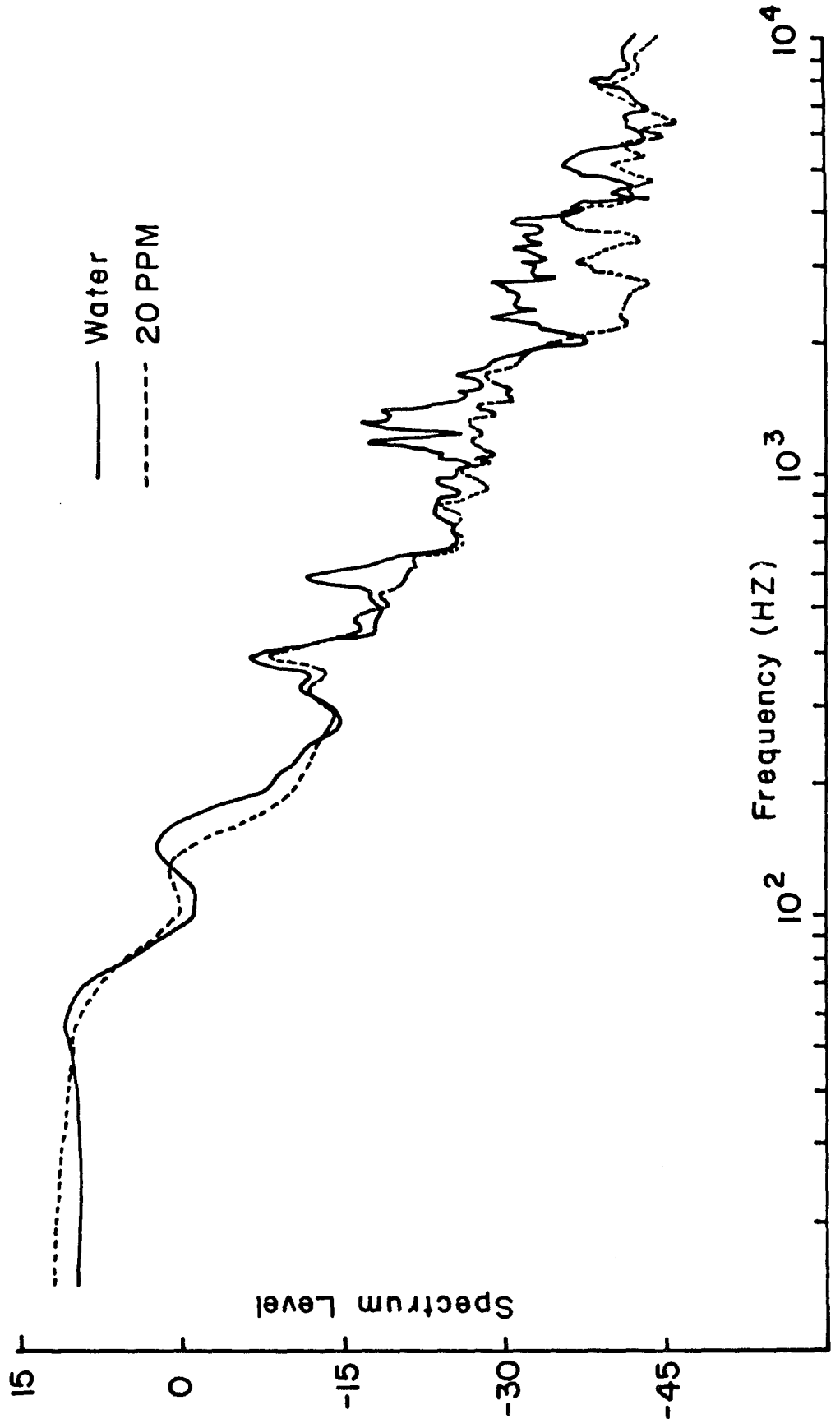

Figure 51. Noise spectra of water and 20 ppm polyox: y = 2.5 cm; x = 83 cm.

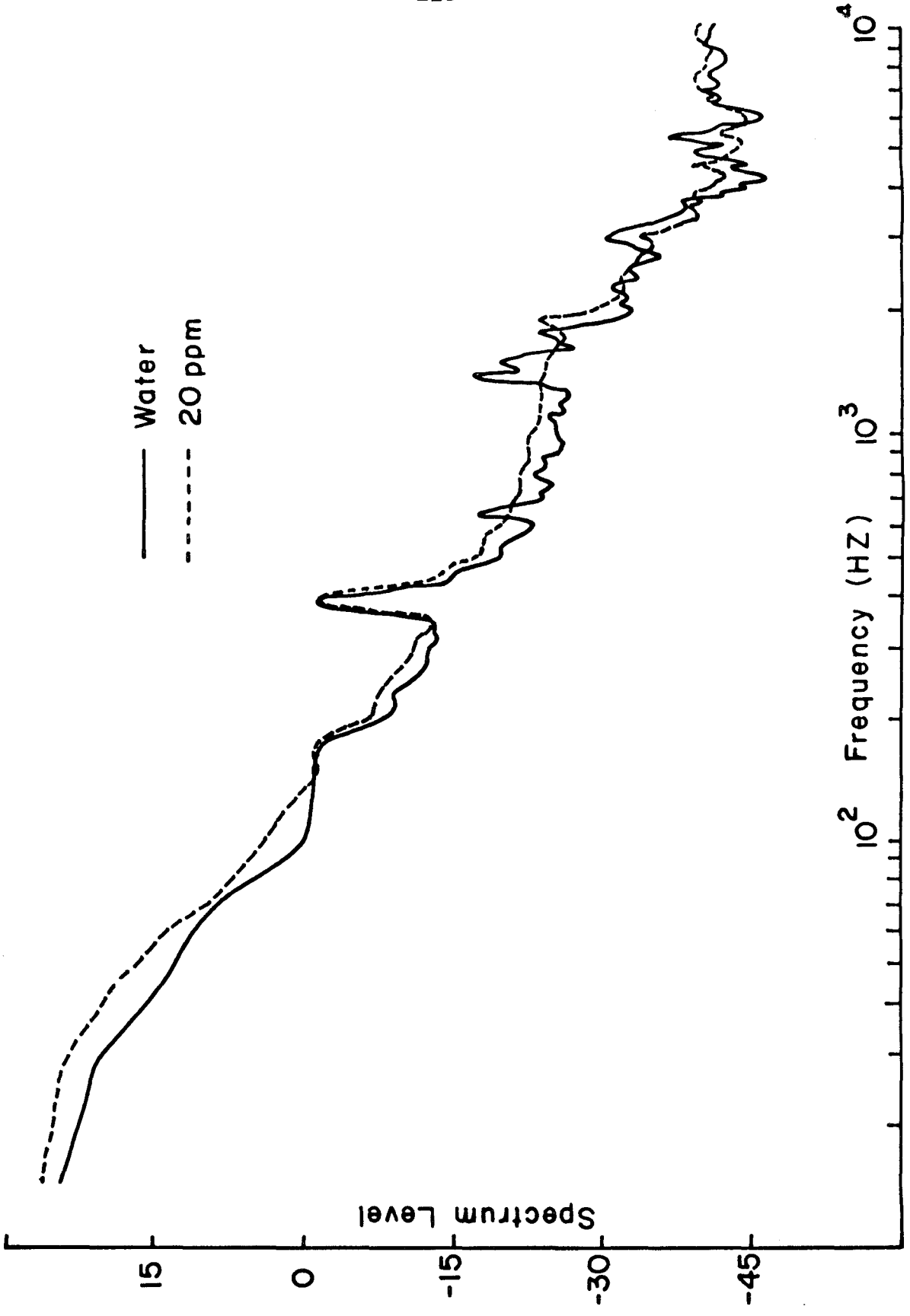

Figure 52. Noise spectra of water and 20 ppm polyox: y = 2.5 cm; x = 194 cm.

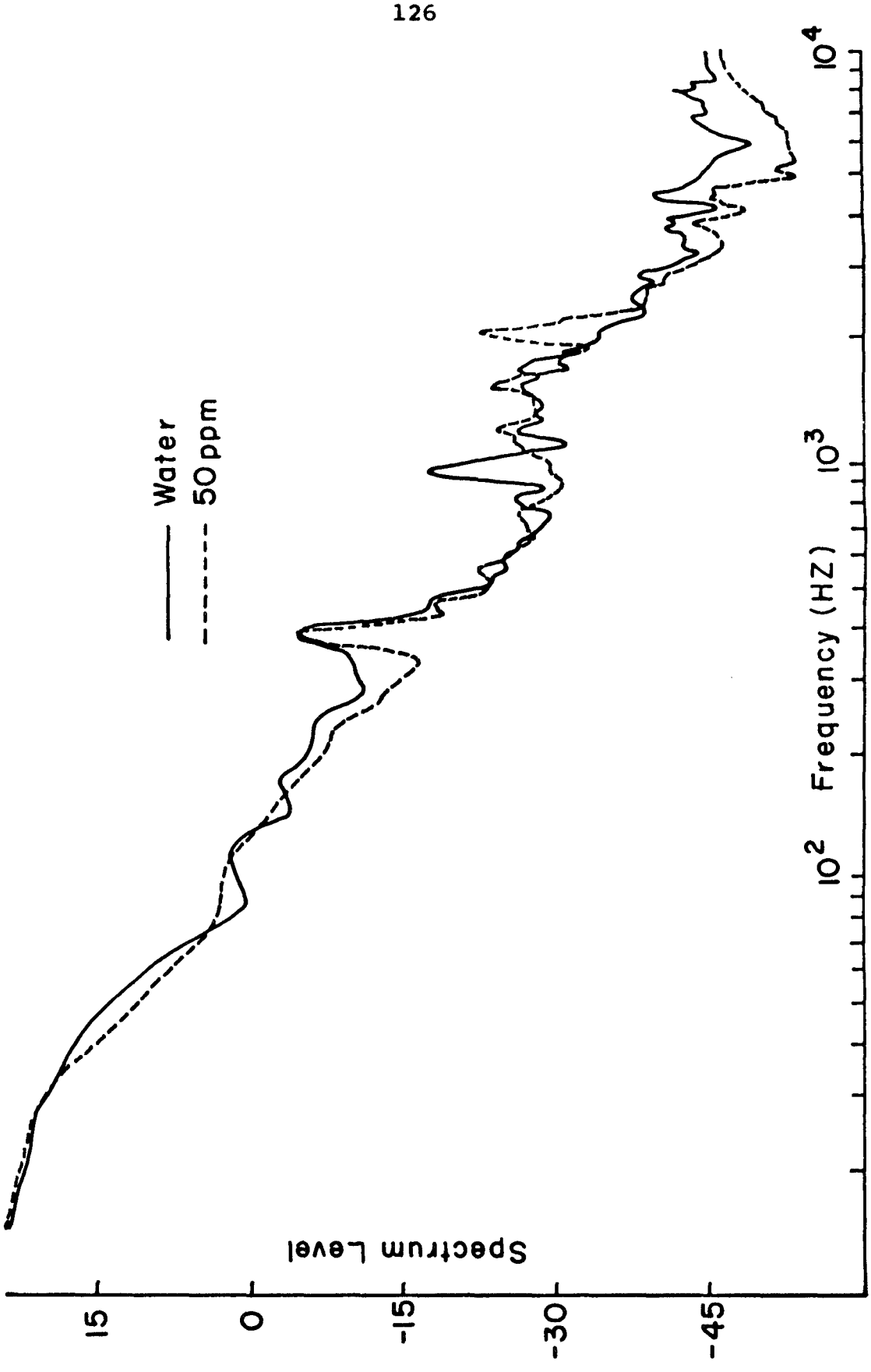

Figure 53. Noise spectra of water and 50 ppm polyox: y = 5.1 cm; x = 9.3 cm.

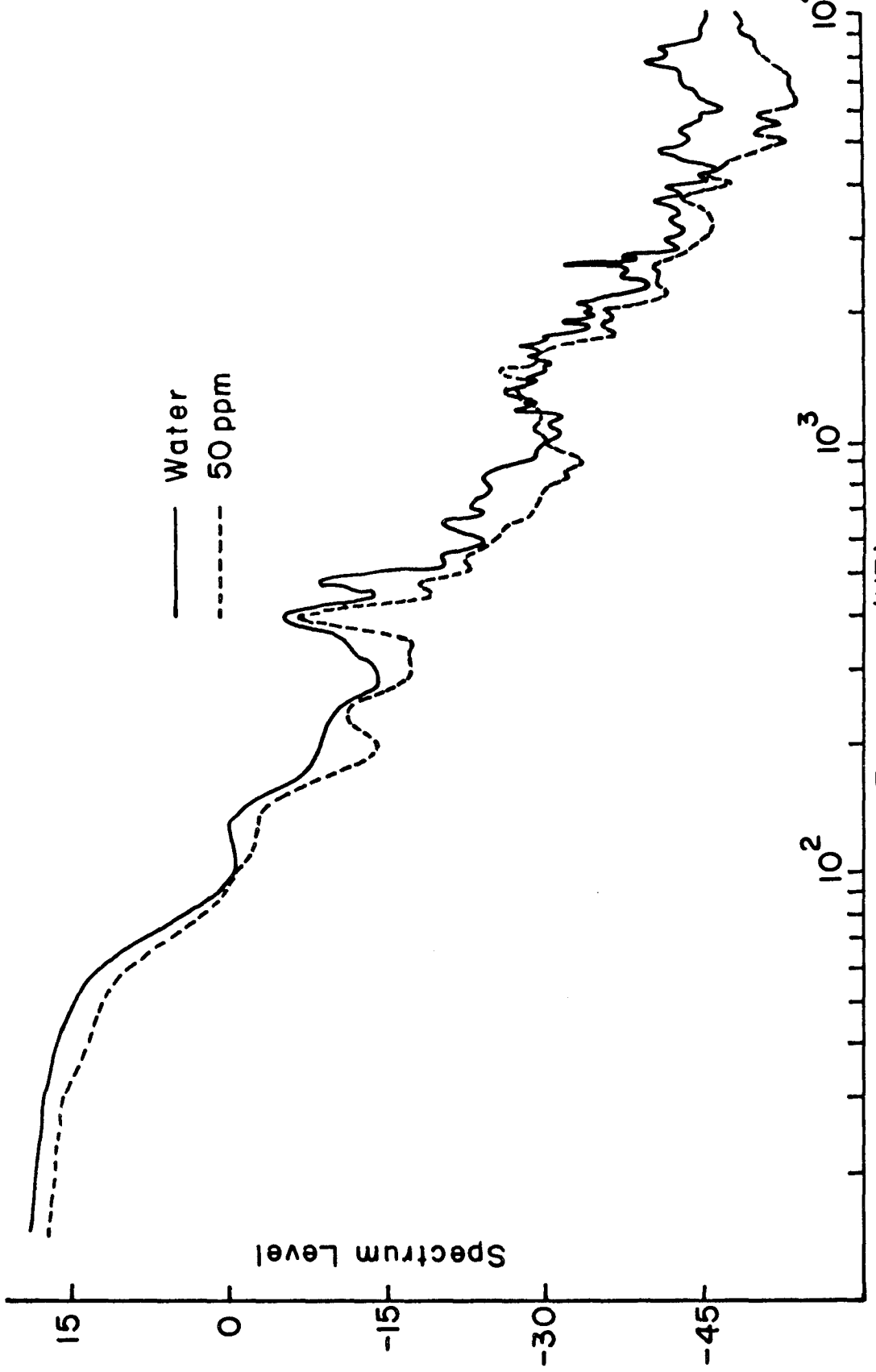

Figure 54. Noise spectra of water and 50 ppm polyox: y = 5.1 cm; x = 46 cm.

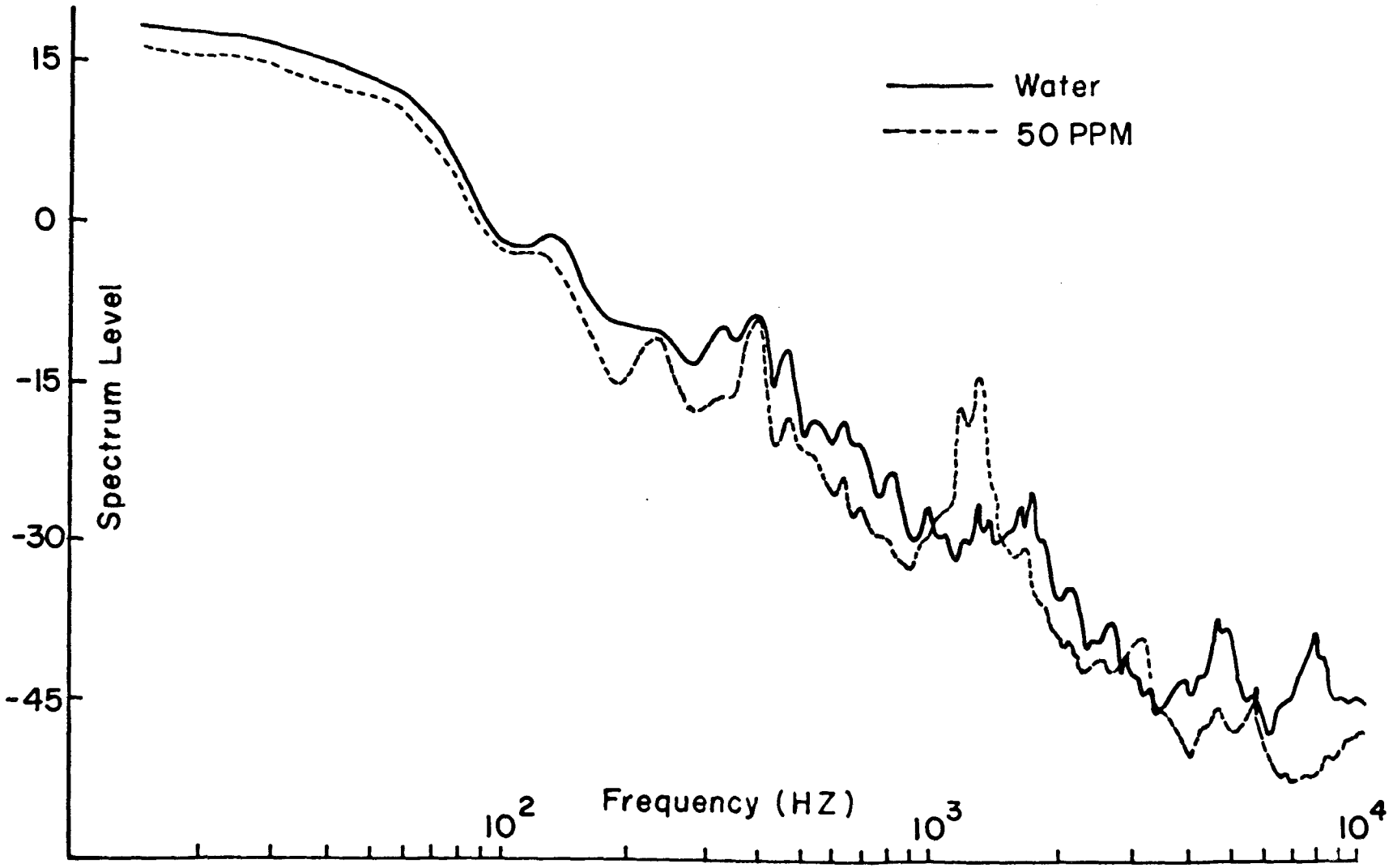

Figure 55. Noise spectra of water and 50 ppm polyox: y = 5.1 cm; x = 83 cm.

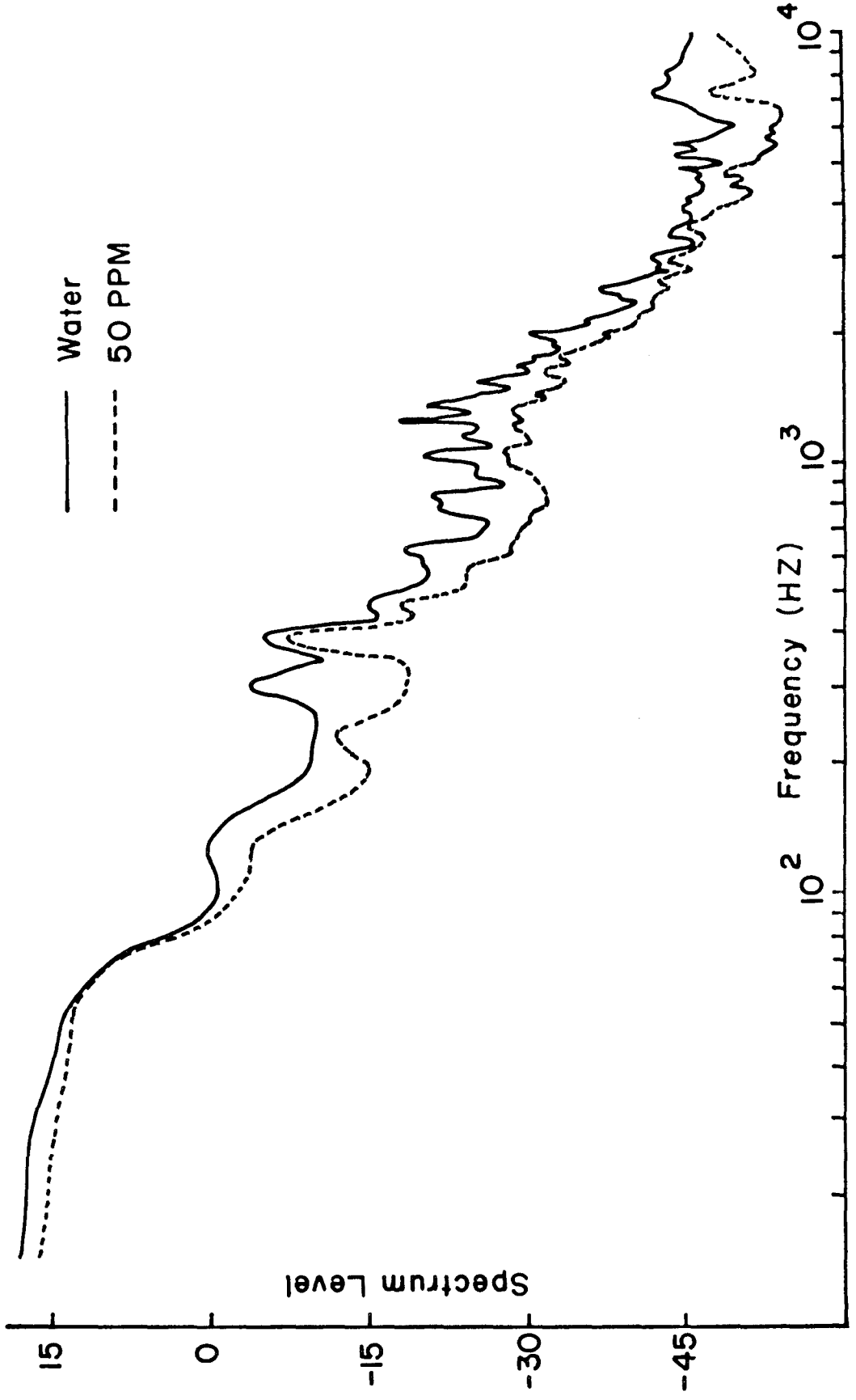

Figure 56. Noise spectra of water and 50 ppm polyox: y = 5.1 cm; x = 120 cm.

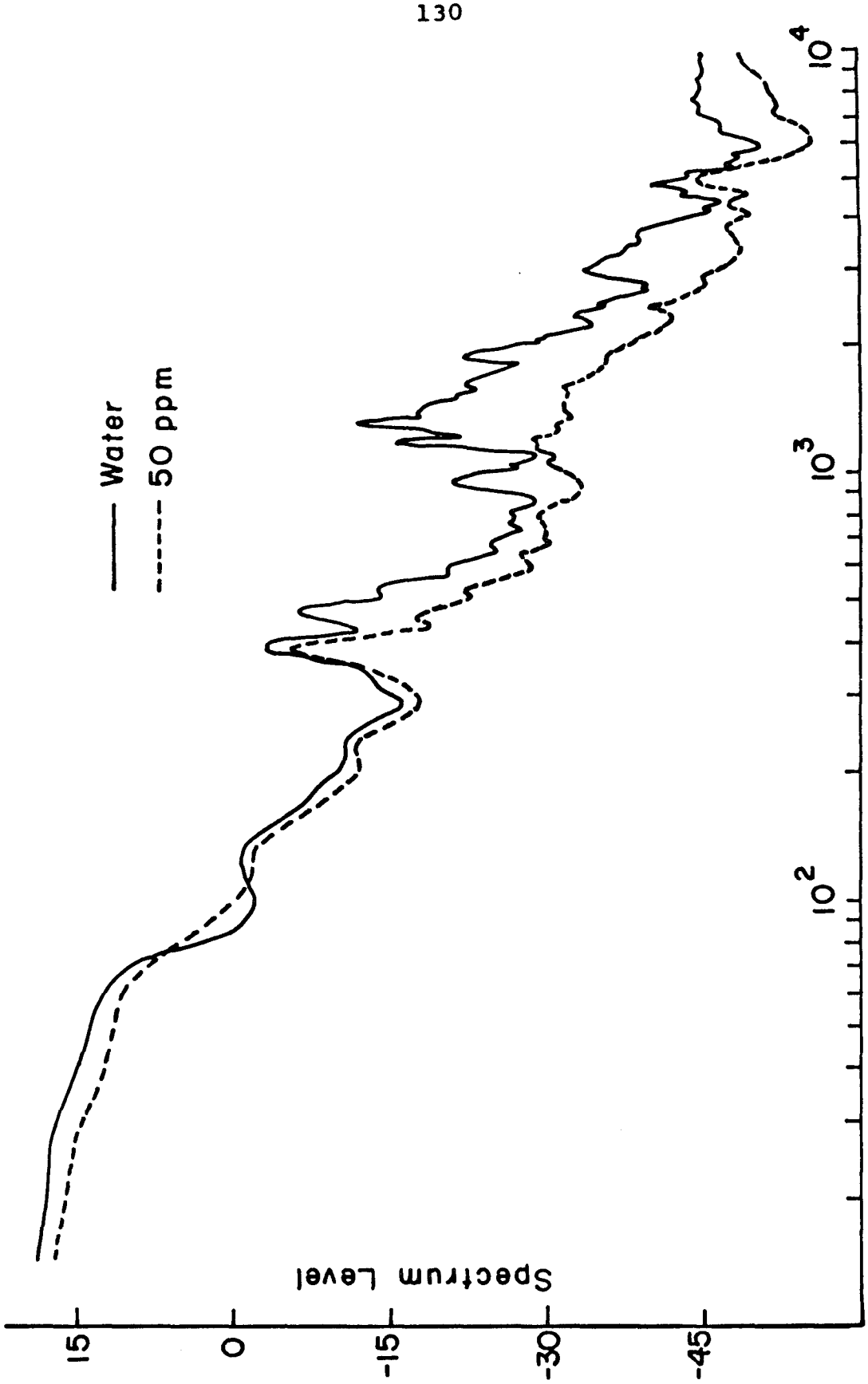

Figure 57. Noise spectra of water and 50 ppm polyox: y = 5.1 cm; x = 157 cm.

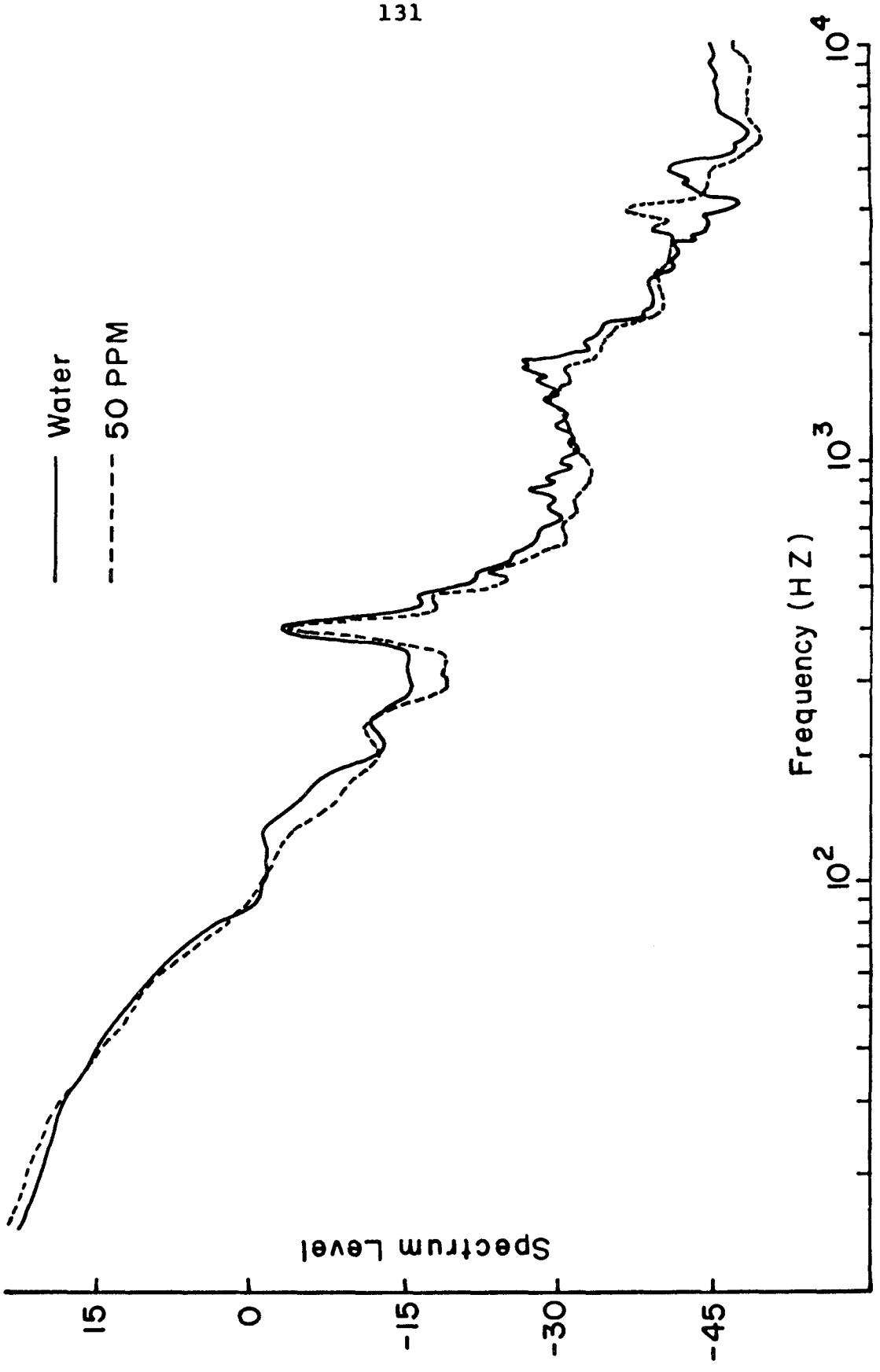

Figure 58. Noise spectra of water and 50 ppm polyox: y = 5.1 cm; x = 194 cm.